Dissertation

submitted to the

Combined Faculties for the Natural Sciences and for Mathematics

of the Ruperto-Carola University of Heidelberg, Germany

for the degree of

Doctor of Natural Sciences

presented by

M.Sc. Aishwarya Sundaram

born in: Chennai, India

Oral examination: 9th December, 2016

Linking Metabolic Syndrome And Pancreatic Cancer Through Transcriptional Regulation and Secreted Factors From White Adipocytes

Referees:

PD Dr. Renate Voit

Prof. Dr. Stephan Herzig

Summary

Obesity has reached pandemic proportions, and is associated with several co-morbidities like cardiovascular disorders, hypertension, dyslipidemia, and Type 2 diabetes mellitus. The dysregulated adipose tissue metabolism in obesity leads to an altered adipokine secretion, which can influence energy homeostasis, promote insulin resistance, as well as provide pro-tumorigenic signals to tumor cells. We investigated the link between obesity, and the progression of pancreatic ductal adenocarcinoma (PDAC). Although, obesity has been associated with a poor prognosis in PDAC, the underlying mechanisms are unclear.

At first, we used adipose tissue specific knockout of TBLR1 (ATKO) mice as a model of obesity, to investigate if the transcriptional inactivation of the transcriptional co-factor Transducin beta like related 1 (TBLR1) promoted PDAC progression. Although, subcutaneous (SC) Panc02 tumors grew significantly larger in the ATKO mice, compared to wt littermates, histological examination of the tumors did not reveal increased proliferation, or adipocyte infiltration in the tumors from ATKO mice. Also, gene expression analysis in tumors from wt and ATKO mice did not reveal any significantly differentially regulated genes. Finally, *in vivo* effects could not be validated by treating PDAC cells with conditioned media (CM) generated from primary adipocytes of ATKO mice, or from *Tblr1* knockdown 3T3-L1 adipocytes. Therefore, we could not establish a robust link between the absence of *Tblr1* in the adipose tissue, to PDAC progression.

Using *in vitro* assays, we demonstrated that adipocyte-conditioned media (ACM) from differentiated 3T3-L1 adipocytes, but not fibroblasts, promoted PDAC cell viability, proliferation, migration, and invasion *in vitro*. Therefore, we hypothesized that secreted factors from adipocytes mediate pro-tumorigenic effects on PDAC. Previously it was shown by our group that SC Panc02 tumors grew significantly larger in db/db mice, compared to wt mice. Microarray analysis of the SC inguinal white adipose tissue (iWAT) of db/db, and wt mice identified *ob gene* encoding leptin as one of the most significantly differentially regulated genes. Although, recombinant leptin did not affect proliferation, or migration of PDAC cell monolayer cultures, it increased the invasion of BxPC3 spheroids through collagen matrix. Most importantly, leptin increased the viability of PDAC cells upon treatment with gemcitabine. Thus, we hypothesized that leptin improves the chemo-resistance of PDAC cells to gemcitabine. However, knockdown of *Lepr* in PDAC cells did not affect proliferation, and viability upon gemcitabine treatment. Also, *Lepr* kd Panc02 tumors implanted subcutaneously into wt mice, displayed similar chemo-sensitivity to gemcitabine treatment *in vivo*, as compared to wt Panc02 tumors. Finally, pharmacological inhibition of human LEPR with anti-LEPR antibody did not affect the chemo-resistance of PDAC cells to gemcitabine.

In conclusion, although there was a strong effect of ACM from 3T3-L1 cells on PDAC growth *in vitro*, the effects could not be attributed entirely to leptin. Further investigation is required to identify the secreted factors from dysregulated adipocytes which could play a potential pro-tumorigenic role on PDAC progression, thus providing a link between obesity and PDAC development.

Zusammenfassung

Fettleibigkeit, welches pandemische Ausmasse erreicht, geht mit mehreren Erkranungen, wie Kardiovaskuläre-, Bluthochdruck, erhöhte Cholesterin Level und Type 2 Diabetes, einher. Der durch Fettleibigkeit gestörte Fettgewebsmetabolismus führt zu einer geänderten Sekretion von Adipokinen, welche die Energie-Homeostase beeinflussen, Insulinresistenz fördern und pro-tumorigene Wirkung auf Krebszellen haben können. Wir haben den funktionellen Zusammenhang zwischen Fettleibigkeit und der Entwicklung des pankreatischen duktalen Adenokarzinoms (PDAC) untersucht. Obwohl Fettleibigkeit mit einer schlechteren Prognose für PDAC assoziiert ist, sind die zugrundeliegenden Mechanismen noch relativ unbekannt.

Wir nutzten die Fettgewebsspezifische Knockout Maus für TBLR1 (ATKO) als Modelorganismus für Fettleibigkeit, um zu untersuchen ob die transkriptionelle Inaktivierung des Transkriptionellen Ko-Faktors Transducin Beta like related 1 (TBLR1) PDAC Entwicklung fördert. Obwohl subkutan implantierte (SK) Panc02 Tumore von ATKO Mäusen signifikant erhöhtes Wachstum gegenüber Wildtyp (WT) Wurfgeschwistern aufzeigten, konnten nach histologischer Analyse keine erhöhte Proliferation oder Adipozyten Infiltration in die Tumore von ATKO Mäusen gemessen werden. Genexpressionsanalysen von Tumoren aus WT und ATKO Mäusen zeigte keine signifikant differentiell regulierten Gene. Es konnten die in vivo Effekte auch nicht validiert werden, indem PDAC Zellen mit Konditionertes Medium von primären Adipozyten der ATKO Mäuse oder *Tblr1* knockdown 3T3-L1 Adipozyten behandelt wurden. Insofern konnte keine Verbindung zwischen dem Fehlen von *Tblr1* im Fettgewebe und PDAC Entwicklung gefunden werden.

In *in vitro* Assays konnte demonstriert werden, dass Adipozyten-konditioniertes Medium von differenzierten 3T3-L1 Adipozyten, aber nicht Fibroblasten, PDAC Zellviabilität, Proliferation, Migration und Invasion bewirkt. Daher wurde die Hypothese aufgestellt, dass sekretierte Faktoren von Adipozyten die pro-tumorigenen Effekte auf PDAC bewirken. Kürzlich wurde von unserem Labor gezeigt, dass SK Panc02 Tumore in db/db Mäusen signifikant grösseres Wachstum aufzeigen als in WT Mäusen. Microarray Analysen des SK inguinalen weissen Fettgewebes (iWAT) der db/db und WT Mäuse identifizierte das *ob* Gen, welches für Leptin kodiert, als eines der am höchsten signifikant differentiell exprimierten Gene. Obwohl rekombinantes Leptin keine Proliferation oder Migration von PDAC Zellen in Einzelschichten wachsend bewirkte, erhöhte es jedoch die Invasion von BxPC3 Spheroiden durch eine Kollagen Matrix. Interessanterweise erhöhte Leptin die Viabilität von Gemcitabine behandelten PDAC Zellen. Daher wurde hypothetisiert, dass Leptin die Chemoresistenz von PDAC Zellen gegenüber Gemcitabine erhöht. Jedoch bewirkte der Leptinrezeptor (Lepr) knockdown in PDAC Zellen keine Änderung in Proliferation oder Viabilität bei Gemcitabine Behandlung. Überdies zeigten SK in WT Mäuse implantierte Lepr knockdown Zellen ähnliche Sensitivität gegenüber Gemcitabine im Vergleich zu Kontroll Panc02 Tumoren. Auch pharmakologische Inhibierung des humanen LEPR mit einem anti-LEPR Antikörper hatte keinen Effekt auf Chemoresistenz der PDAC Zellen gegenüber Gemcitabine.

Zusammenfassend kann gesagt werden, dass, obwohl ein starker Effekt von AKM der 3T3-L1 Zellen auf PDAC Wachstum *in vitro* festgestellt werden konnte, konnten diese Effekte nicht vollständig auf Leptin zurückgeführt werden. Weitere Untersuchungen sind nötig, um die Sekretierten Faktoren von dysregulierten Adipozyten zu identifizieren, welche eine potentiell pro-tumorigene Rolle bei der PDAC Entwicklung spielen um damit einen Zusammenhang zwischen Fettleibigkeit und PDAC Entwicklung herzustellen.

Acknowledgements

I would firstly like to thank Prof. Dr. Stephan Herzig, for giving me this great opportunity to join his research group and work on my doctoral thesis. He has inspired me with his relentless optimism, enthusiasm, and great ideas. Secondly, I would like to thank Dr. Mauricio Berriel Diaz for all the supervision, support during my PhD, and of course for proof-reading my thesis.

Thirdly, I would like to thank my former lab colleagues from A170 group at DKFZ, particularly Maria Rohm for all the guidance, and brainstorming in the early stages of my PhD. I am extremely grateful to Marcos, for being a great post-doc mentor during my PhD. I also would like to thank Adriano, and Götz for helping me with my thesis. I would like to thank the technicians from A170 – Dani, Yvonne, Annika, and Kati for their great support during experiments. I would then like to thank Eveline, my master student, for reminding me why I chose a scientific career through her curiosity to understand, and unravel biological processes.

I am very grateful to our collaborators in Heidelberg, and Mannheim, who contributed to the progress of this project. Thanks to PD. Dr. Karin Müller-Decker for tremendous support with mouse experiments. And thanks to Carsten Sticht for microarray data analysis, and Maria Muciek for performing microarray.

I would like to thank my thesis advisory committee, PD. Dr. Renate Voit, and Dr. Med. Oliver Ströbel for very good scientific discussions, and inputs throughout my PhD.

I would like to thank my close friends Irem, Asrar, Paula, and Krishna for their constant support, for memorable trips, and for being there for me during tough times. PhD wouldn't have been as much fun without them. I would like to thank Jess for nice discussions at lunch, and for making delicious cupcakes on my birthday. I really loved the hiking trips in Bavarian Alps with fellow lab mates at the IDC, Munich, and would like to thank Maude for organizing them. And thanks to Miriam for being a great friend and for helping me innumerable times.

Finally, and most importantly, I would like to thank my family. Arun is my pillar of strength, my best friend and husband, and I want to thank him for his undying support throughout my PhD. It wouldn't have been possible for me to follow and realize my dreams without his encouragement, sacrifices, and faith in me. I owe my PhD to him. I would like to thank my parents, and my sister, and Arun's parents, and the entire family for their tremendous support, and for having belief in me. Thank you all!

Success is not final; failure is not fatal;
It is the courage to continue that counts.
-Winston Churchill

INDEX

1 INTRODUCTION

1.1 Metabolic syndrome and obesity: A Global Pandemic

1.1.1 Metabolic syndrome: Definition, and epidemiology

The term "Metabolic Syndrome" (MetS), was first used by Haller and Hanefeld in 1975 [1]. MetS is defined by the clustering of several interconnected biochemical, clinical, and metabolic factors, like central obesity, insulin resistance, hypertension, and dyslipidemia, that synergistically increase the risk for developing cardiovascular disease (CVD), and type 2 diabetes mellitus (T2DM) [1], [2].

The global occurrence of MetS ranges between 10% to as much as 84% based on the geographical location, age, gender, and ethnicity of the population being examined (WHO fact sheet No. 311, 2015). Greater socio-economic status, reduced physical activity, and high body mass index (BMI) were significantly correlated with MetS [2]. Overweight, and obesity, are defined as having a BMI ≥ 25 kg/m², and ≥ 30 kg/m² respectively, and have reached epidemic proportions. Globally, more than 1.9 billion adults aged 18 and above were found to be overweight in 2014, of which 600 million were obese (WHO fact sheet No. 311, 2015). The number of obese individuals has more than doubled between 1980 and 2014 (WHO fact sheet No. 311, 2015). Although considered as a disease of affluence, obesity is now spreading to poorer nations and is a growing threat to the developing world [3]. Currently, bariatric surgery is the best treatment option available for severely obese patients [4]. Therefore, there is a huge need for improved pharmacological treatment strategies to address the global obesity epidemic [5]. Better understanding of the molecular mechanisms that regulate obesity, and its influence on other organs is necessary to develop novel therapeutics for this condition [6].

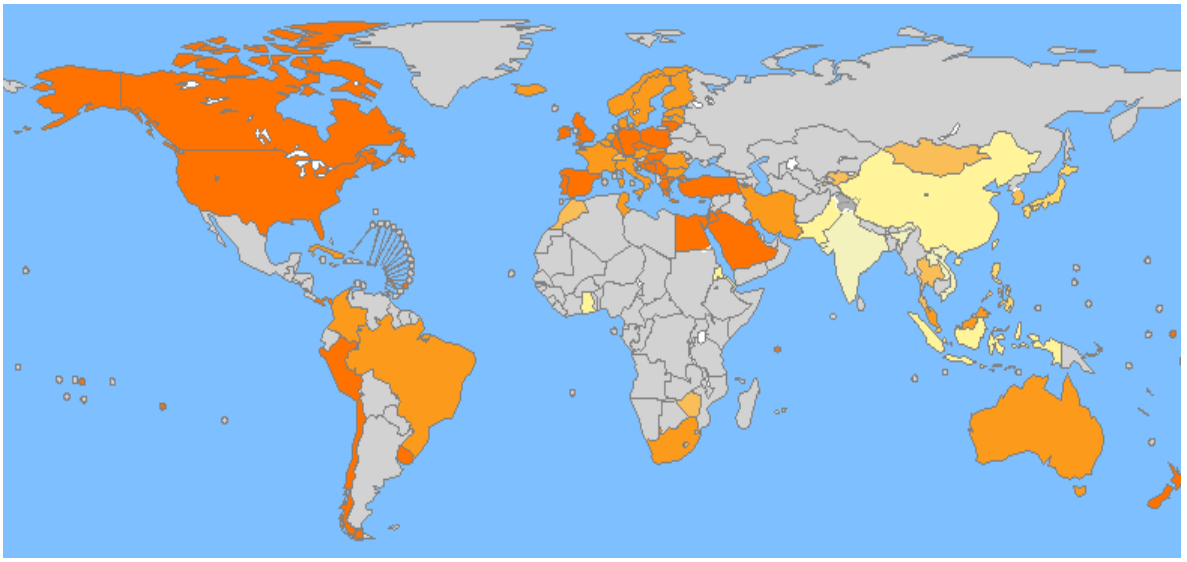

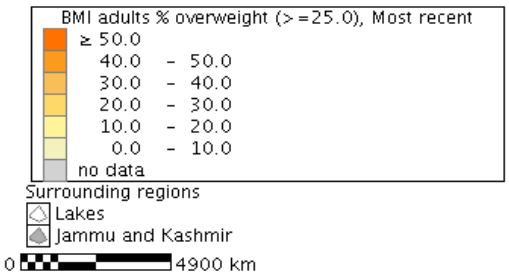

Figure 1: Global Database on Body Mass Index. *Mean body mass index trends (kg/m2), ages 18+, 2014 (age standardized estimate). Source: WHO (http://apps.who.int/bmi/index.jsp)*

1.1.2 Obesity is fundamental for development of metabolic syndrome

The underlying cause of obesity is a sustained imbalance between energy intake and expenditure (WHO fact sheet No. 311, 2015), [5]. Consumption of calorie rich diet, in combination with a sedentary lifestyle has contributed greatly to the epidemic of obesity. Although dyslipidemia, hypertension, hyperglycemia, and a chronic pro-inflammatory state are well-accepted risk factors for the development of MetS, abdominal obesity, and insulin resistance (IR) are considered as the underlying causes [7].

The mechanisms causing MetS are a subject of ongoing research due to the complex interaction between different metabolic, genetic, and environmental factors [8]. It is known that overweight and obesity result in hypertrophic expansion of the adipose tissue, particularly the visceral fat depot [9]. These hypertrophic abdominal adipocytes contribute to increased amounts of circulating free fatty acids (FFAs) [10]. FFAs have been known to inhibit insulin mediated glucose transport and/or phosphorylation, and contribute to insulin resistance [11]. The increased amounts of FFAs thus cause a state of peripheral muscle insulin resistance, and hyperglycemia. In order to compensate for the reduced peripheral insulin action, and achieve a normoglycemic state, more insulin is secreted which results in hyperinsulinemia, and ultimately β-cell hypertrophy [12], [13]. Hence, obesity associated insulin resistance is one of the key mechanisms causing MetS.

1.2 Adipose tissue in energy homeostasis and metabolic disorders

1.2.1 Classification of adipose tissue, and its role in metabolic homeostasis

Historically, the adipose tissue was considered merely as an organ responsible for storing energy, and hence did not gain much attention from researchers. However, the global rise in obesity has led to a renewed interest in understanding the role of adipose tissue in the regulation of systemic energy homeostasis. Adipose tissue is classified into two main categories in humans, the white adipose tissue (WAT), and the brown adipose tissue (BAT). Based on its anatomy, the WAT is further classified into two depots namely, the subcutaneous WAT, and the visceral WAT. The adipocytes and progenitor cells from

distinct depots differ in their proliferative capacities, developmental origin, and response to hormonal stimuli [14]. The primary function of the WAT is to store energy, and to provide insulation. On the other hand, the BAT is rich in mitochondria and is distinguished by its expression of the uncoupling protein-1 (UCP1) which is involved in cold induced thermogenesis [15].

Adipose tissue is composed of different cell types, such as the mature adipocytes, and the stromal vascular fraction consisting of fibroblasts, precursor cells, immune cells, and blood cells. The adipocytes secrete a variety of proteins called adipokines, which contribute to the regulation of systemic energy metabolism by their paracrine and endocrine effects on multiple other organs like brain, liver, muscle, vasculature, and pancreas [16], [17].

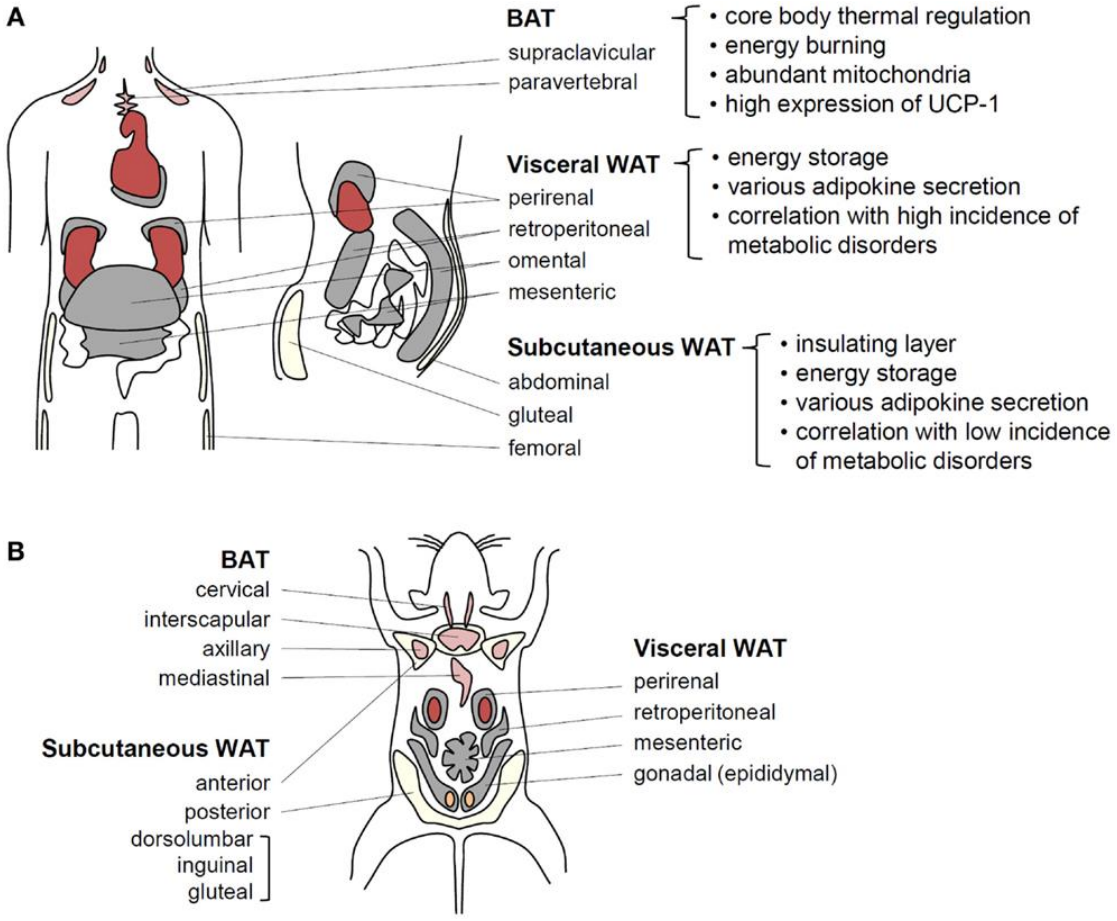

Fig. 2: Classification and function of adipose tissue in humans and mice. *(A) In humans, BAT is located near the shoulders and ribs, and is thought to regulate body temperature. The brown adipocytes are rich in mitochondria and express UCP-1. The visceral WAT surrounds the intra-abdominal organs, and the subcutaneous WAT is present under the skin. Both the white, and brown adipocytes release several adipokines, which regulate whole-body energy homeostasis. Obesity and MetS are associated with the dysregulation of the visceral WAT. (B) In adult mice, the BAT is distinct and easily identifiable. The WAT depot consists of pair of adipose tissue surrounding the gonads (peri-gonadal), and are used as a model of visceral WAT. The subcutaneous inguinal depots found at the back of the hind limbs serve as a model of subcutaneous WAT (Adapted from* [15]*).*

1.2.2 Adipose tissue dysregulation in obesity

Adipocytes function to store the surplus calories in the form of triglycerides within lipid droplets, and release free fatty acids upon energy deficit. When challenged with over nutrition, the adipocytes adapt and expand in order to prevent lipid spill over into other organs. This is achieved either by increasing the size of pre-existing adipocytes (hypertrophy), or by increasing the number of adipocytes (hyperplasia) [18]. The number of adipocytes stays constant in adults, and is determined during childhood and adolescence [19]. Terminally differentiated adipocytes in adults, adapt to positive energy balance predominantly by hypertrophic expansion [19]. The expandability of hypertrophic adipocytes is not unlimited, and is dependent on several factors like the formation of new blood vessels (angiogenesis), and the remodeling of matrix components [20]. Obesity associated nutrient overload causes hypertrophic expansion of adipocytes, which become dysfunctional due to their limited capacity to store further lipids. Finally, the inability of adipocytes to store the excess calories results in the ectopic accumulation of lipids, and lipotoxicity, which is one of the contributing factors to the pathologies associated with MetS [21].

Adipose tissue is an active endocrine organ, secreting several hormones, and adipokines. Leptin was one of the first adipokines to be discovered [22]. Leptin regulates central energy metabolism, and promotes satiety by its action on the hypothalamic neurons. The expanding fat mass in obesity is associated with increased plasma leptin concentrations. However, the higher circulating levels of leptin fails to prevent the development of obesity in mouse models of obesity, and as well as in obese human subjects [23]. Ultimately, a combination of factors including reduced expression of leptin receptor in the hypothalamus, and an impaired leptin signaling, lead to leptin resistance [23].

Adiponectin is one of the most abundantly secreted adipokines by the healthy adipose tissue [24]. However, plasma adiponectin levels drop significantly in obese individuals [25]. The injection of adiponectin in mouse models has been shown to improve insulin resistance [26], [27]. Therefore, obesity induced reduction in adiponectin levels promotes insulin resistance.

The dysfunctional adipocytes have an impaired secretion of adipokines, and release more of the pro-inflammatory cytokines like TNFα, and IL-6, and chemo-attractants like MCP-1 [28]. The pro-inflammatory cytokines and chemo-attractants alter the local and systemic inflammatory milieu, and attract macrophages, and infiltrating immune cells, causing a state of chronic low grade inflammation in the adipose tissue. Adipose tissue inflammation is fundamental to the pathophysiology of obesity related metabolic dysfunction [29].

Obesity related adipocyte hypertrophy increases the size of adipocytes, resulting in diminished blood supply and restricted access to nutrients and oxygen, causing a hypoxic stress [30]. Studies indicate the

involvement of hypoxia in adipose tissue fibrosis, and inflammation [31], [30]. Moreover, hypoxia has been shown to cause polarization of the adipose tissue macrophages (ATMs) to the more inflammatory M1 state [32]. The paracrine and endocrine effects of adipokines can impact the metabolism of different organs and contribute further to the pathology of obesity and associated disorders. Therefore, it is necessary to understand the molecular mechanisms underlying the dysregulation of adipose tissue in obesity, and its effects on adipokine secretion in order to develop novel therapeutics for obesity. The figure below describes the key features of obesity mediated adipose tissue dysregulation.

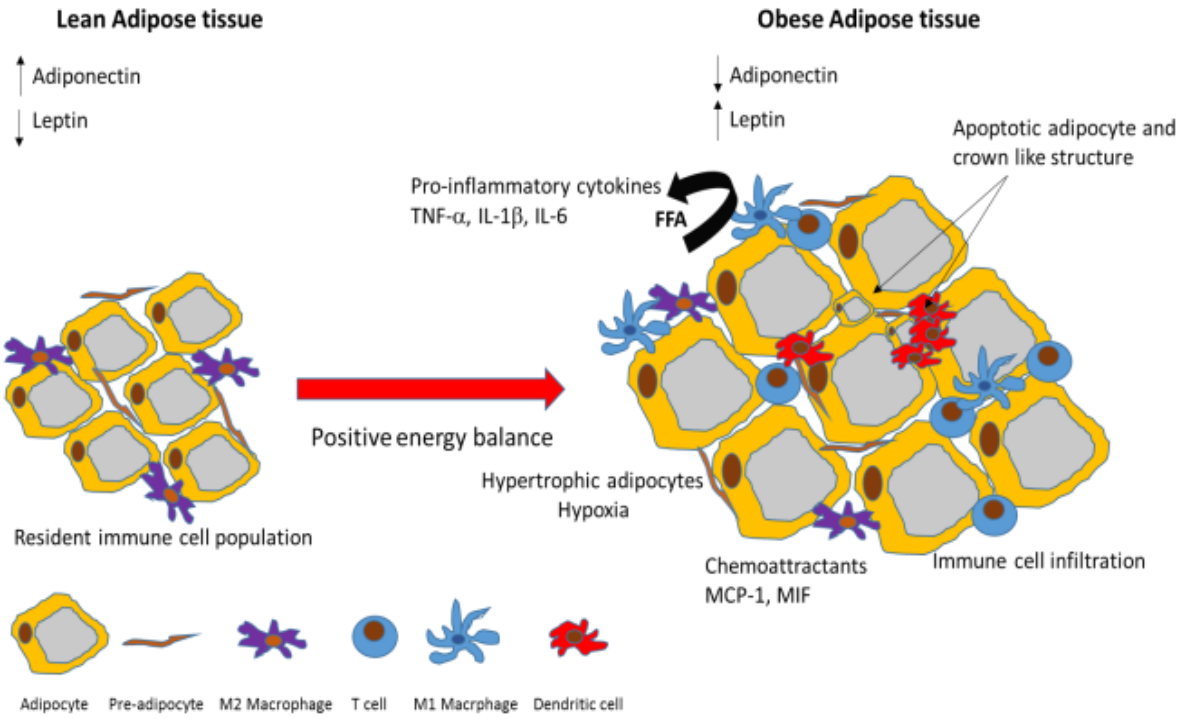

Fig. 3: Dysregulation of adipocytes in obesity. *Obesity promotes the hypertrophic expansion of adipocytes, alters adipokine secretion, and augments the release of free fatty acids, and chemo-attractants. Plasma leptin concentration goes up, and adiponectin level decreases during obesity. The dysregulated adipocytes secrete more pro-inflammatory adipokines, which promotes Infiltration of macrophages and immune cells into the dysfunctional adipose tissue, and triggers a chronic inflammatory state characterized by the presence of pro-inflammatory M1 macrophages. The increased amounts of free fatty acids, and inflammation, promote insulin resistance(Adapted from* [28]*).*

1.3 Pancreas

1.3.1 Anatomy and functions

The pancreas is an elongated, tapered organ located in the upper abdomen behind the stomach. It consists of three main parts namely, the head, the body, and the tail. The head of the pancreas is positioned on the right side of the organ, and lies in the loop of the duodenum. The body of the pancreas is tapered, and extends upwards, and the tail of the pancreas ends near the spleen.

The pancreas consists of the exocrine, and the endocrine glands. The pancreas has digestive and hormonal functions. The exocrine tissue constituting the majority of the pancreas, is composed of the acinar tissue, and secretes enzymes like trypsin and chymotrypsin, amylase, and lipase that help digest the ingested proteins, carbohydrates, and fats respectively. The enzymes are secreted in an inactive form by the pancreas, and are drained into the pancreatic duct, which joins the common bile duct. Upon entering the duodenum, they get activated.

The endocrine pancreas consists of the islets of Langerhans, which is composed of several different types of cells. The α-cells (produce glucagon), β-cells (secrete insulin and amylin), δ-cells (secrete somatostatin), PP-cells (produce pancreatic polypeptide), and ε-cells (produce ghrelin). The main hormones secreted by the endocrine pancreas are insulin, glucagon, and somatostatin. Insulin is an anabolic hormone, and regulates the levels of glucose in the bloodstream, and promotes uptake of glucose by liver, muscle, adipose tissue, and other organs. Glucagon on the other hand has the opposite effect of insulin in glucose regulation, and promotes the release of stored energy into the bloodstream. Somatostatin reduces the rate of absorption of nutrients from the contents in the intestine. Finally, the pancreatic polypeptide is involved in the auto-regulation of the secretory activities of pancreas, and functions to reduce appetite.

1.4 Pancreatic cancer

1.4.1 Epidemiology

The worldwide annual incidence rate for pancreatic cancer is approximately 8 out of 100,000 persons [33]. As of 2012, pancreatic cancer was the 10^{th} most common cancer in men, and 6^{th} most common cancer in women, in Germany (Fig. 4). Pancreatic cancer was the 4^{th} most common cause of cancer related mortality in both men and women in 2012, in Germany (Fig. 5). Pancreatic cancer is one of the most aggressive malignancies, as its rate of incidence almost equals the mortality rate. Pancreatic cancer has one of the most dismal prognosis, with a 5-year survival rate of a mere 8% for both sexes, in Germany [34], (Zentrum für Krebsregisterdaten, Robert-Koch-Institut). Due to the absence of specific symptoms, the disease escapes diagnosis in its formative stages [35].

Incidence

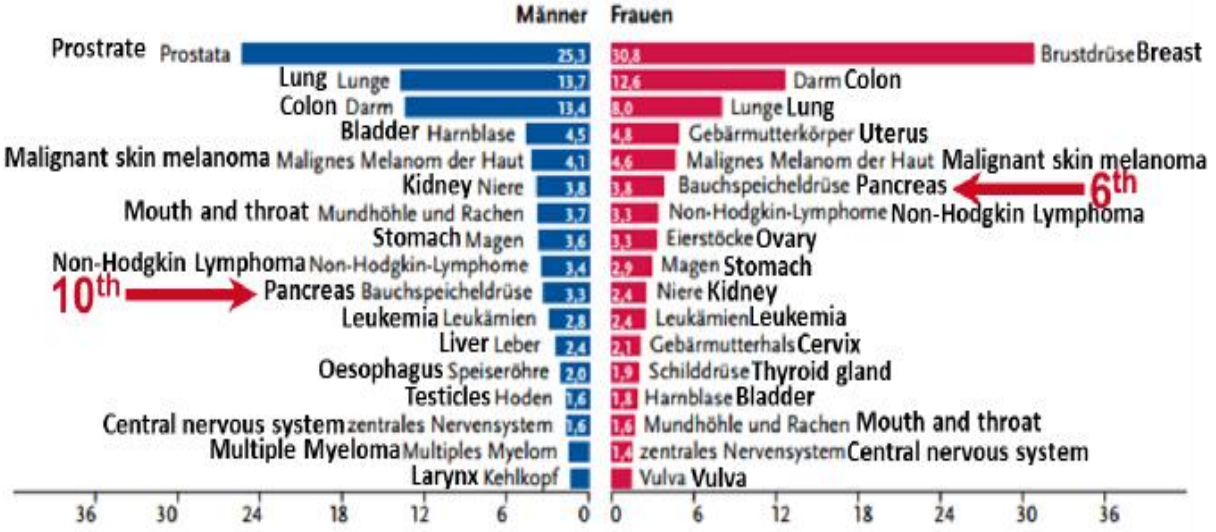

Fig. 4: Cancer incidence in Germany: *Percentage of common tumor sites on all new cancer cases in Germany in 2012 (Excluding non-melanotic skin cancer) - Zentrum für Krebsregisterdaten. Robert-Koch-Institut*

Mortality

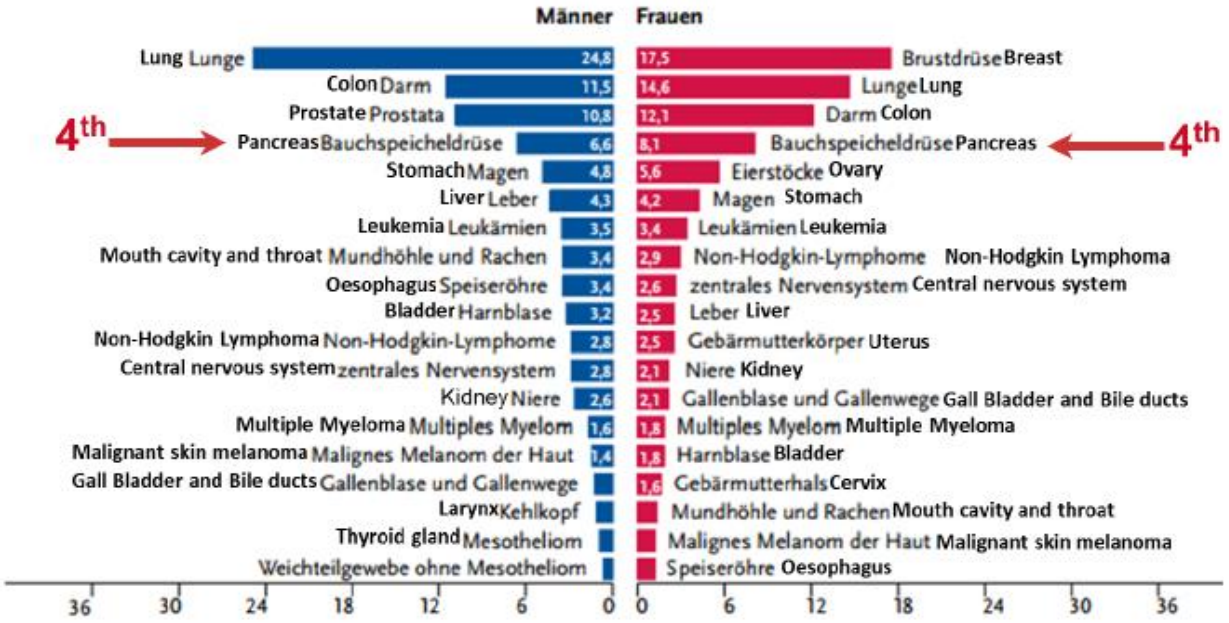

Fig. 5: Cancer mortality in Germany: *Percentage of common tumor sites of all cancer deaths in Germany in 2012. - Zentrum für Krebsregisterdaten. Robert-Koch-Institut*

1.4.2 Common gene mutations in PDAC

Studies have identified certain signature gene mutations in *KRAS, CDKN2A, TP53, BRCA2,* and *SMAD4/DPC4* genes, which contribute to the biological characteristics and progression of pancreatic carcinoma (Table. 1) [35]. The majority of the tumors originate in the exocrine ductal tissue. It has been

observed that abnormal ductal structures called PanIN lesions (pancreatic intraepithelial neoplasia), often precede the occurrence of pancreatic ductal adenocarcinoma (PDAC) [35].

Tumor type	Histological features	Mutation
Adenocarcinoma	Ductal morphology	*KRAS, CDKN2A, TP53, SMAD4*
Acinar cell carcinoma	Zymogen granules	*APC/β-catenin*
Pancreatic endocrine tumors	Hormone production	*MEN1*
Serous cystadenoma	Ductal morphology, cystic growth	*VHL*

Table 1: Types of pancreatic cancer neoplasms. *Different types of tumors can originate in the pancreas, determined by their histological similarity to different cell types. They show specific clinical and genetic profiles. Pancreatic ductal adenocarcinoma (PDAC), originating in the exocrine ductal cells, is the most common type of cancer in the pancreas, contributing to as much as 85% of pancreatic malignancies (Adapted from* [35]*).*

1.4.3 Risk factors for development of PDAC

1.4.3.1 Hereditary, gene mutations, pancreatitis, and type 2 diabetes mellitus (T2DM)

Having a family with at least 2 affected first degree relatives, poses an 18-fold higher risk for PDAC than random cases [36]. Germline mutations in genes like *BRCA, p16, STK11/LKB1*, and *PRSS1*, have been linked to the development of hereditary pancreatic cancer syndromes [36].

Hereditary pancreatitis significantly increases the risk for PDAC [37]. It is a rare disease, and is thought to arise due to a mutation in the trypsinogen gene, which might be affecting the activation of trypsinogen or preventing its autolysis, leading to pancreatic inflammation [37], [38]. Hereditary pancreatitis poses a 53-fold higher risk of developing pancreatic cancer, in comparison to unaffected individuals [38].

Meta-analyses have shown that diabetics have a 2-fold higher risk for developing pancreatic cancer, compared to non-diabetics [13]. It is not clear if diabetes is a cause or consequence of pancreatic cancer. Diabetes could manifest due to impairment of pancreatic β-cells, as a consequence of pancreatic cancer. However, in the presence of diabetes, the tumor cells could be exposed to high levels of insulin, and insulin is known to promote tumor growth. Therefore, hyperinsulinemia could be the link between T2DM and pancreatic cancer [39].

1.4.3.2 Age, sex, smoking, and alcohol consumption

Pancreatic cancer is rare before the age of 55, and the median age of onset is 71 years [33]. Also, the incidence of pancreatic cancer is higher in men than in women [33]. Pancreatic cancer incidence rates are significantly greater in persons of an African origin, compared to any other racial origin (http://seercancergov/statfacts/html/pancreashtml). The reason for these racial differences are unknown [33].

Smoking is one of the most well-known modifiable risk factor for PDAC, contributing upto 20-30% of PDAC cases [40]. Long-term smokers have a 2-fold higher probability of developing PDAC than non-smokers [41]. Alcohol was identified as an independent risk factor for PDAC, however only in heavy alcohol consumers [40]. Smoking was found to be a strong confounding factor for alcohol-induced pancreatic cancer [42].

1.4.4.3 Obesity and PDAC risk

Overweight, and obesity not just increase the risk of CVD, and T2DM, but also of many different types of cancers [16]. In fact, studies have shown that obesity accounts for 20% of all cancers [43]. Cancers that are most frequently associated with a higher BMI are those of the endometrium, breast, kidney, liver, esophagus, and pancreas. The altered hormonal milieu in obesity influences these tumors selectively. Obesity causes significant pathological modifications in the morphology and functions of adipose tissue, involving alterations in pro-inflammatory adipokine secretion, lipolysis and free fatty acid generation, and immune cell infiltration. Together, these changes lead to insulin resistance, and a state of chronic inflammation, both of which are involved in carcinogenesis [16]. BMI $\geq$ 30 is significantly associated with increased risk of pancreatic cancer [44].

The metabolic dysregulation of visceral fat in obesity has been shown to cause fat accumulation or steatosis in the pancreas, which is a risk factor for pre-cancerous lesions (PanIN) that might progress to pancreatic cancer [45]. Autophagy is a process that under normal conditions, reduces inflammation. However, in mouse models, obesity and high-fat diet are known to inhibit autophagy, thereby augmenting inflammation [46]. Pancreatic cancer is known to be highly desmoplastic, characterized by activated stellate cells and build-up of the extra-cellular matrix (ECM) [47]. Desmoplasia promotes tumor cell migration, and metastasis, and most importantly prevents drug diffusion, causing chemo-resistance. Obesity associated inflammation augments desmoplastic response in the pancreas, and contributes to drug-resistance [47]. Understanding the connection between inflammation, autophagy, and obesity could help identify new therapeutic targets, and develop effective treatments for PDAC [46].

Communication between dysfunctional adipocytes, and pancreas through secreted adipokines could be an important mechanism linking obesity and PDAC progression. Better understanding of the tumor promoting effects, and mechanism of action of such secreted factors on PDAC progression would pave the way for development of better therapeutics.

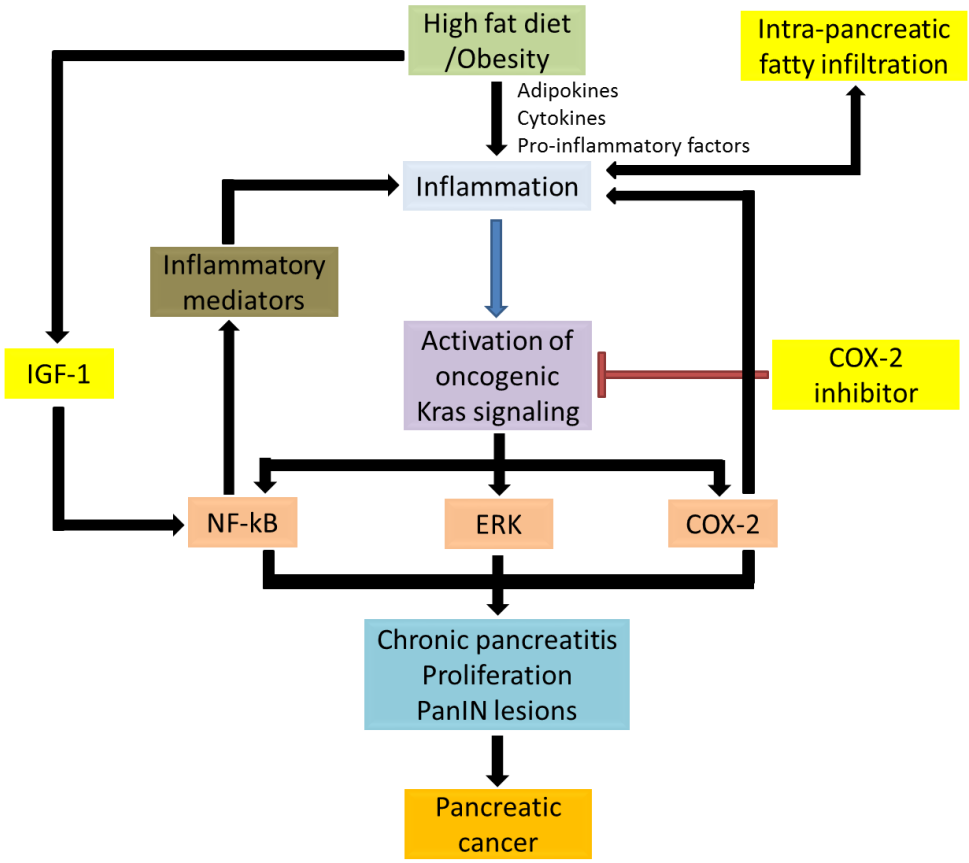

Fig. 6: Mechanisms linking obesity and PDAC. *The interaction between HFD/obesity, inflammation, and oncogenic Kras signaling promotes PDAC progression. Studies in mouse models (LSL-Kras/Ela-CreERT mouse) showed that HFD feeding for 30 days increases Kras activity, upregulates COX-2 expression, activates Erk, causes significantly more PanIN lesions, and increases the severity of chronic pancreatitis compared to the mice on control diet. The same mice, when placed on a HFD for a prolonged period, proceed to develop PDAC from PanIN lesions. Inhibition of COX-2 ameliorates the effects of HFD on pancreatic tumor progression* [48]*. On the contrary, caloric restriction impedes obesity, and reduces the growth of murine Panc02 allografts, and xenografts from human pancreatic cancer. Calorie restricted mice had lower IGF-1 levels, and the reduced pancreatic cancer growth was potentially mediated through reduced NFκB activation associated with IGF-1 signaling (Adapted from* [49], [50]*).*

1.5 Transcriptional co-factor: Transducin beta like related (TBLR) 1

1.5.1 Nuclear transcription factors and cofactors

Eukaryotic transcription is a complex process involving an intricate, and concerted action of several macromolecules. Nuclear receptors (NR) are transcription factors that are activated by ligand binding, and function to activate (or repress) the transcription of specific downstream target genes [51]. Several receptors like the steroid receptors, estrogen receptor (ER), glucocorticoid receptor (GR), retinoic acid receptor (RAR), thyroid hormone receptor (TR), and receptors for fatty acids and prostaglandins, belong to the nuclear receptor class. Orphan receptors without any clearly identified ligands, are also a part of the NR superfamily [52]. Upon binding to its ligand, a series of events are triggered wherein the NR undergoes a conformational change, and can for e.g. induce receptor dimerization, import to the nucleus,

and bind to target DNA sequences [51]. The conformational change can also expose binding sites for transcription co-factors.

Transcription cofactors interact with NRs, and other transcription factors to activate (coactivators) or repress (corepressors) target gene expression [53]. They do so by modifying specific lysine residues on histones, which changes the local chromatin structure, making it more or less accessible to the transcription machinery. The coactivators most often have an intrinsic histone acetyltransferase (HAT) activity, and acetylate specific lysine residues of histone proteins, neutralizing its charge and promoting the unwinding of DNA from the associated histone to promote transcription. On the other hand, most corepressors recruit histone deacetylases (HDAC) to hydrolyze the acetyl residues and restore the positive charge to histones, strengthen the DNA-histone interaction, and inhibit basal transcription machinery. Both the coactivators, and corepressors, have distinct binding motifs. The NR coactivators are recruited in a ligand-dependent fashion (e.g.: CREB binding protein, p300 etc.). The NR corepressors on the other hand, specifically bind to ligand free receptor (e.g.: NCoR2/SMRT, RIP140 etc.).

1.5.2 TBLR1 is part of a transcriptional corepressor complex

TBLR1 (Transducin beta like related 1) is a transcriptional co-factor, and a component of the SMRT/NCoR1 corepressor complex [54]. TBLR1 promotes repression of target gene expression, upon binding to ligand free nuclear receptors like TR (Thyroid hormone receptor) [55], [56]. The human gene encoding TBLR1 is located on chromosome 3, and contains 18 exons [54], [55]. TBLR1 has two more isoforms, namely TBL1X and TBL1Y, which are also encoded by the same gene [57].

Previously, it has been demonstrated that TBLR1 plays a critical role in adipocyte lipid metabolism, and that mice lacking TBLR1 (**A**dipose **T**issue specific **K**nock**O**ut of *Tblr1*, ATKO) in their adipose tissue have an impaired lipolysis [58]. Upon exposure to a high fat diet, the ATKO mice were found to gain more weight, develop glucose intolerance, and become insulin resistant [58].

Transcriptional dysregulation in the adipocyte, particularly those that lead to aberrant adipocyte energy metabolism, can serve as a link between obesity and adipose tissue dysfunction. Such changes in the adipose tissue can result in an altered adipokine secretion, potentially mediating pro-tumorigenic signals to tumors. Given that, ATKO mice have an impaired adipose tissue metabolism, they can serve as an experimental mouse model of metabolic dysfunction. The link between TBLR1 and PDAC is not known. Therefore, further research is required to understand the contribution of TBLR1 deficient adipose tissue to PDAC progression.

1.6 Adipokines and PDAC

1.6.1 Dysregulated adipokines provide pro-tumorigenic signals

Adipokines are secreted polypeptide cytokines, predominantly secreted by white adipocytes [59]. Obesity leads to alterations in the morphology, immune status, and vasculature of the adipose tissue, and causes changes in the secretory profile of adipose tissue [17]. The obese adipose tissue secretes more of the pro-inflammatory adipokines like TNFα, IL-6, leptin, and Plasminogen activator inhibitor 1 (PAI1), resistin etc. [17]. The altered adipokine secretion, and a pro-inflammatory state favor tumorigenesis [59]. Adipokines like IL-6, and leptin have been linked to activation of cancer stem cells, and increased tumor cell survival [59]. On the other hand, the serum levels of adiponectin, an anti-inflammatory adipokine associated with improving insulin sensitivity, , goes down in obesity [60], [61]. Serum adiponectin levels have been negatively correlated to CRC (Colorectal cancer) [62], [63]. The association between reduced adiponectin levels in obesity and PDAC are not clearly understood, however it is possible that increased insulin resistance, and inflammatory cytokines linked to lower adiponectin levels, could be an indirect mechanism [61]. Effect of adipokines on PDAC tumorigenesis is an ongoing field of research, and efforts in this direction would help gain a better understanding of the paracrine and endocrine effects of dysregulated adipose tissue on pancreatic cancer progression, and find safer and better treatment options for this deadly malignancy.

1.7 Aim of the project

Dysregulated adipose tissue metabolism is known to be associated with the progression of several cancers. The aim of this study was to investigate how obesity affects PDAC progression. We hypothesized that the adipose tissue, communicates with the tumor cells through secreted protein factors, which have a pro-tumorigenic effect on PDAC. This was to be achieved by comprehensive *in vitro* experiments exposing PDAC cells to the conditioned media from murine 3T3-L1 cells, or from primary mouse adipocytes. We aimed to investigate the *in vitro* effects of the conditioned media on tumor cell viability, proliferation, migration, and invasion and to validate these effects *in vivo* using different mouse models of obesity. Subcutaneous Panc02 tumor implantations were performed to study the effects of obesity on PDAC progression *in vivo*. The ultimate goal was to identify differentially regulated candidate genes between lean and obese white adipose tissue, that encoded secreted proteins. With these studies, we aimed to identify potential crosstalk between dysfunctional adipose tissue and PDAC.

2 RESULTS

2.1 3T3-L1 adipocyte conditioned media has pro-tumorigenic effects on PDAC cell lines *in vitro*

2.1.1 3T3-L1 ACM increases the viability and proliferation of Panc02 cells *in vitro*

To investigate the effect of adipocyte-conditioned media (ACM) on PDAC progression *in vitro*, 3T3-L1 cells were used as an *in vitro* model of mouse adipocytes. Panc02 cells were either treated with the supernatant from differentiated adipocytes, or undifferentiated fibroblasts, generated from 3T3-L1 cells. The effects on tumor cell proliferation, and viability were measured by EdU assay, and CCK-8 assay, respectively.

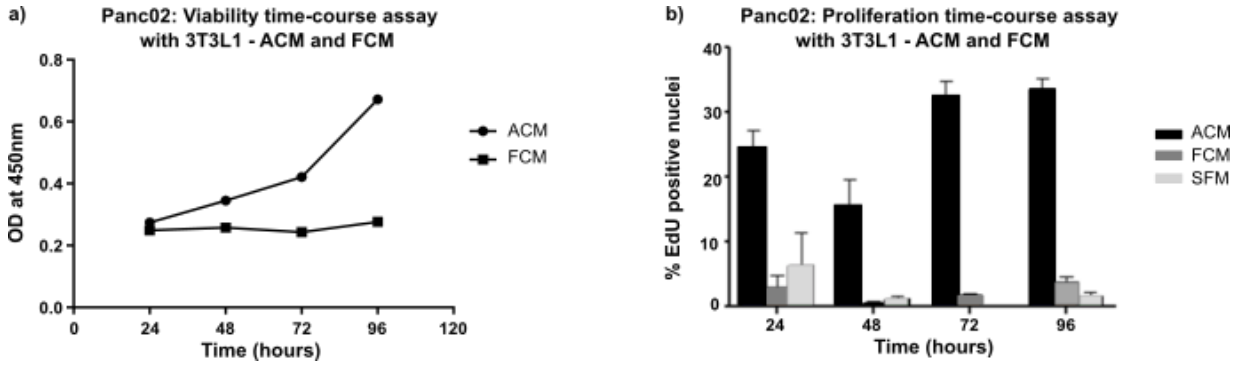

Fig. 7: Viability and proliferation time course assay of Panc02 with 3T3-L1 ACM and FCM. *a) CCK-8 Viability assay b) EdU Proliferation assay. n=4,*

Compared to the fibroblast-conditioned media (FCM), the adipocyte conditioned media (ACM) significantly increased the viability of Panc02 cells, with increasing treatment time (Fig. 7 a). The ACM also increased the proliferation of Panc02 cells all time-points, and the proliferation effects did not increase further after 72 hrs. of treatment with ACM. The serum-free media (SFM) was used as a negative control. We were further interested to investigate the effects of ACM on other tumor characteristics like migration.

2.1.2 Adipocyte conditioned media from 3T3-L1 cells increases the migration of PDAC cell lines *in vitro*

To determine if the ACM affected the migration of PDAC cells, we performed trans-well migration assays. Here, the tumor cells were plated on the upper compartment of a cell permeable membrane, and the conditioned medium (ACM/FCM) from 3T3-L1 cells was placed on the bottom compartment as the chemo-attractant. DMEM with 10% FBS was used as a positive control, and serum-free media (SFM) was used as a negative control. After an incubation period of 16-18 hrs. in the cell culture incubator at

37°C and 5% CO_2, the cells that migrated to the bottom side of the permeable membrane were stained with crystal violet, and quantified manually or using the ImageJ software.

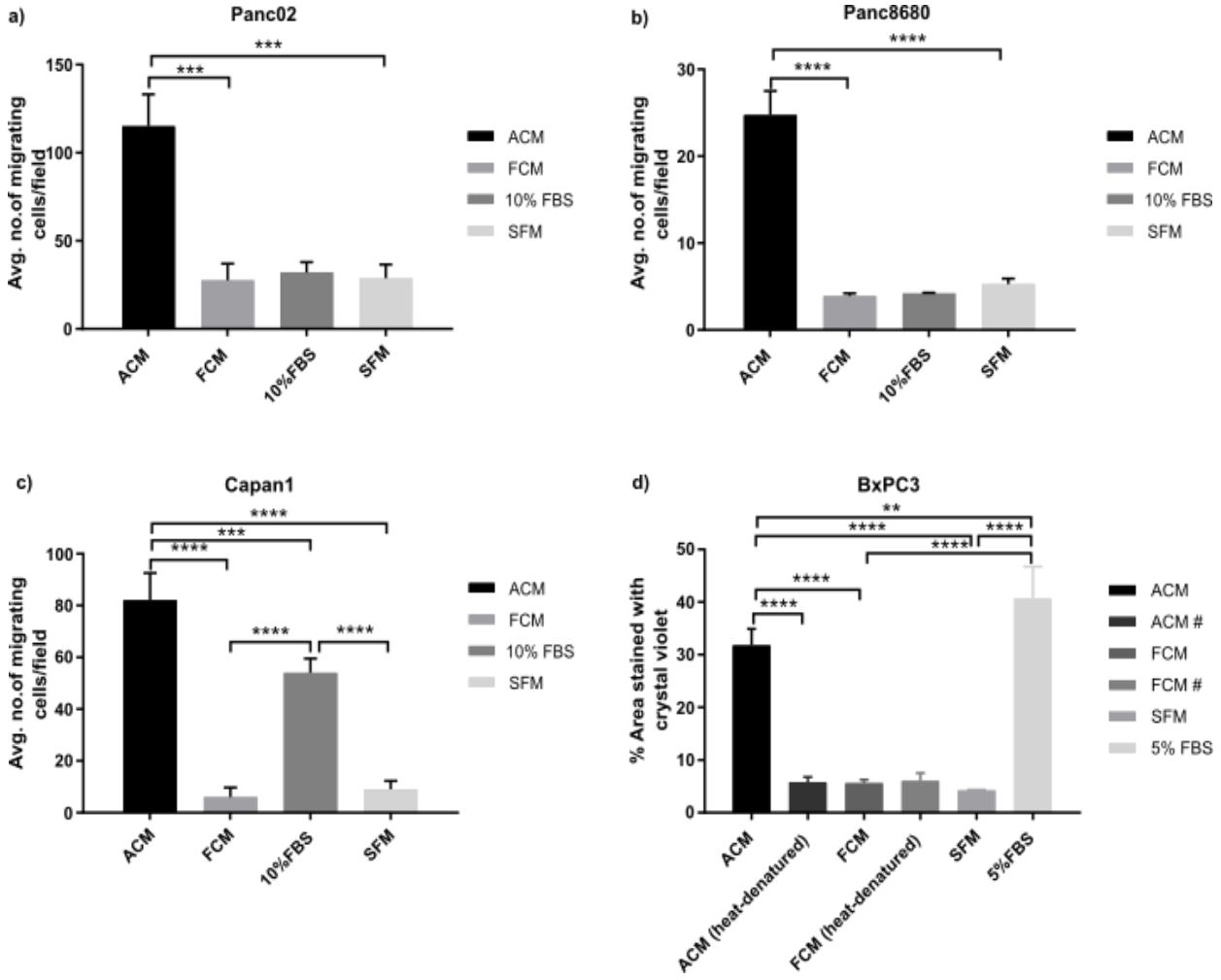

e) Panc02 migration

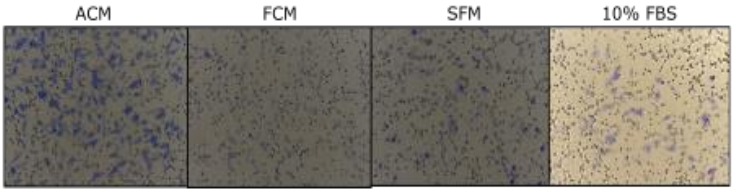

f) Capan1 migration

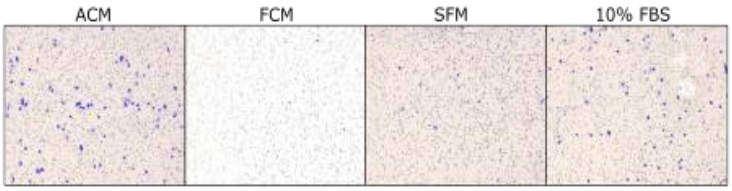

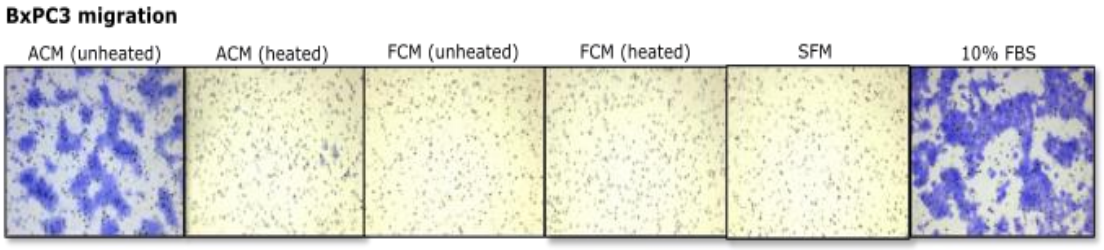

Fig. 8: Trans-well migration of Panc02, Panc8680, Capan1 and BxPC3 with 3T3-L1 conditioned media. *PDAC cell lines were plated on trans-well permeable membranes, and ACM or FCM from 3T3-L1 cells were added on the lower compartments. 10% FBS containing DMEM, and SFM were used as positive and negative controls, respectively. The cells were allowed to migrate for 16-18 hrs. in the cell culture incubator. The cells that migrated to the bottom surface of the membrane were stained and quantified manually for- a) Panc02, b) Panc8680, c) Capan1, and using ImageJ software for d) BxPC3 cells. Microscope image for migration of a) Panc02 f) Capan1 g) BxPC3 with intact and heat-denatured conditioned media. n=4, means ±SEM, *indicates significance.*

The ACM significantly increased the migration of the murine cells: Panc02, and Panc8680 (Fig. 8 a, b, e), and the human cell line Capan1 (Fig. 8 c, f). Compared to the negative control-SFM, only the ACM from the 3T3-L1 cells induced migration, and not the FCM.

For the human PDAC cell - BxPC3, we additionally heat-inactivated the conditioned media. This was performed to evaluate if there were any changes in the migration promoting effects of the 3T3-L1 - ACM upon heat-denaturation. The BxPC3 cells migrate as tightly packed colonies, and are difficult to quantify manually. Therefore, ImageJ software was used to quantify the area of migrating cells. Surprisingly, only the intact, non- heat denatured ACM promoted the migration of BxPC3 cells. However, the heat-inactivated ACM lost its migration promoting effects (Fig. 8 d, g).

Next, we wanted to investigate the effects of 3T3-L1 conditioned media on PDAC tumor invasion *in vitro*. For this we decided to utilize matrigel-coated trans-well membranes as an *in vitro* system.

2.1.3 3T3-L1 adipocyte conditioned media significantly increases the invasion of Panc02 cells

Tumor cell metastasis is a key process for the development of secondary tumors at distant organs. The metastatic cascade is complex, and involves several coordinated and sequential processes. Some of the early steps involved in tumor cell metastasis are: the loss of cell-cell contact to be able to dissociate from the primary tumor site, followed by invasion of the stroma by the secretion of factors/enzymes that help to degrade the basement membrane and the extra-cellular matrix (ECM) components, and the modulation of proteins involved in tumor cell motility/migration.

We hypothesized that adipocyte secreted factors could potentially alter the tumor cell invasiveness. This prompted us to investigate if the ACM from 3T3-L1 cells affected the invasiveness of PDAC cell lines. We performed trans-well invasion assays by plating Panc02 cells on the top part of a matrigel-

coated trans-well permeable membrane, and placed ACM/FCM from 3T3-L1 cells in the bottom compartment, as the chemoattractant. DMEM supplemented with 10% FBS, and SFM were used as positive and negative controls, respectively. Following an incubation time of 24 hrs., the invading cells on the bottom part of the invasion chambers were stained with crystal violet, and counted manually under the microscope.

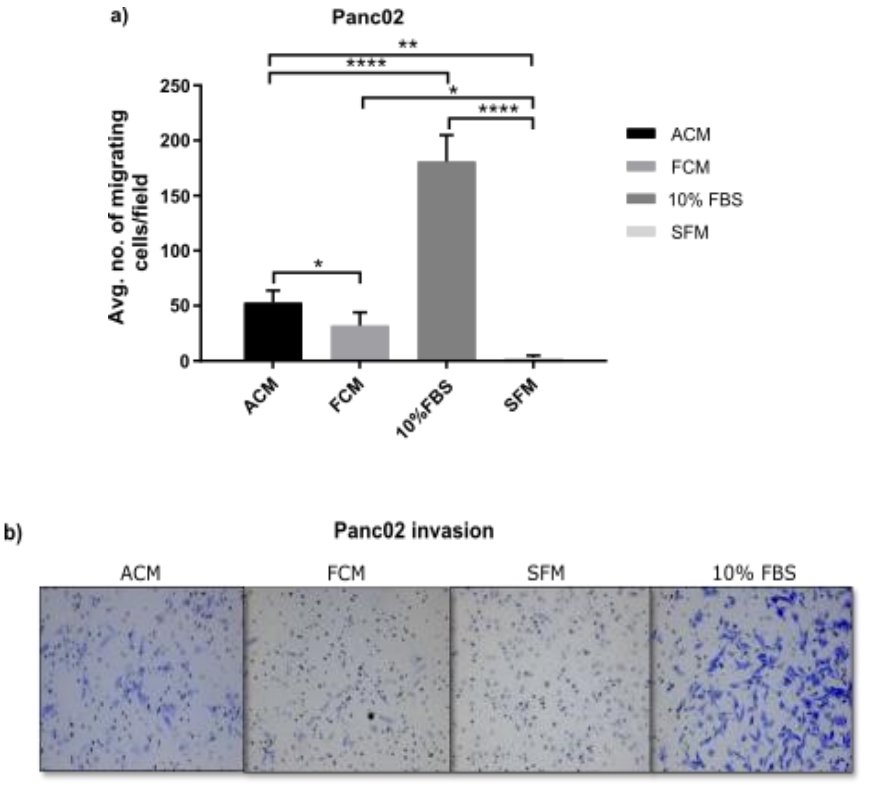

Fig. 9: Trans-well invasion of Panc02 with 3T3-L1 conditioned media. *Panc02 cells were plated overnight on matrigel-coated trans-well invasion inserts, with ACM or FCM from 3T3-L1 cells as the chemo-attractant in the bottom chamber. The invading cells were stained with crystal violet and counted manually after 24 hrs. a) Quantification of invading Panc02 cells b) Microscopic images of invading Panc02 cells.*

The ACM from 3T3-L1 cells significantly increased the invasiveness of Panc02 cells through the matrigel coated membrane, compared to the conditioned media from undifferentiated 3T3-L1 fibroblasts, or the SFM (Fig. 9 a, b).

Based on the above results, we hypothesized that secreted factors from adipocytes have tumor promoting effects on PDAC cell lines *in vitro*. Going forward, we aimed to validate our hypothesis using different *in vivo* mouse models. Above all, we wanted to identify the secreted factors from white adipocytes that could potentially mediate these effects on PDAC cells. Therefore, we decided to employ ATKO (Adipocyte specific Knockout of *Tblr1*) mice, as well as ob/ob and db/db mice, as *in vivo* mouse models of obesity.

2.2 Analysis of subcutaneous Panc02 tumors implanted into wt and ATKO mice

2.2.1 ATKO mice have significantly higher body weight and fat mass compared to wt control mice

We used ATKO mice as an experimental model of MetS. It has been shown before that the ATKO mice have an impaired lipolysis, have hypertrophic adipocytes, and gain more weight upon high-fat feeding [58]. In order to investigate, if the absence of *Tblr1* in the adipose tissue accelerates PDAC progression *in vivo*, we implanted Panc02 cells subcutaneously into the flanks of 12 weeks old- wt and ATKO mice.

Tumor progression was monitored non-invasively by measuring luminescence signal from the SC tumors, using the *in vivo* imaging system (IVIS). We measured the body weight, blood glucose, fat mass, and lean mass of the mice during the entire course of the experiment. The fat mass, and lean mass were determined by placing the mice inside the ECHO MRI system. Finally, the tumor, the abdominal WAT, and the inguinal WAT, were harvested after sacrificing the mice.

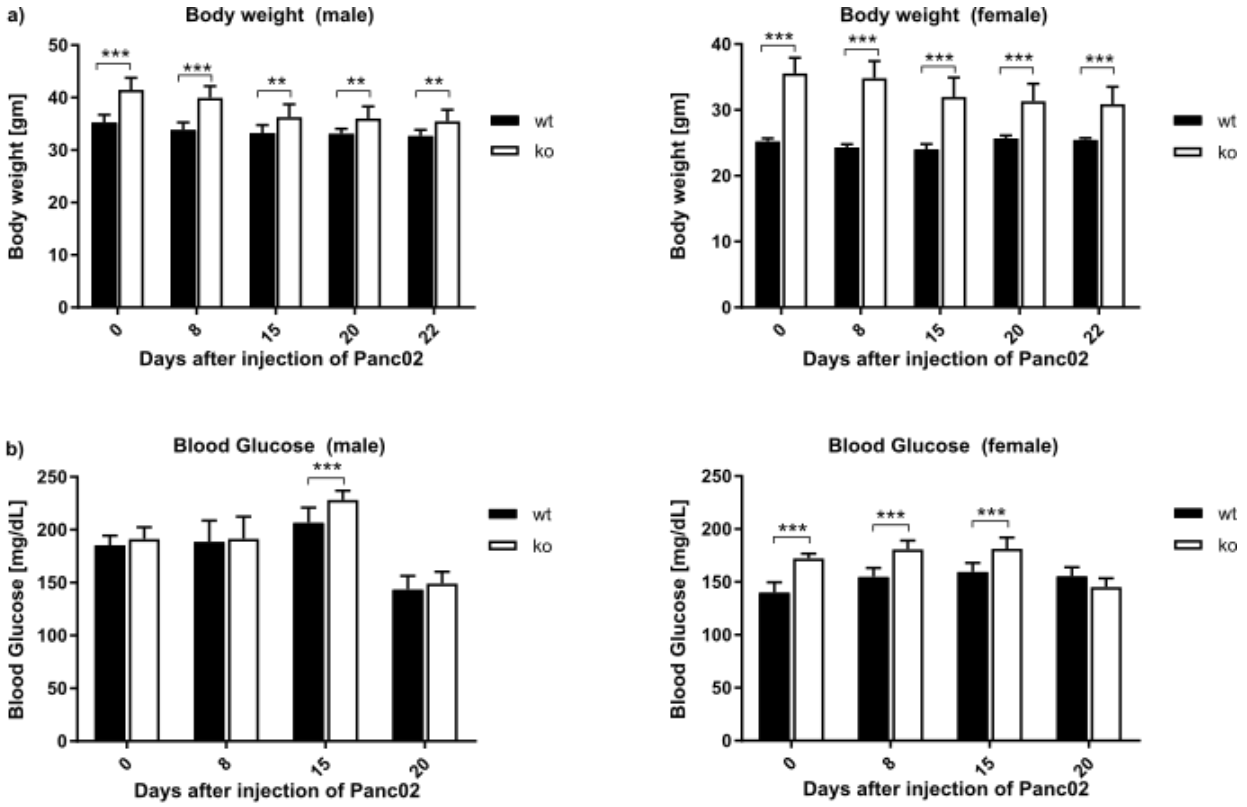

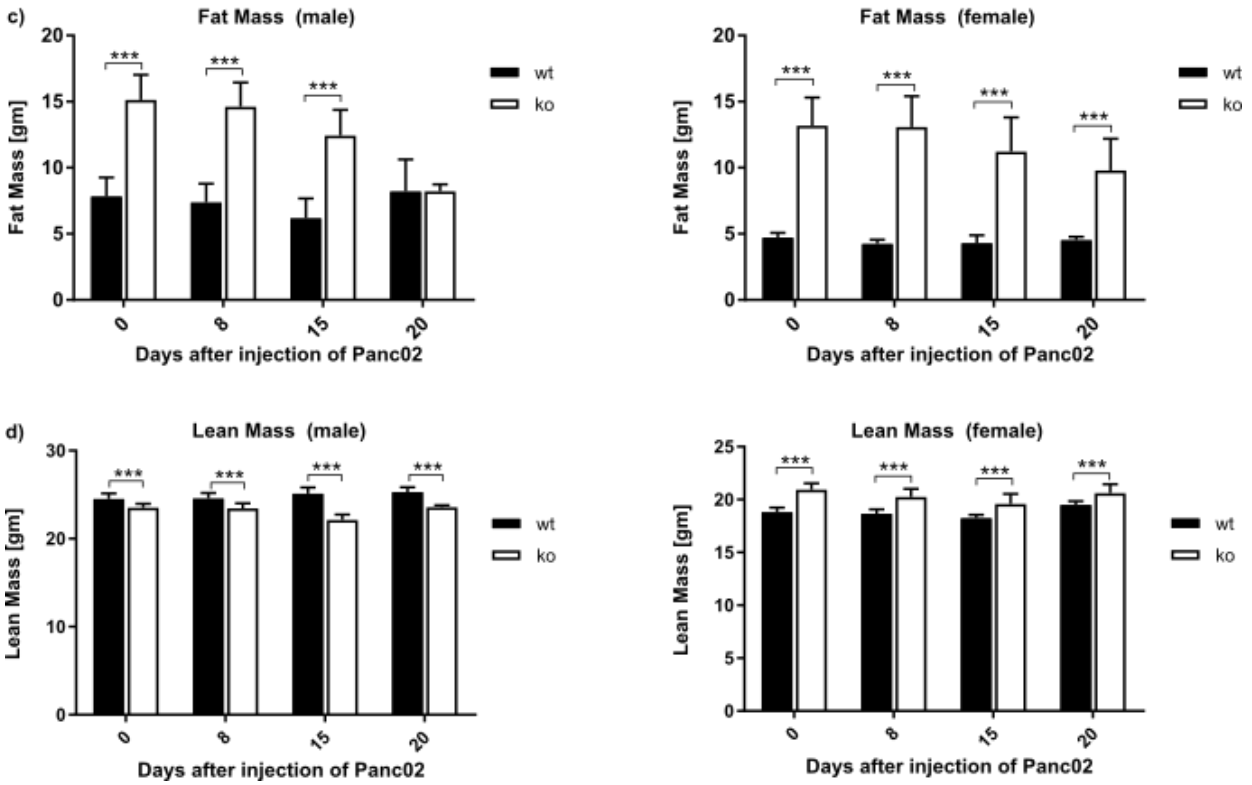

Fig. 10: Body weight, blood glucose, and body composition measurements by ECHO MRI, for wt and ATKO mice*. A) Body weight, b) Blood glucose c) Fat mass, and d) Lean mass, of wt and ATKO mice were measured using weighing scales and ECHO MRI system. n=10, means ±SEM, *indicates significance.*

The ATKO male, and female mice had significantly higher body weights than the wt control mice (Fig. 10 a). There was no significant difference in the blood glucose levels of wt and ATKO male mice, but the ATKO female mice had significantly higher serum glucose levels, than wt mice (Fig. 13 c). In line with the higher body weight, the fat mass was significantly higher, and the lean mass was significantly lower in the ATKO mice, compared to the wt littermates (Fig. 10 c, d).

Next, we performed IVIS measurements to evaluate if the increased body weight and fat mass of the ATKO mice could contribute to greater tumor growth.

2.2.2 Subcutaneous Panc02 tumors grew significantly larger in the ATKO mice

To monitor the tumor progression non-invasively, we measured luminescence output from the luciferase-expressing Panc02 tumors, using the IVIS system. The ATKO and wt mice were intra-peritoneally injected with a luciferin solution, at a dosage of 150 μg/g of body weight, and anesthetized with vaporized isoflurane before placing them inside the IVIS imaging system. Pairs of wt and ATKO mice were imaged simultaneously for a better comparison.

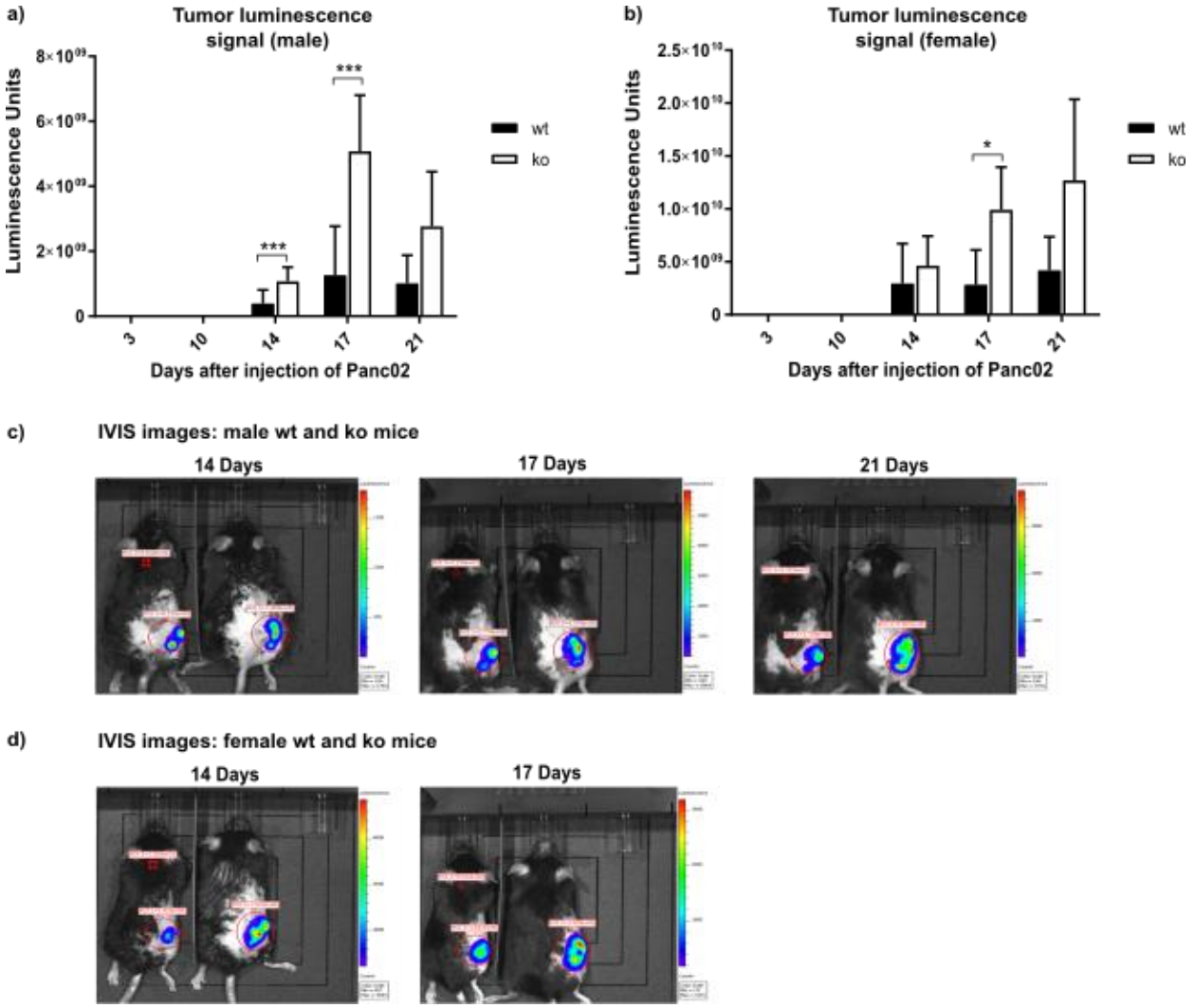

Fig. 11: IVIS measurement of tumor luminescence from male and female wt and ko mice bearing SC Panc02 tumors: *Mice were injected with luciferin (150 μg/g of body weight, 10 μl/g body weight), and anesthetized with vaporized isoflurane before measuring the luminescence signal. Quantification of IVIS luminescence signals for tumors from (a) male wt and ko mice, (b) female wt and ko mice, IVIS images for tumors from (a) male wt and ko mice (d) female wt and ko mice. n=10, means ±SEM, *indicates significance.*

The luminescence signal was significantly higher from the tumors of ATKO male and female mice. As the luminescence measurement is directly proportional to the tumor size, we concluded that the subcutaneous Panc02 tumors were significantly larger in the ATKO mice (Fig. 11 a, b). Furthermore, we wanted to quantify the tumor mass, and the abdominal-, and inguinal- fat mass from wt and ATKO mice.

2.2.3 Tumors, abdominal WAT, and inguinal WAT from ATKO mice weighed significantly more compared to wt mice

In order to quantify the tumor mass, abdominal (ABD) fat mass, and inguinal (ING) fat mass, we weighed the respective tissue explants after sacrificing the mice. The ABD, and ING fat mass from the ATKO mice weighed significantly more in comparison to wt controls (Fig. 12 a, b). In line with the higher luminescence signal from tumors in the ATKO mice, the tumor mass was significantly greater in the ATKO mice, as compared to wt littermates (Fig. 12 c).

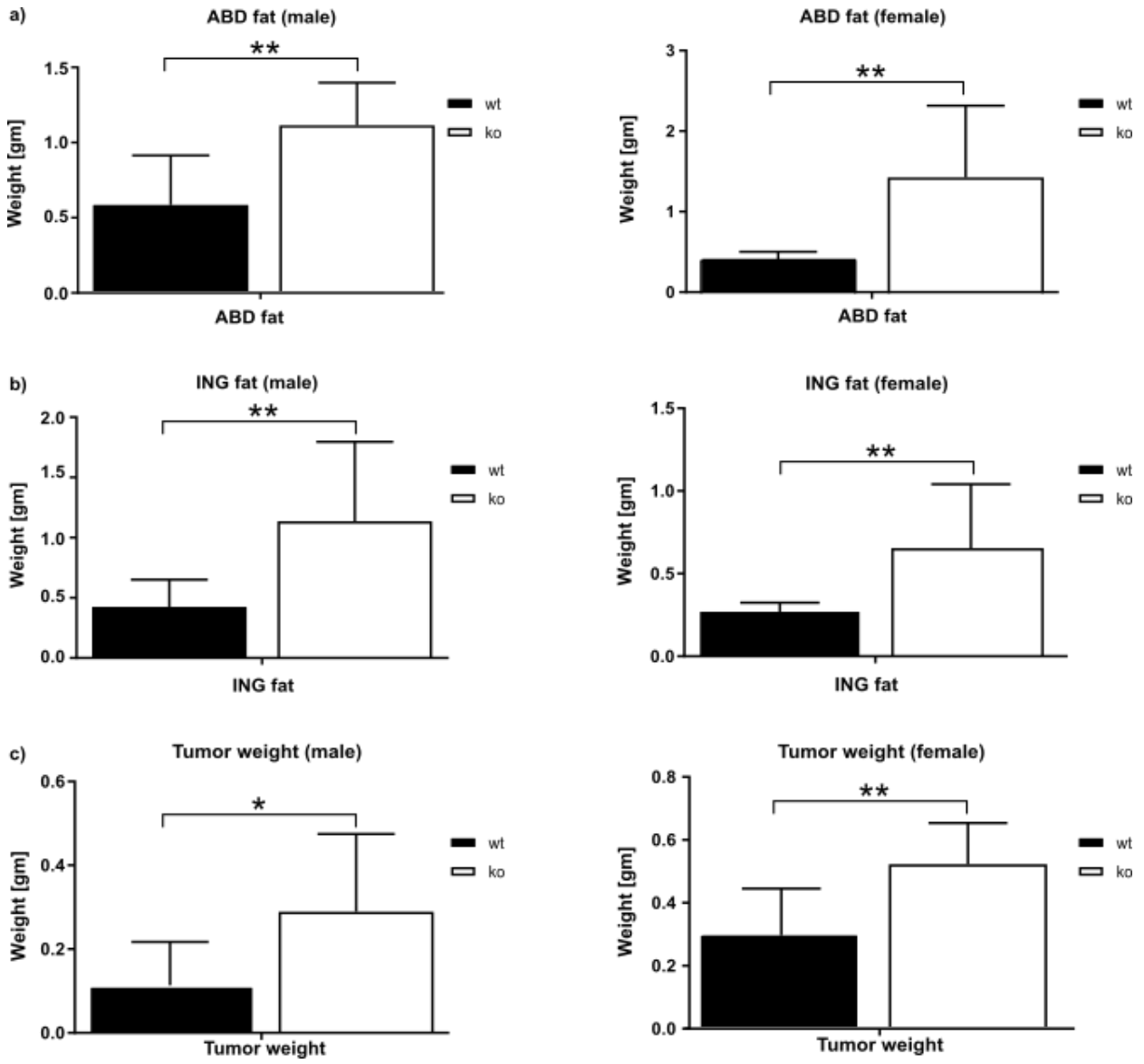

Fig. 12: Tumor, ABD, and ING fat mass from wt and ATKO mice: *Mice were sacrificed after three weeks of tumor implantation and their a) ABD fat mass b) ING fat mass c) tumor weight and d) TG from tumor were measured on a weighing scale.*

We speculated if the higher tumor mass in the ATKO mice could be attributed to a higher fat content within the tumors. Therefore, we decided to quantify the triglyceride contents in the tumors from the wt and ATKO mice.

2.2.4 Triglyceride levels in the tumors of wt and ATKO mice were similar

In order to find out if the triglyceride (TG) content in the tumors contributed to the increased tumor mass in the ATKO mice, we extracted the TGs from the tumors and quantified them. Surprisingly, the TG content was lower in male ATKO mice compared to controls, while there was no significant difference between the females (Fig. 13 a, b).

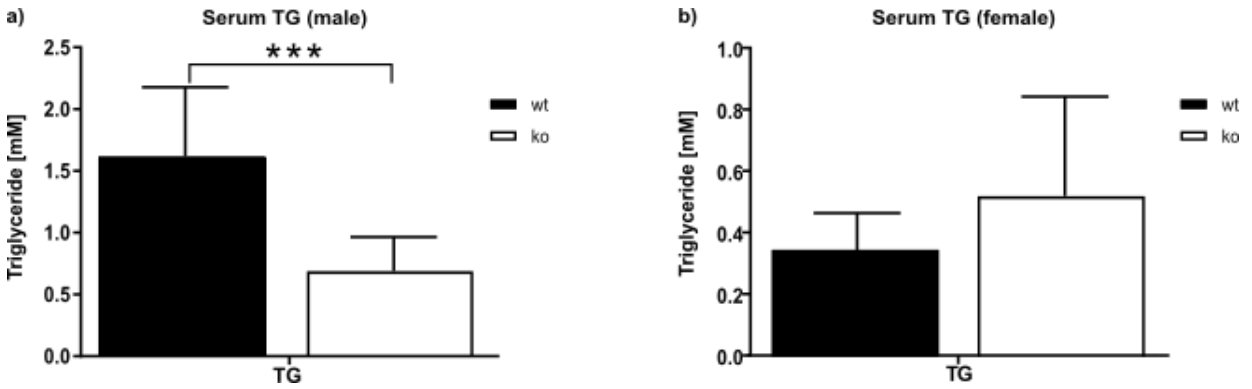

Fig. 13: TG measurement from SC tumors. *Quantification of tumor TG content from male (a), and female (b) wt and ATKO mice. n=10, means ±SEM, *indicates significance.*

As the TGs from the tumors were not consistently higher in the tumors from both male and female ATKO mice, we rationalized that TG could not be a reason for the higher tumor mass in the ATKO mice. Therefore, we performed histological analysis to investigate the cause of the greater tumor size in the ATKO mice. We reasoned that the tumors could be larger in the ATKO mice due to an increased adipocyte infiltration, or increased proliferation. To this end, we decided to perform H and E-, and Ki67- staining on the tumor paraffin sections.

2.2.5 H and E- staining of subcutaneous Panc02 tumors from wt and ATKO mice did not show significant differences

In order to investigate if adipocyte infiltration into tumors could be a contributing factor for the greater tumor mass observed in ATKO mice, we performed H and E- staining on the tumor paraffin sections. We did not observe any striking differences between the tumors from the wt and ATKO mice upon H and E- staining (Fig. 14). Also, we did not observe any particularly striking differences in the tumor adipocyte content between the treatment groups, by visually analyzing the H and E- stained sections under the microscope (Fig. 14).

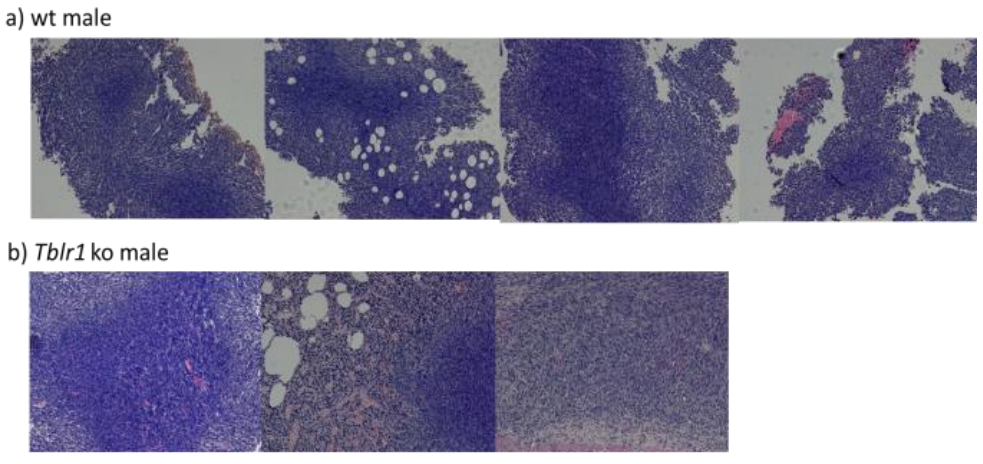

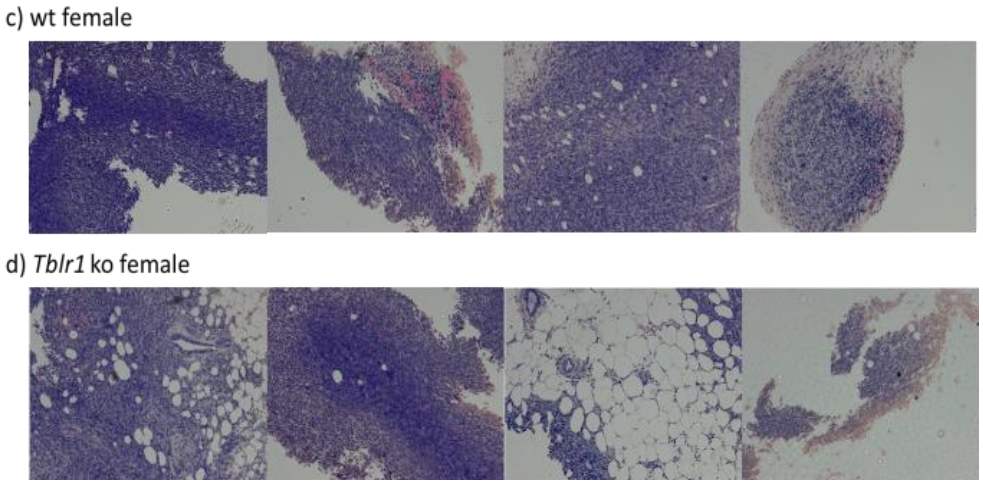

Fig. 14: H and E- staining of Panc02 SC tumor sections from wt and ATKO mice. *(a) Male wt and ATKO mice, (b) female wt and ATKO mice.*

We further wanted to investigate if the greater tumor size in the ATKO mice could be due to adipocyte infiltration into the tumors implanted in the ATKO mice.

2.2.6 Ki67 staining from wt and ATKO mice did not show any striking differences in tumor cell proliferation

To investigate if there were differences in proliferation between wt and ATKO tumors, we performed Ki67 staining on tumor paraffin sections. The Ki-67 protein is localized in the nucleus of a cell during the G_1, G_2, S, and M phase of the cell cycle [64]. It is not present in the cells at G_o phase, or in the resting cells [64]. Therefore, Ki-67 protein is routinely used as a proliferation marker, and anti-Ki67 antibodies are used to detect Ki-67 expression immuno-histochemically, in the paraffin embedded tissue sections.

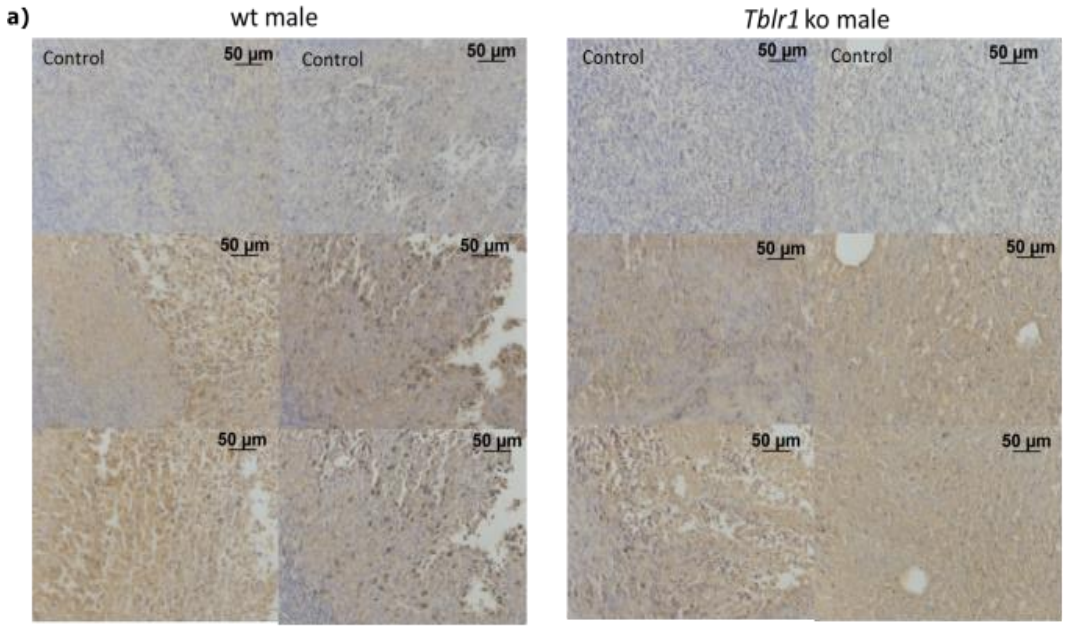

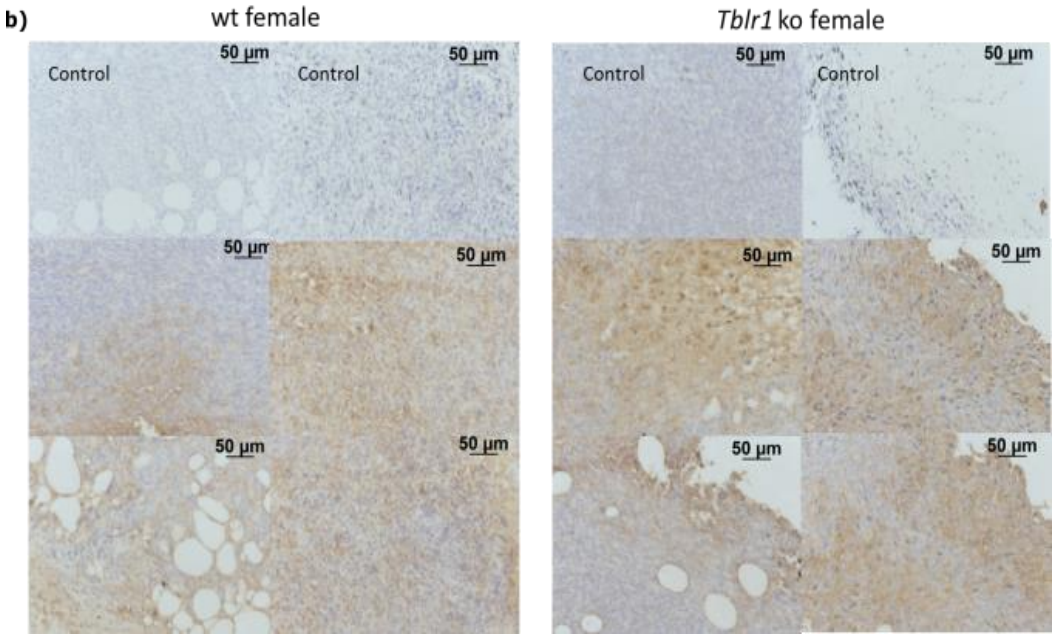

Fig. 15: Ki67 staining of SC Panc02 tumors from wt and ATKO mice. *(a) wt and ATKO males (b) wt and ATKO females*

As can be observed from the staining depicted in Fig. 15, there was no significant difference in the Ki-67 staining between SC Panc02 tumors grown in wt and ATKO mice. Therefore, we could not detect any difference in the tumor proliferation between SC Panc02 tumors in wt and ATKO tumors.

Going forward, we wanted to identify target genes that could be differentially regulated between tumors from wt and ATKO mice, which could explain the higher tumor mass in the ATKO mice.

2.2.7 Gene expression analysis from tumors grown in wt and ATKO mice did not reveal any significantly differentially regulated candidate genes

We performed microarray analysis to identify potential candidate genes, that could be differentially regulated between SC Panc02 tumors grown in the wt and ATKO mice. By doing so, we wanted to determine potential underlying genes, and pathways contributing to larger tumor growth in the ATKO mice that we observed. Three samples were tested per treatment group.

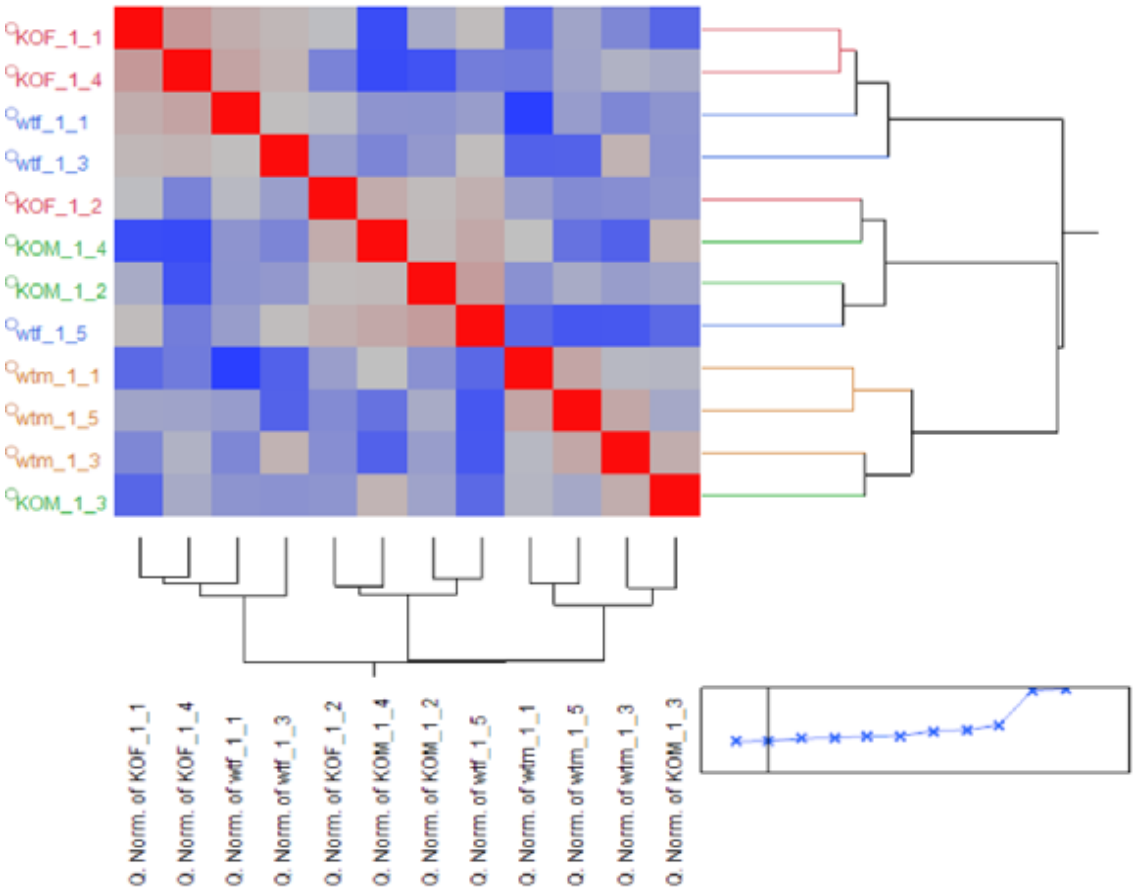

Fig. 16: Heat map for Microarray samples from wt and ATKO SC Panc02 tumors*. n=3 per condition.*

Unfortunately, samples from the same treatment group did not cluster together due to high standard deviations (Fig. 16). Based on a p-value cut off of < or = 0.05 for significance, the microarray analysis could not identify any differentially regulated genes between wt and ATKO tumors.

We decided to focus on *in vitro* trans-well assays, using conditioned media from wt or *Tblr1* kd adipocytes, to establish a link between PDAC and *Tblr1*.

2.3 Trans-well assay of Panc02 with wt or Tblr1 knockdown ACM

2.3.1 Adenovirus mediated knockdown of Tblr1 in 3T3-L1 adipocytes

To investigate the effect of ACM from *Tblr1* kd adipocytes on Panc02, 3T3-L1 adipocytes were infected with adenovirus encoding an shRNA *Tblr1*. The cells were differentiated until 10 days, followed by serum starvation for 4 hours, and the conditioned media was harvested. The knockdown was confirmed both at the mRNA, and the protein levels by qPCR and western blot analysis, respectively (Fig. 17).

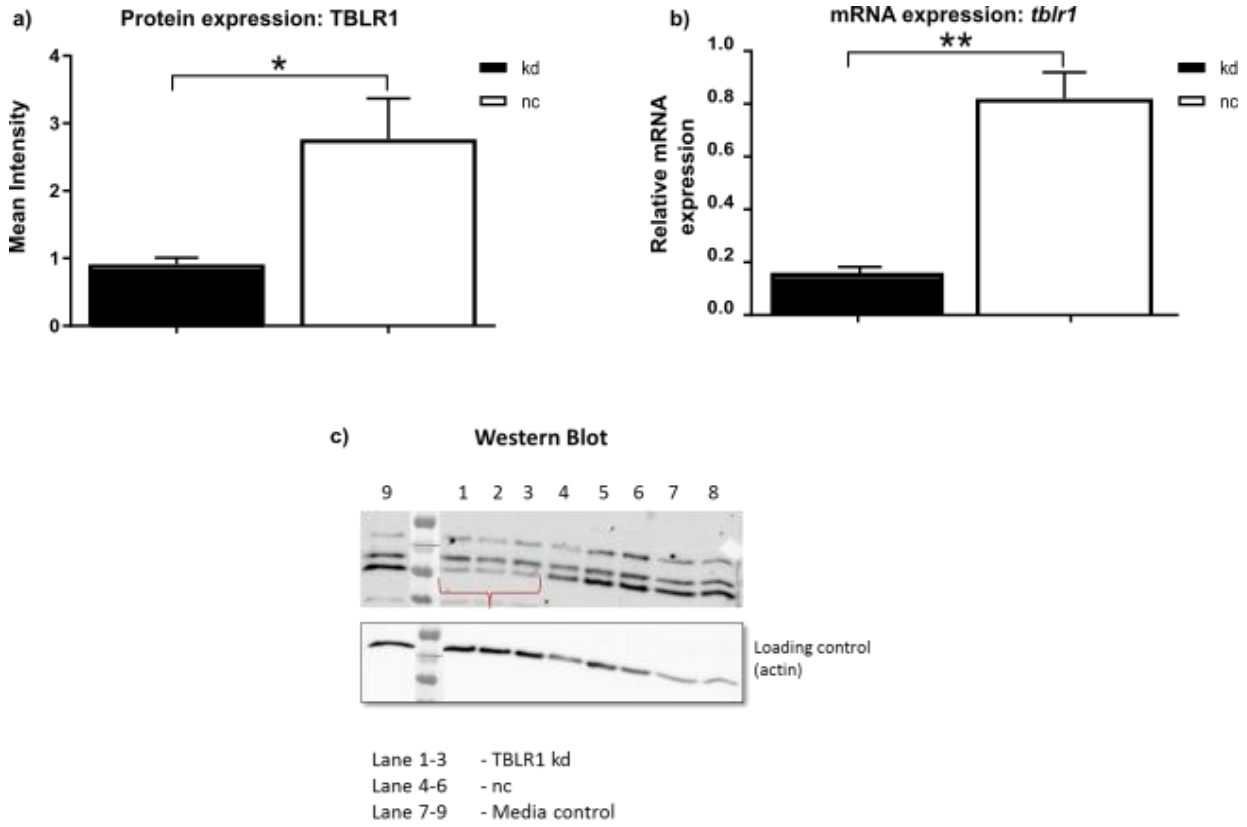

Fig. 17: Adenovirus mediated knockdown of Tblr1 in 3T3-L1 adipocytes. *a) TBLR1 protein expression quantification b) Relative mRNA expression of Tblr1 measured by qPCR, and c) Western blot image showing TBLR1 kd. n=3, means ±SEM, *indicates significance.*

We generated conditioned media from control and *Tblr1* kd adipocytes, to utilize them as a chemo-attractant in trans-well assay with Panc02.

2.3.2 Viability and proliferation of Panc02 was not significantly affected upon treatment with Tblr1 kd conditioned media from 3T3-L1 adipocytes

To investigate if the ACM from *Tblr1* kd - 3T3-L1 cells had an impact on Panc02 cell viability and proliferation, we performed CCK-8 assay, and EdU assay, respectively. We treated Panc02 cells with the respective conditioned media for different time-points.

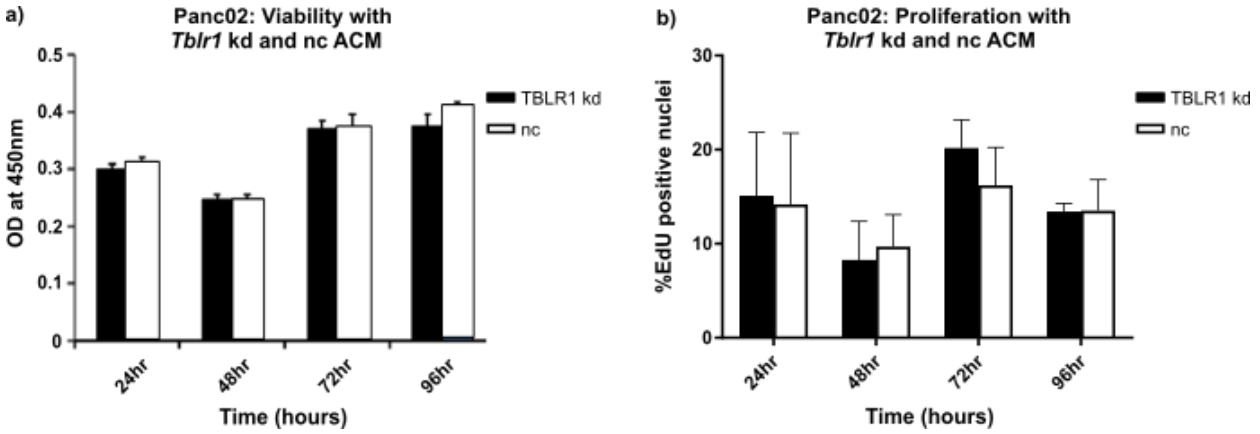

Fig. 18: Treatment of Panc02 cells with 3T3-L1- nc or Tblr1 kd ACM a) Viability by CCK-8 assay b) Proliferation by EdU Assay. *n=4, means ±SEM.*

There were no significant differences in viability, as well as proliferation of Panc02 cells at any given time-point of treatment with the control or the *Tblr1* kd conditioned media from 3T3-L1 adipocytes (Fig. 18).

We previously demonstrated that ACM from differentiated 3T3-L1 cells had a strong impact on PDAC cell proliferation, viability, migration, and invasion in vitro, which could be mediated by factors secreted from adipocytes. Hence, we decided to perform gene expression analysis from the WAT of a distinct congenital model of obesity, to identify differentially regulated genes between lean and obese adipose tissue mediating these effects.

2.3.3 Microarray analysis from the inguinal WAT of wt and db/db mice reveals significantly regulated genes, including such which encode secreted proteins

Microarray gene expression analysis was performed from the subcutaneous inguinal WAT of wt and db/db tumor bearing mice. The db/db mice lack the receptor for leptin (*Lepr*), and are a well-accepted monogenic mouse model of obesity. We observed that the subcutaneous Panc02 tumors grew significantly larger in the db/db mice, and therefore we hypothesized that secreted factors from the WAT of the db/db mice could potentially play a pro-tumorigenic role.

With this analysis, we aimed to identify candidate genes that were differentially regulated in WAT of wt and db/db mice and hence could serve as a link between obesity and PDAC.

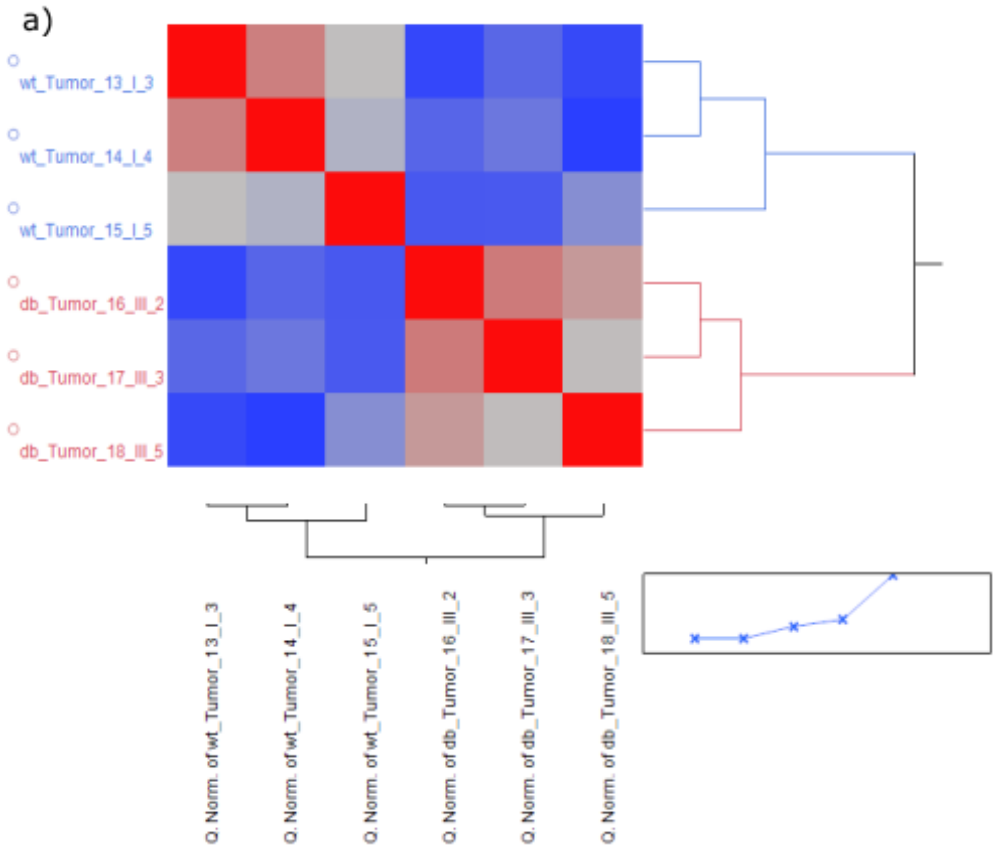

Fig. 19: Microarray from the WAT of wt and db/db, SC Panc02 tumor bearing mice: *A) Heat map distribution for Microarray samples b) One Way ANOVA distribution.*

Although a total of 195 genes were significantly differentially regulated between the iWAT of wt and db/db mice, we were particularly interested to identify such candidate genes which encoded for secreted proteins. Based on the above criteria, five candidate genes were identified to be significantly differentially regulated:

1. *Lep* (leptin)	Significantly upregulated in db/db iWAT
2. *Lcn2* (Lipocalin 2)	Significantly upregulated in db/db iWAT
3. *Lbp* (Lipo-polysaccharide binding protein)	Significantly upregulated in db/db iWAT
4. *Saa3* (Serum amyloid a 3)	Significantly upregulated in db/db iWAT
5. *Angpt1* (Angiopoietin 1)	Significantly downregulated in db/db iWAT

We aimed to determine if the above candidates were mediating their effects from the WAT on PDAC cells. For evaluating this, we decided to perform in vitro assays of PDAC cells following treatment with respective candidate in the form of conditioned medium. In order to generate such conditioned media, these candidates were to be overexpressed (OE) using plasmid OE constructs in human HEK293A cells, and knocked-down using siRNAs in murine 3T3-L1 cells.

2.3.4 Overexpression of candidate genes in HEK293A cells

HEK293A cells were transfected with plasmid constructs to overexpress the candidate genes. We confirmed the overexpression of the candidate genes by qPCR (Fig. 20). Conditioned media enriched with secreted candidates was generated, by serum starving the HEK293A cells transfected with OE plasmid constructs, for 4 hours. HEK293A cells transfected with *Gfp* plasmid construct was used to generate control conditioned media.

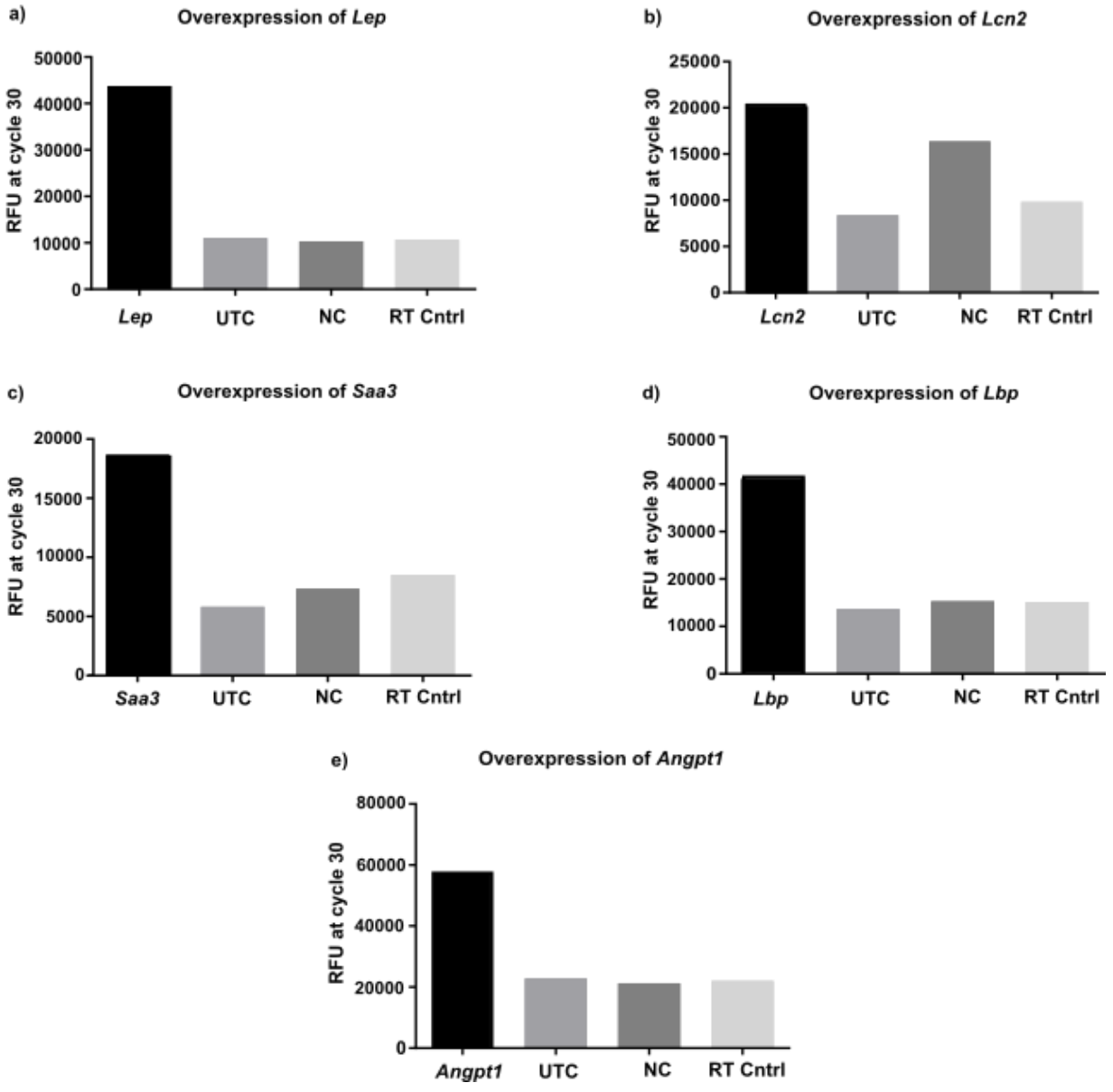

Fig. 20: qPCR data depicting the overexpression of candidate genes in HEK293A cells.

Next, we performed viability and migration assays of PDAC cells with candidate OE-conditioned media from HEK293A cells. With such read-outs we aimed to investigate the potential effects of the candidates on PDAC tumorigenesis *in vitro*.

2.3.5 Migration of Panc02 with candidate overexpression-conditioned media

In order to identify if any of the overexpressed candidates affected the migration of Panc02 cells, we serum starved the HEK293A cells that were transfected with OE constructs *for Lep, Lcn2, Lbp, Saa3,* and *Angpt1* for 4 hours and collected the CM. The CM was used as a chemo-attractant for the trans-well migration assay and Panc02 cells were plated on the top part of the trans-well permeable membranes, and allowed to migrate for 16-18 hrs. in the cell culture incubator.

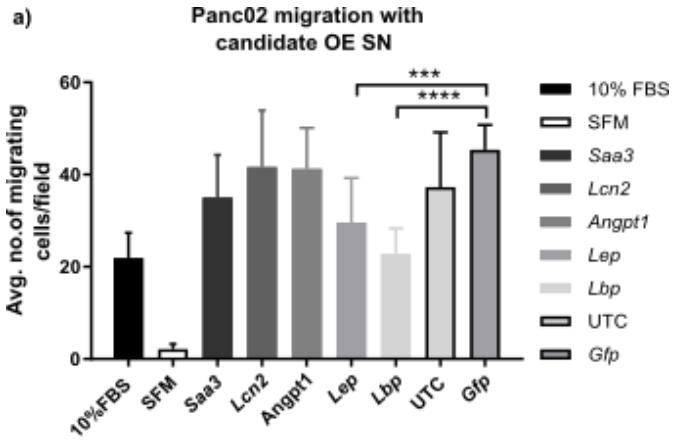

Fig. 21: Trans-well migration of Panc02 with candidate overexpression-conditioned media from HEK293A cells.

There was no significant effect of any of the candidate OE-CM on Panc02 migration. The control supernatant with *Gfp* overexpression induced the migration of Panc02 cells as well (Fig. 21). Also, we did not see any effect of the candidate OE-CM on Panc02 proliferation, and viability (data not shown).

As we did not see any effect of candidate OE-CM on PDAC cell proliferation, and viability, we decided to use alternate approach and perform transient knockdown of candidate genes in mature 3T3-L1 adipocytes using siRNA. The knockdown-CM was to be generated from the siRNA transfected 3T3-L1 cells, to be used later for assays with Panc02 cells.

2.3.6 Knockdown of microarray candidates in mature 3T3-L1 adipocytes

We performed transient knockdown of candidate genes in 3T3-L1 adipocytes by transfecting them with multiple siRNAs on day 9 of differentiation. We then changed media on day 10, serum starved the adipocytes on day 12 for 4 hrs., and collected the respective knockdown conditioned media on day 12. We performed qPCR analysis to identify the siRNA construct that gave the best knockdown (Fig. 22).

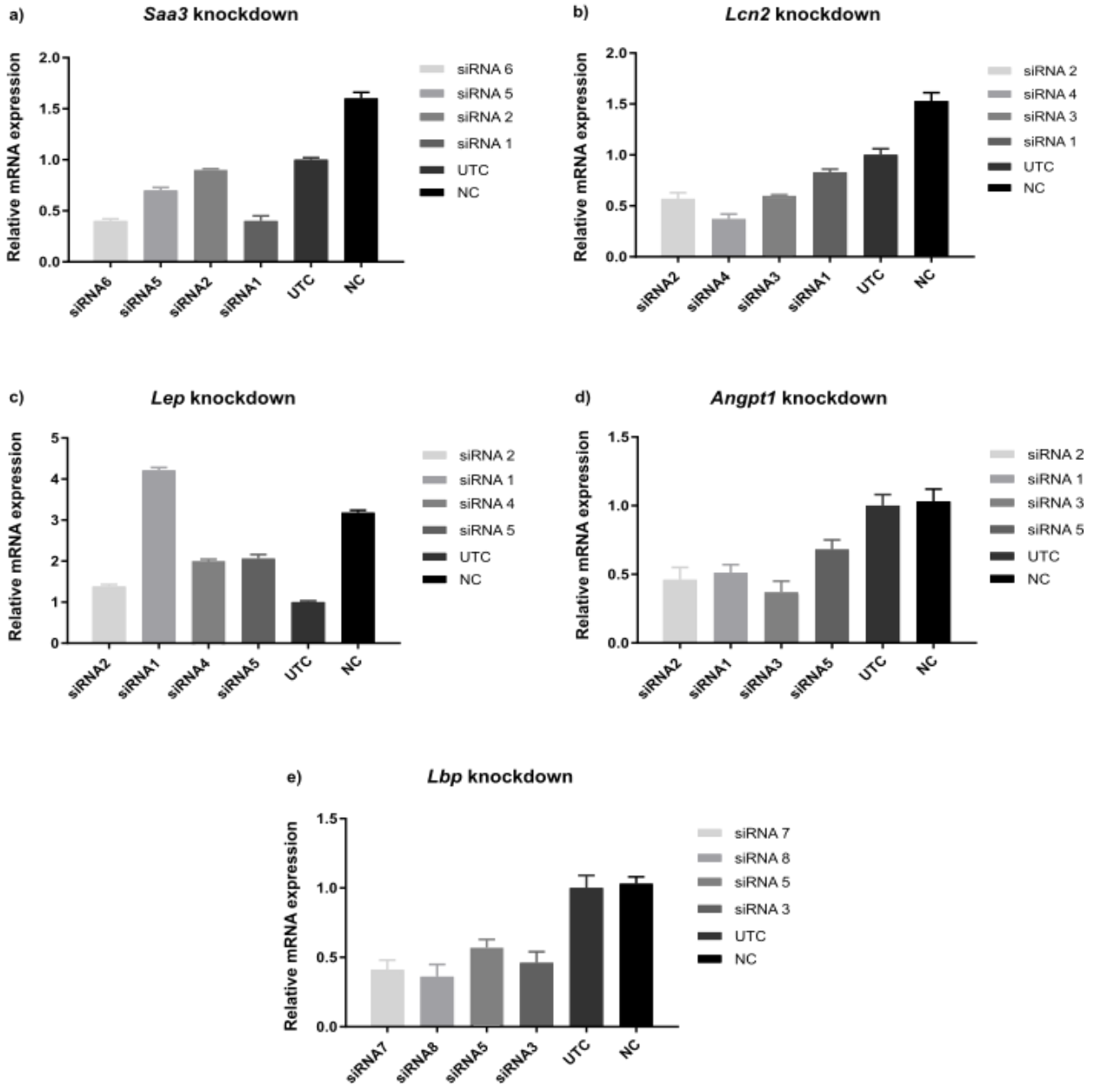

Fig. 22: qPCR data showing the knockdown of candidate genes in mature 3T3-L1 adipocytes. *3T3-L1 cells were transfected on day 9 of differentiation with siRNAs against candidate genes, and the media was changed on day 10, and knockdown condition media was collected 48 hours later on day 12, after serum staving cells for 4 hrs.*

There was no significant effect of any of the knockdown-CM on Panc02 migration, proliferation, and viability (data not shown).

As we did not see any effect of OE as well as kd conditioned media treatments, we decided to use recombinant candidate proteins instead to evaluate their effects on PDAC cell line viability, proliferation, and migration.

2.3.7 Viability, and migration of PDAC cells with recombinant candidate proteins

We treated PDAC cell lines with different concentrations of recombinant candidate proteins, and performed viability, and migration assays. None of the candidate proteins had any effect on the proliferation, and migration of cell lines that we tested (data not shown). However, we found that recombinant leptin (LEP) increased the viability of Panc02 and BxPC3, compared to serum free media (SFM) (Fig. 23).

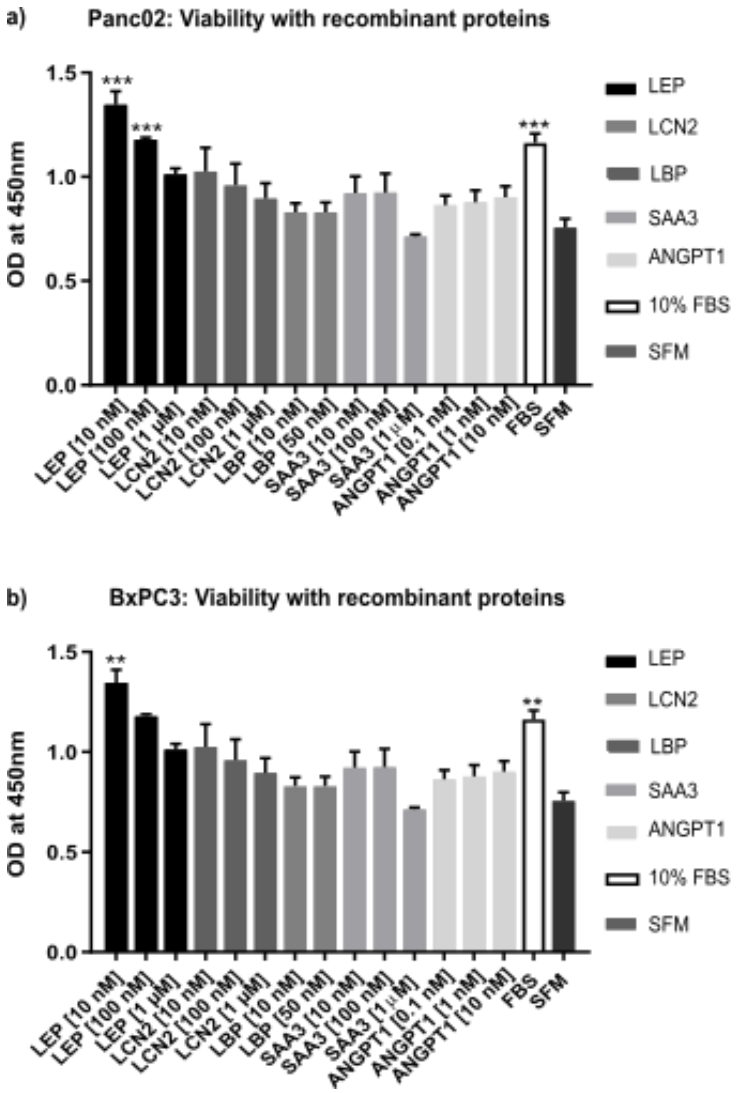

Fig. 23: Viability of Panc02 and BxPC3 with recombinant candidate proteins. *a) Panc02, and b) BxPC3.*

Leptin was the primary candidate that affected the viability of PDAC cell lines tested above. As PDAC forms a solid tumor mass *in vivo*, we wanted to investigate the effect of recombinant candidates on 3-dimensional spheroid invasion *in vitro*.

2.4 Recombinant leptin increases the invasiveness of tumor 3D spheroids, and chemo-resistance of PDAC cell lines to gemcitabine

2.4.1 Leptin increases the invasiveness of BxPC3 spheroids through collagen I matrix

Traditionally, anti-cancer drugs were screened for their *in vitro* potency against tumor cells, cultivated as 2-dimensional (2D) cultures in cytotoxicity assays [65]. However, several of them with great efficacy against tumor cells in the 2D monolayer cultures *in vitro*, have failed in clinical trials [66], [67]. Although, 2D monolayer cultures are an invaluable research tool, they do not reflect the complexity, and heterogeneity of an *in vivo* tumor [65]. Tumors grow as a closely packed 3-dimensional (3D) mass *in vivo*. Therefore, 3D spheroid cultures of tumor cell lines are a better representative of the *in vivo* tumors [65].

In order to investigate the effect of recombinant LEP on 3D spheroid cultures of PDAC cells, we generated spheroids of BxPC3, and Panc8680 by the hanging drop method. The spheroids were carefully placed within collagen I matrix in 96 well plates. Throughout the procedure, recombinant LEP was present in the cell culture media/collagen matrix at specific concentrations as indicated below. The spheroids were imaged at different time-points with a microscope to measure the area of the spheroid invasion.

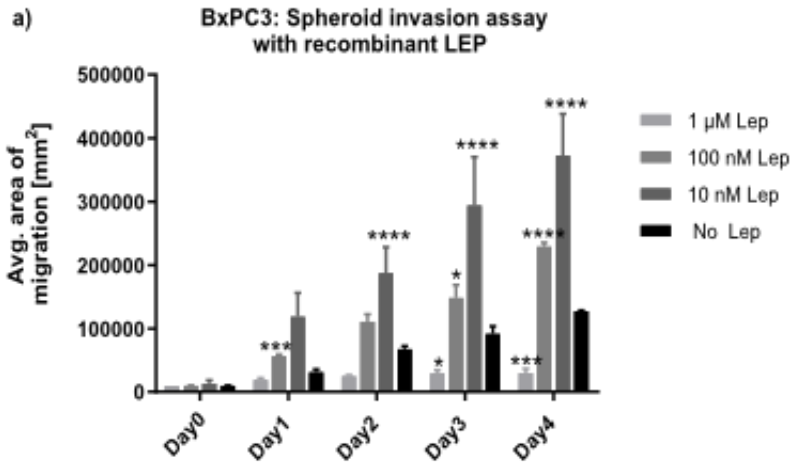

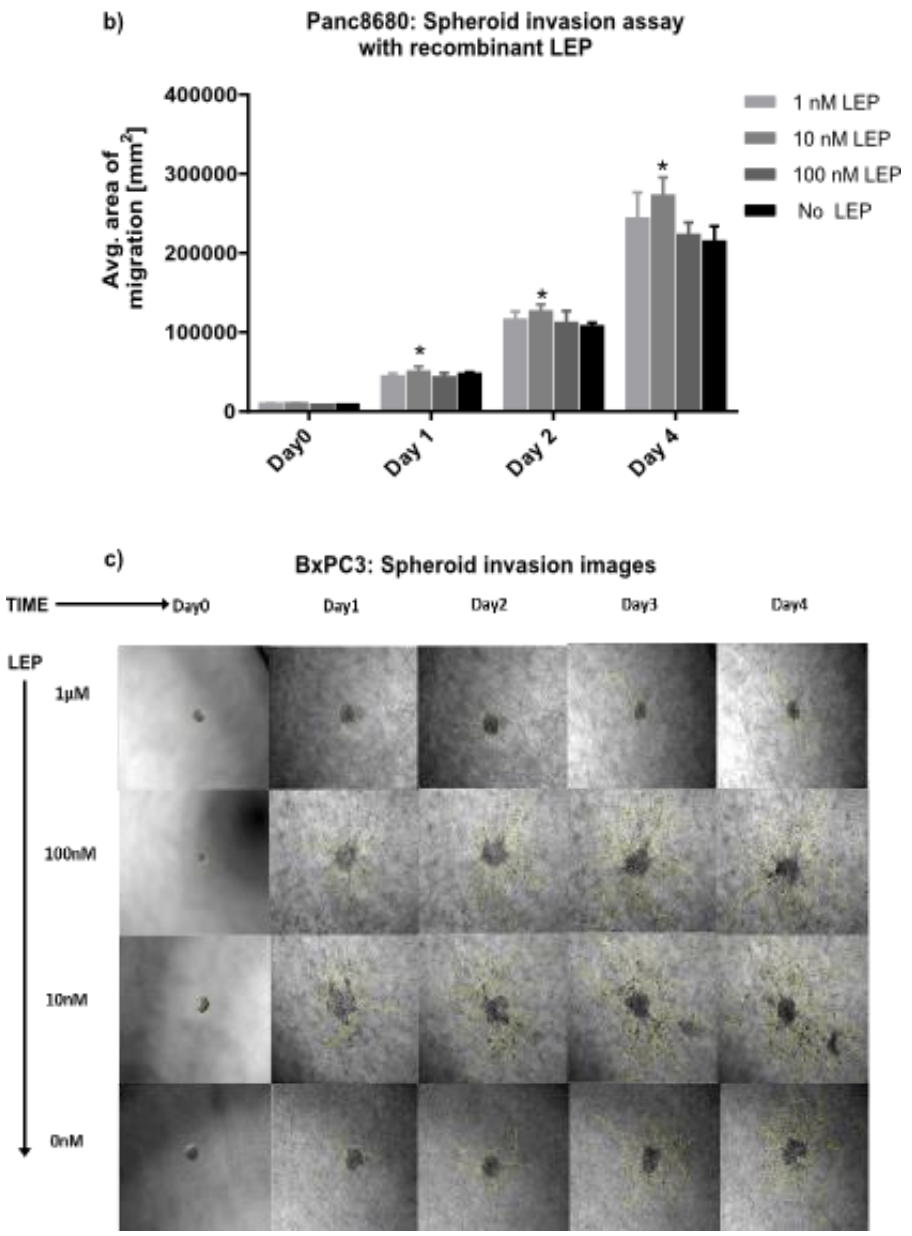

Fig. 24. Effect of recombinant LEP on BxPC3, and Panc8680 spheroid invasion through collagen I matrix. *BxPC3, and Panc8680 spheroids were generated by hanging drop method, and transferred into collagen I matrix. Different concentrations of LEP was added, and the spheroid area was calculated from microscopic images at different time points. Quantification of the area of spheroid invasion of a) BxPC3 and b) Panc8680. c) Microscopic images of BxPC3 spheroids in collagen I matrix after treatment with different concentrations of LEP.*

Recombinant LEP at a concentration of 10 nM, significantly increased the invasion of BxPC3, and Panc8680 spheroids through collagen I matrix (Fig. 24). We therefore, decided to focus on the role of LEP based on its effects on viability, and invasion of PDAC cell lines.

Gemcitabine is the primary chemotherapeutic for treating pancreatic cancer. It is a nucleoside analog, with a H-atom being replaced by a F-atom at the 2’ carbon of deoxycytidine. As chemo-resistance to gemcitabine is a major issue in the treatment for PDAC that affects the disease prognosis, we wanted to evaluate if leptin affected the chemo-resistance of PDAC cell lines to gemcitabine.

2.4.2 Recombinant leptin significantly increases the viability and chemo-resistance of PDAC cell lines in vitro

Chemo-resistance is a huge problem in pancreatic cancer. Gemcitabine is the standard chemotherapy administered to treat PDAC. We therefore, wanted to investigate if recombinant leptin treatment affected PDAC sensitivity to gemcitabine *in vitro*. Tumor cell viability and proliferation were measured after treating PDAC cell lines with LEP and gemcitabine.

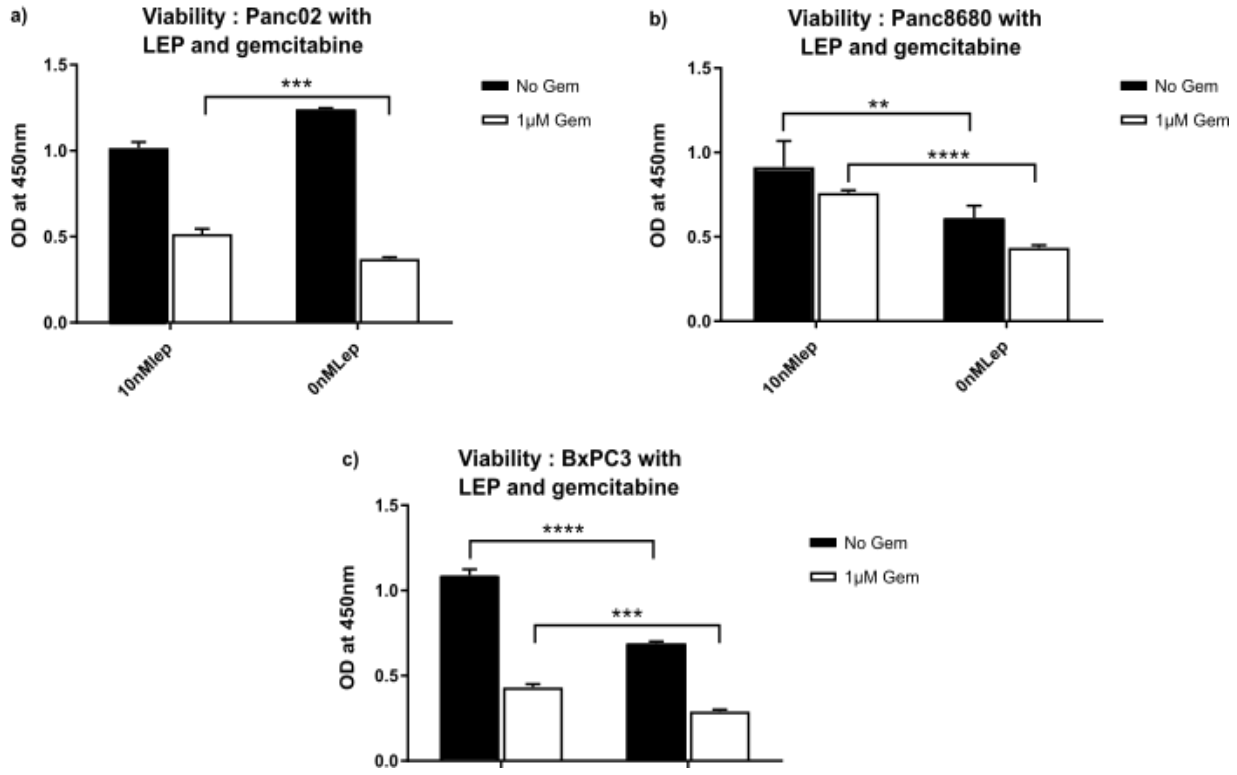

Fig. 25: Viability and chemo-resistance of PDAC cell lines after recombinant leptin treatment, measured by CCK-8 assay. *PDAC cell lines were plated on 96-well plates on day1, and allowed to attach overnight. LEP was added on the following day2, and 1 µM gemcitabine was added on day 3. The viability measurement was performed with CCK-8 reagent for a) Panc02 b) BxPC3 c) Panc8680.*

Recombinant LEP treatment significantly increased the viability and chemo-resistance of the PDAC cell lines: Panc02, Panc8680, and BxPC3 after treatment with gemcitabine (Fig. 25).

We found that recombinant LEP strongly affected the *in vitro* viability-, spheroid invasion-, and chemo-resistance to gemcitabine-, of distinct PDAC cell lines. Going forward, we wanted to investigate the progression of subcutaneous Panc02 tumors in mouse models of obesity with an impaired leptin signaling.

2.5 PDAC progression in congenital mouse models of obesity: ob/ob and db/db mice

2.5.1 Experiment plan for study of Panc02 tumor progression and chemo-sensitivity to gemcitabine in distinct monogenic mouse models of obesity: db/db and ob/ob mice

We performed subcutaneous Panc02 tumor implantations in wt, db/db, and ob/ob mice to investigate if the tumors progressed at different rates in these mice, and responded differently to gemcitabine treatment, depending on the *in vivo* leptin signaling. The db/db mice harbor a glycine to threonine mutation in the *Lepr* gene, which leads to a non-functional form of the long form of *Lepr*: Ob-Rb [68]. The mice homozygous for the mutation become markedly obese by three to four weeks after birth, have hyperinsulinemia by two weeks of age, and display polyphagia, polydipsia, polyuria, and have excess circulating leptin due to impaired leptin signaling at the cellular level. The ob/ob mice on the other hand, have a non-sense mutation in the *ob* gene encoding leptin. This mutation converts an arginine residue to a stop codon, leading to a non-functional and truncated protein [68]. Homozygous mutant ob mice gain significant weight compared to the control mice, and exhibit polyphagia, hyperinsulinemia, hyperglycemia, and suffer from reduced fertility. Both db/db, and ob/ob mice are well characterized congenic mouse models of obesity.

The experiment was performed as shown in the schematic below (Fig. 28). We subcutaneously injected 100,000 Panc02 cells per mouse, into the right flanks of all mice (20 mice/genotype). Once the tumors became palpable, half of the mice per genotype were treated with gemcitabine at 20mg/kg dose, on alternate days. The other half were treated with the vehicle, i.e. PBS. The tumor volumes were measured thrice a week. The experiment was terminated as soon as the tumors in the PBS group reached the barely acceptable limit (humane end point; 1.5 cm on any single dimension).

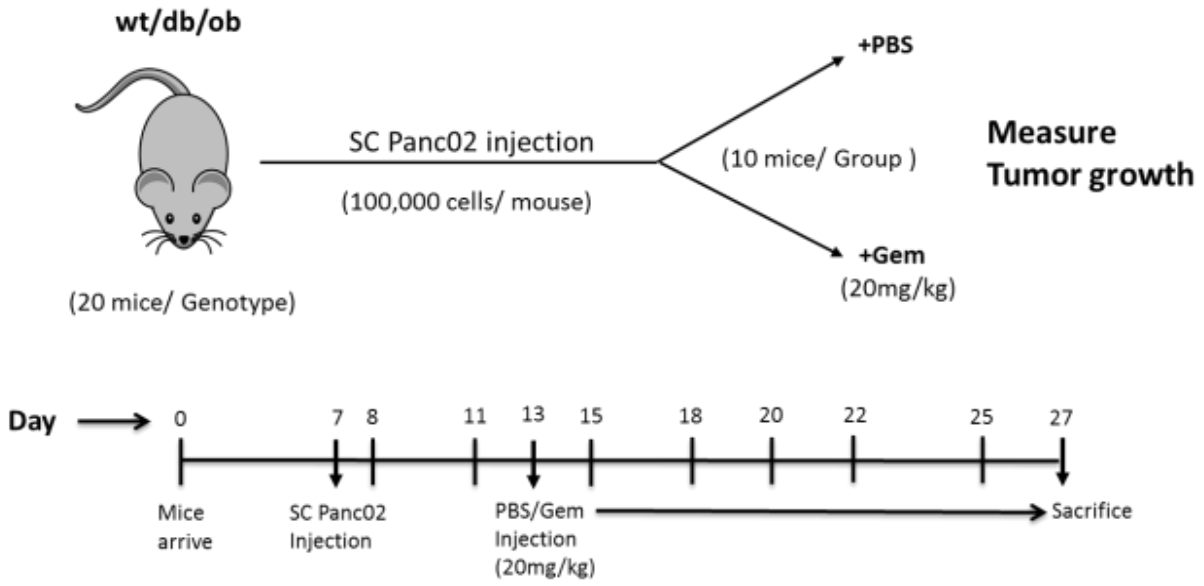

Fig. 26: Experimental plan for study of SC Panc02 tumor progression and chemo-sensitivity to gemcitabine in wt, ob/ob and db/db mice. *Mice were acclimatized for a week in the housing facility, and then implanted with Panc02 cells (100,000 cells/ mouse). Once the tumors were palpable, they were treated with gemcitabine (20mg/kg), or vehicle (PBS), on alternate days. Body weight, and tumor volumes were measured on alternate days. The mice were sacrificed when the PBS group developed tumors that reached the limit of 1.5 cm length on any dimension.*

2.5.2 Tendency for slower tumor growth, and better response to gemcitabine treatment observed in ob/ob mice compared to db/db mice

To evaluate the impact of *in vivo* leptin signaling on pancreatic cancer progression, we performed subcutaneous Panc02 tumor implantations in wt, db/db, and ob/ob mice. The experiment was performed as explained in Fig. 26 above.

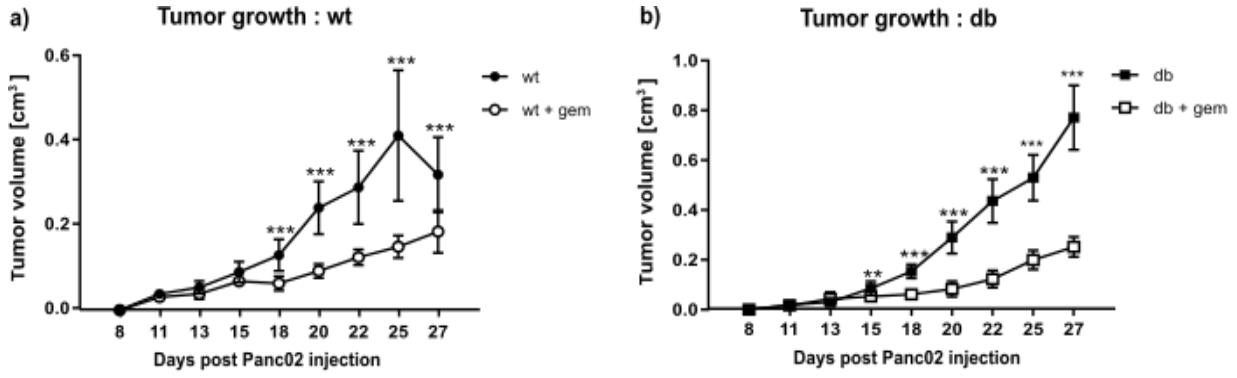

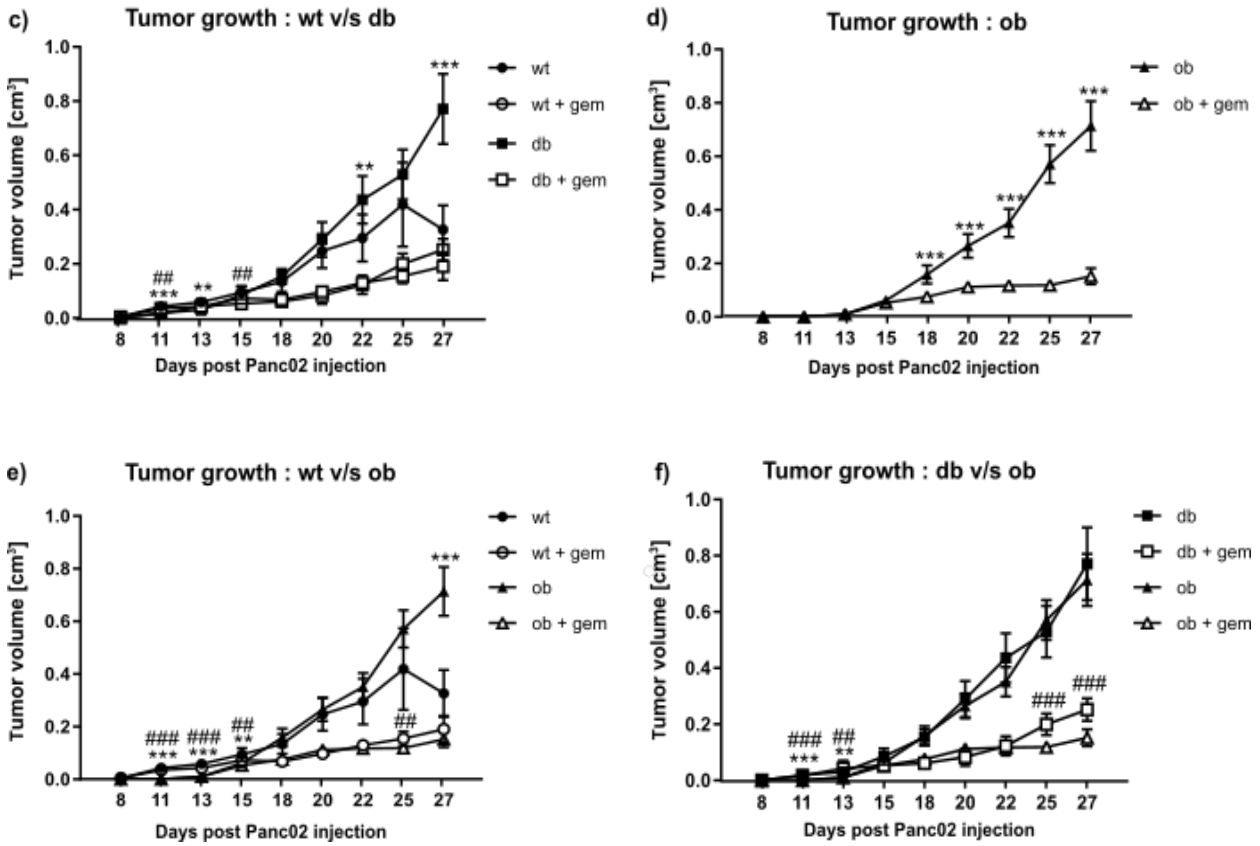

Fig. 27: Progression of SC Panc02 tumors in wt, ob/ob, and db/db mice. *n=10 per group, means ±SEM. *,# indicates significance.*

The subcutaneous tumors grew significantly larger in the PBS group for all three genotypes (Fig 27 a, b, d). The tumor growth curves for wt, db/db, and ob/ob mice with and without gemcitabine treatment, are represented multiple times to clearly compare different treatment groups and genotypes (Fig. 27). The db/db-, and ob/ob- PBS group developed significantly larger tumors than the wt controls (Fig. 27 c, e). There was no significant difference between wt and db/db mice treated with gemcitabine, or wt and ob/ob mice treated with gemcitabine (Fig. 27 c, e). However, towards the end, there was a tendency for the ob/ob tumors to respond better to gemcitabine, compared to the db/db mice on gemcitabine, and the tumor volumes were significantly smaller in ob/ob gemcitabine group than the db/db on gemcitabine (Fig. 27 f). However, the experiment was terminated after four weeks of tumor implantation, as the PBS group in all genotypes developed tumors beyond the acceptable limit.

As we previously observed that recombinant LEP increased the viability-, spheroid invasion-, and chemo-resistance to gemcitabine-, of multiple PDAC cell lines, we wanted to generate stable *Lepr* knockdown cells, and determine their growth characteristics and response to gemcitabine *in vitro*, in comparison to wt cells.

2.5.3 Knockdown of *Lepr* in the murine PDAC cell line: Panc02

Panc02 cells with a stable *Lepr* kd were generated using lentivirus mediated shRNA expression. The cell lines were generated by clonal selection. qPCR assay was performed to select the clones with lowest expression of the *Lepr*. The clones were selected, expanded, and stored in liquid nitrogen for future experiments.

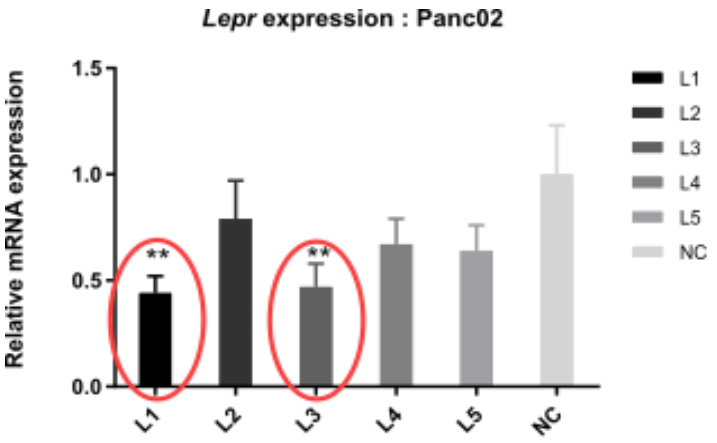

Fig. 28: Lentivirus mediated knockdown of Lepr in mouse PDAC cell line Panc02. *Five different shRNA constructs were used to generate stable Lepr kd cell lines. The knockdown cell lines were generated from single clone. n=4, means ± SEM, *indicates significance.*

As shown in the figure above, we could get best knockdown with the lentivirus construct 1 and 3 (Fig. 28). We performed *in vitro* assays with these cell lines. However, we observed that the kd status was lost in stable cells with the due course of time, and with increasing passage numbers.

In order to circumvent this issue, we decided to generate pooled knockdown cells with the same lentiviral shRNA constructs, and freeze several aliquots, and use shortly for *in vitro* experiments. The cells were to be used only for few passages, and fresh vials were thawed after 2-3 passages. The construct L2 gave the best knockdown, and hence we generated pooled cells with *Lepr* kd using shRNA construct 2, and used these cells for future experiments (Fig. 29).

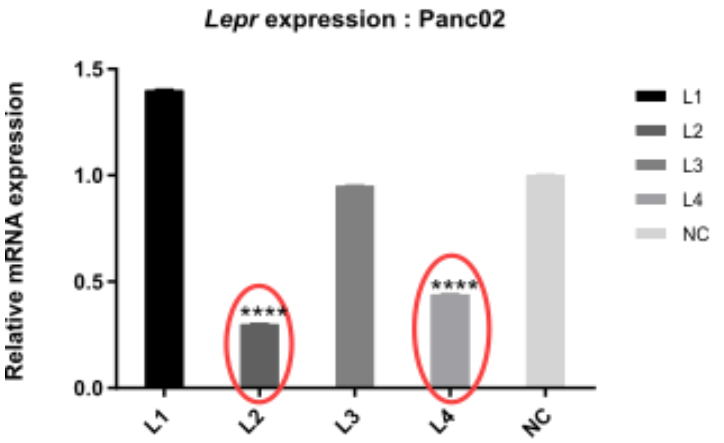

Fig. 29: Lentivirus mediated knockdown of Lepr in mouse PDAC cell line Panc02. *Five different shRNA constructs were used to generate stable Lepr kd cell lines. The knockdown cell lines were generated from pool of cells infected with a specific shRNA construct. n=4, means ± SEM, *indicates significance.*

We wanted to compare the proliferation and viability of control and *Lepr* kd Panc02 cells.

2.5.4 Viability and proliferation of wt (nc) and *Lepr* kd Panc02 cells in vitro

In order to investigate the effects of *Lepr* knockdown on Panc02 viability and proliferation, we treated the wt and *Lepr* knockdown cells with gemcitabine, and performed the respective assays.

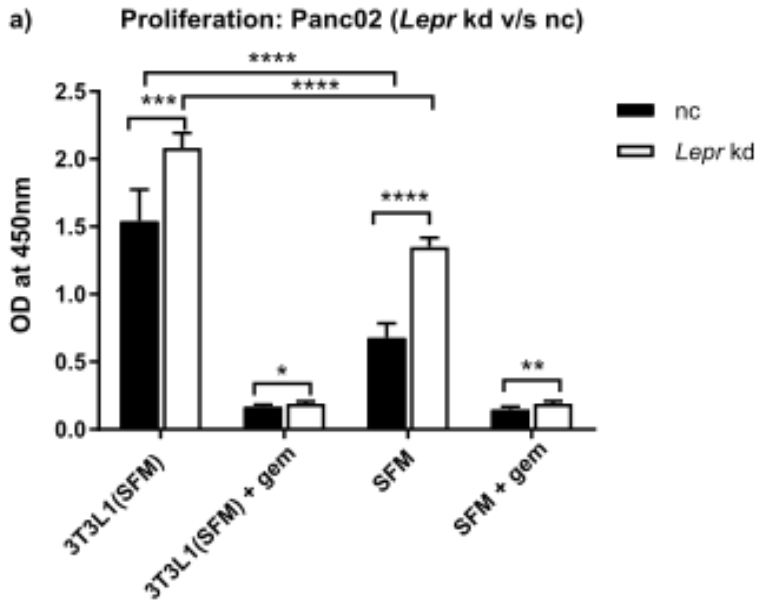

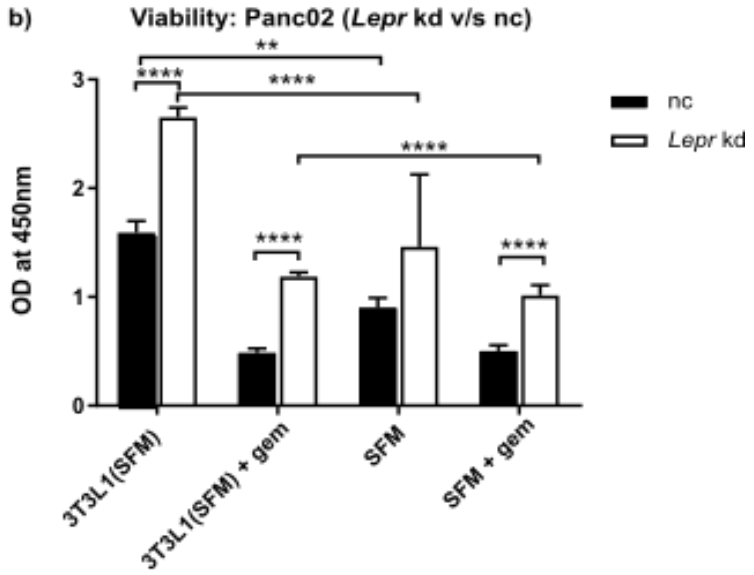

Fig. 30: Proliferation and viability of wt and Lepr kd Panc02 cells*. wt and Lepr kd Panc02 cells were treated with gemcitabine a) Proliferation measured by BrDU assay b) Viability measured by CCK-8.*

To our surprise, the kd of *Lepr* in Panc02 cells increased the proliferation, and viability of Panc02 cells upon treatment with 3T3-L1 – ACM, and gemcitabine (Fig. 30 a, b). We also wanted to generate another human PDAC cell line with a stable *Lepr* kd and perform the above experiments.

2.5.5 Knockdown of Lepr in human PDAC cell line AsPC1

We generated AsPC1 cells with a stable *Lepr* kd to evaluate the effects of the kd on cell proliferation, and chemo-resistance upon gemcitabine treatment (Fig. 31). We used lentivirus with human shRNA constructs for the knockdown.

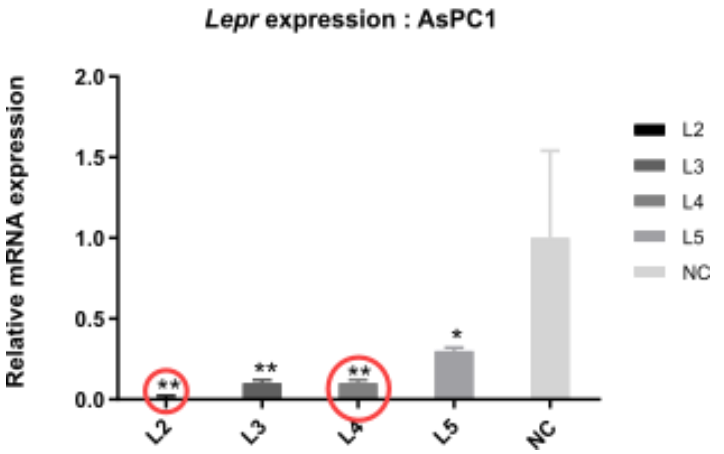

Fig. 31: Lentivirus mediated knockdown of Lepr in human PDAC cell line AsPC1. *Five different shRNA constructs were used to generate stable Lepr kd cell lines. n=4, means ± SEM, *indicates significance. Experiment performed along with Eveline Molocea.*

We wanted to compare the proliferation and viability of control and *Lepr* kd human PDAC cell line: AsPC1.

2.5.6 Viability and proliferation of control and *Lepr* knockdown AsPC1 cells in vitro

Next, we performed proliferation and viability assays with wt and *Lepr* kd AsPC1 cells, with or without gemcitabine treatment. This was done to investigate, if the knockdown of *Lepr* in AsPC1 cells, affected the chemo-sensitivity of AsPC1 cells to gemcitabine.

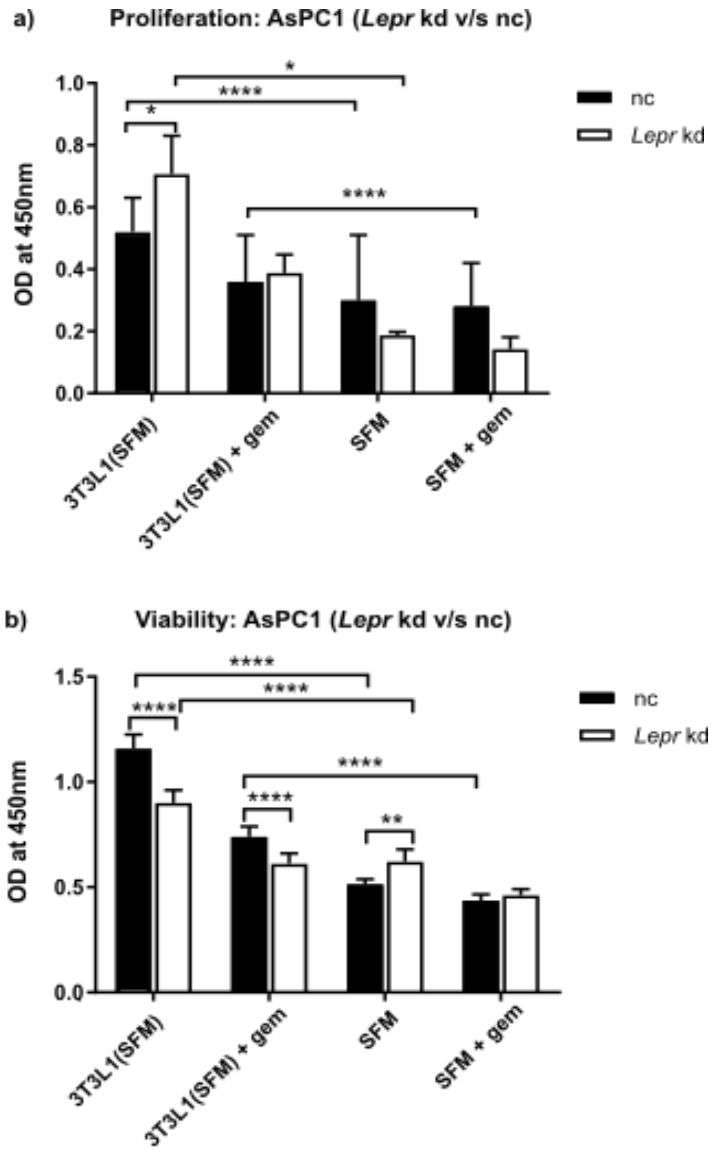

Fig. 32: Proliferation and viability of nc and Lepr kd AsPC1 cells*. NC and Lepr kd AsPC1 cells were treated with gemcitabine a) Proliferation measured by BrDU assay b) Viability measured by CCK-8. Experiment performed along with Eveline Molocea.*

As can be seen in Fig. 32, there was no consistent or significant effect of *Lepr* kd on the viability or proliferation of AsPC1 cells, when treated with ACM/FCM from 3T3-L1 cells, and gemcitabine.

As we previously observed that the knockdown of *Lepr* was unstable with continuous passaging of cells, we decided to pharmacologically inhibit *Lepr* using an antibody against it, and treat cells with primary

adipocyte conditioned media. The primary ACM was used as a source of leptin. This would enable us to evaluate if inhibition of the *Lepr* affects their proliferation and viability when treated with gemcitabine.

2.5.7 Pharmacological inhibition of LEPR in human PDAC cell lines does not affect their viability and proliferation upon gemcitabine treatment.

We identified that lentiviral knockdown of LEPR was not very stable after routine culturing. After a few passages, the cells regained their *Lepr* mRNA expression. Therefore, in order to achieve a more stable inhibition of the LEPR, we pharmacologically inhibited the *Lepr* using anti-*Lepr* antibody. This antibody had 10-fold higher specificity for the human LEPR, therefore we performed our assays with human PDAC cell lines.

We isolated primary subcutaneous iWAT from C57BL/6J mice, separated the stromal vascular fraction (SVF) from the tissue explant, and differentiated them to adipocytes using the standard differentiation cocktail. The differentiated primary cells were then serum starved on day 10 of differentiation for 4 hours, and the supernatant was collected and used as the ACM for this experiment. The ACM was used as a source of leptin, and either LEPR specific antibody or isotype specific control antibody was added, to evaluate if inhibition of the LEPR affected the sensitivity of human PDAC cell lines- Capan1 and AsPC1, to gemcitabine.

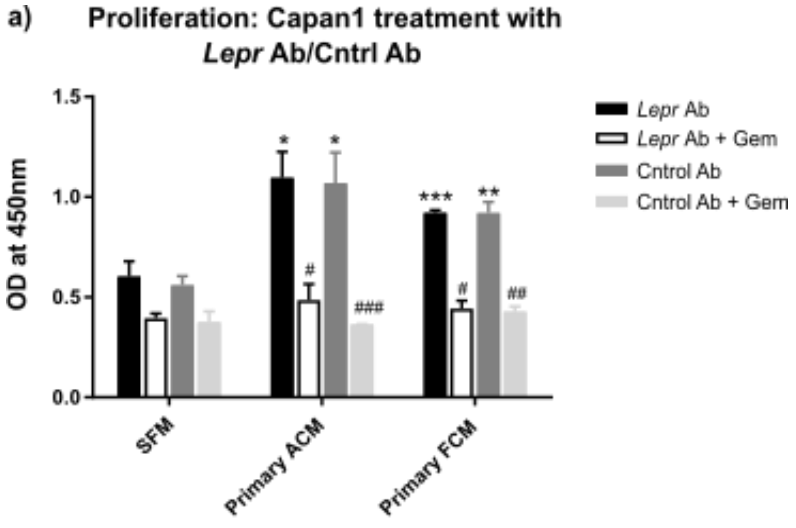

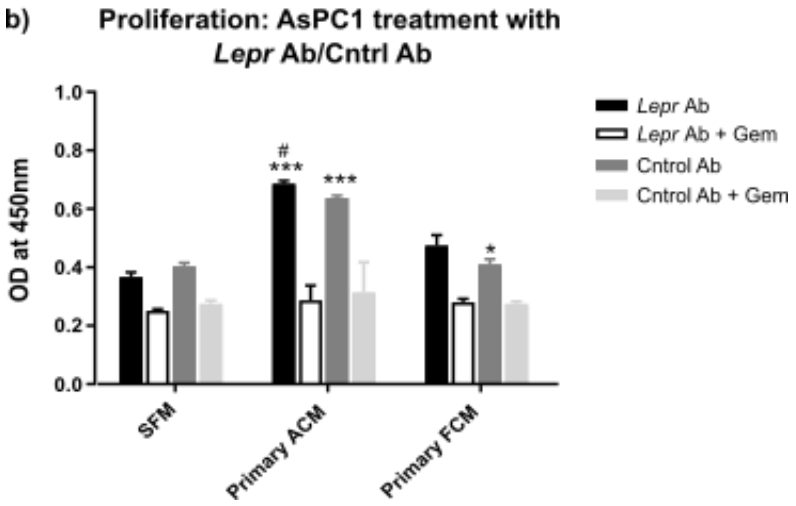

Fig. 33: Effect of LEPR/control antibody treatment on Capan1 and AsPc1 proliferation. *Capan1 and AsPC1 cells were treated with LEPR Ab or control Ab, and primary adipocyte or fibroblast conditioned media from mouse SC WAT. They were treated with or without gemcitabine and proliferation was measured by BrDU assay.*

Anti-LEPR Ab treatment did not have significantly different effect on proliferation upon gemcitabine treatment, compared to control Ab treatment (Fig. 35).

So far, we performed all our experiments of *Lepr* kd cells and gemcitabine treatment, in an *in vitro* setting. However, going forward, we wanted to investigate the *in vivo* chemo-sensitivity of Panc02 - wt and *Lepr* kd tumors to gemcitabine.

2.5.8 Progression and chemo-sensitivity of subcutaneous Panc02 tumors with Lepr knockdown in wt mice

In order to investigate the effect of knockdown of *Lepr* on *in vivo* tumor progression and chemo-sensitivity to gemcitabine, we implanted wt and *Lepr* knockdown Panc02 cells in C57BL6/J mice. The kd cells were generated by pooling lentivirus infected Panc02 cells, that showed lowest *Lepr* expression on qPCR.

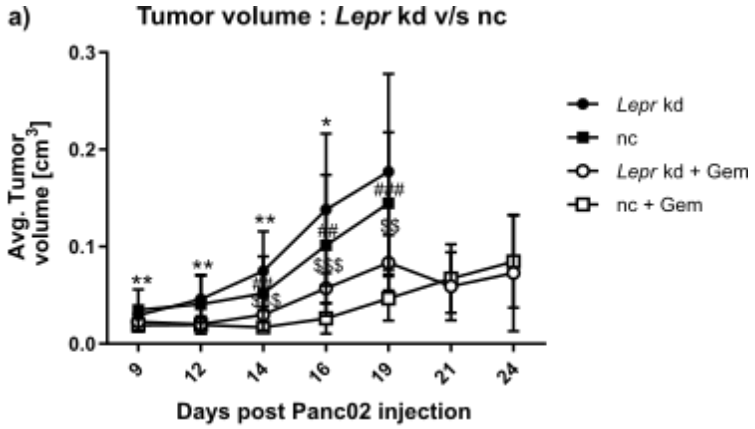

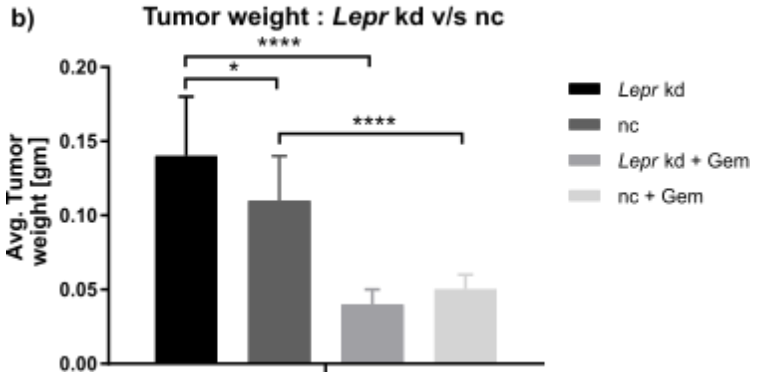

Fig. 34: Progression of SC Panc02 tumors transfected with shnc or shLepr in C57BL6/N mice. *a) Tumor growth comparison between NC and Lepr kd tumors with and without gemcitabine treatment b) Tumor weight comparison between NC and Lepr kd tumors, with and without gemcitabine treatment.*

The *Lepr* kd tumors grew larger than the control tumors. Also initially the *Lepr* kd tumors treated with gemcitabine, grew significantly larger than control tumors treated with gemcitabine. However, by the end of the experiment the gemcitabine groups had similar tumor volumes. The tumor mass was measured after sacrificing the mice. The *Lepr* kd tumors were significantly heavier than the control tumors. However, there was no significant difference in tumor mass between the kd and control tumors treated with gemcitabine (Fig. 34). This prompted us to confirm the *Lepr* expression in the *in vivo* tumor samples by qPCR.

2.5.9 qPCR analysis from in vivo tumor samples revealed the loss of Lepr kd status

As we did not find differences in the tumor volumes between control and *Lepr* kd tumors, we measured the mRNA expression levels of *Lepr* from the *in vivo* tumors, by qPCR.

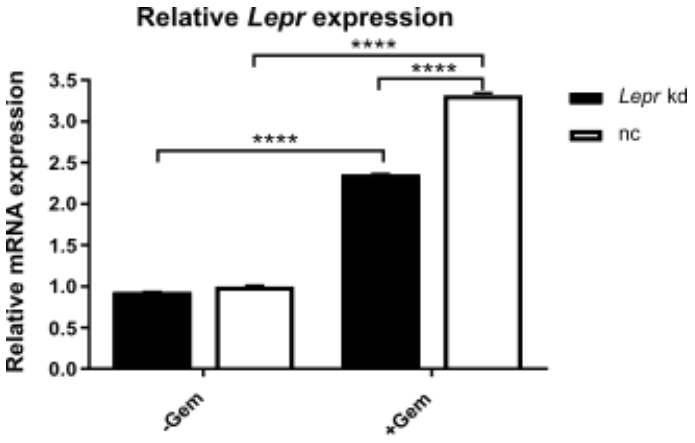

Fig. 35: Relative mRNA expression for Lepr from in vivo Panc02 tumors*. n=3, means ±SEM, * indicates significance*

As can be seen in Fig. 37, the expression level of *Lepr* was similar in the control and *Lepr* kd Panc02 tumors-, without gemcitabine. Therefore, in the vehicle treated mice, the *Lepr* kd tumors regained their *Lepr* mRNA expression during the course of tumor progression. However, in the gemcitabine treated group, the *Lepr* knockdown tumors showed significantly lower receptor expression levels compared to the control tumors. For reasons unknown, gemcitabine treatment significantly increased the expression of *Lepr* mRNA in both the *Lepr* kd and control tumors, compared to the respective PBS treated mice (Fig. 35).

3 DISCUSSION

3.1 Adipocyte conditioned media provides pro-tumorigenic signals to PDAC

It is well known that obesity is associated with the hypertrophic expansion of white adipocytes, and alters the secretion of adipokines, contributes to insulin resistance, and creates a chronic inflammatory state in the adipose tissue. The increased secretion of pro-inflammatory adipokines has been shown to favor tumors of several types including, prostate, colorectal, and breast carcinomas [62].

We investigated the effects of adipocyte conditioned media on PDAC progression. For this, we used immortalized murine 3T3-L1 cells as an *in vitro* model of adipocytes. 3T3-L1 cells are routinely used as an *in vitro* model for studying adipogenesis. Originally generated by the clonal expansion of rodent cells, 3T3-L1 cells serve as a cost-effective alternative to using primary mouse adipocytes [69]. Upon treating PDAC cell lines with conditioned media from mature 3T3-L1 adipocytes, we observed strong pro-tumorigenic effects *in vitro*. We observed that the ACM from 3T3-L1 cells promotes proliferation, migration, and invasion of several PDAC cell lines that we examined. Also, the tumor promoting effects were specific to conditioned media from differentiated 3T3-L1 adipocytes, and not observed with fibroblast conditioned media. This indicates that the pro-tumorigenic effects were mediated by differentiated 3T3-L1 adipocytes, and not fibroblasts.

Moreover, we demonstrated that the migration inducing effect of the 3T3-L1 ACM on BxPC3 cells, was significantly blunted upon heat inactivation of the ACM. We reasoned that the effects were lost because of heat-induced denaturation of secreted protein factors present in the ACM. This led to our hypothesis that secreted adipokines from 3T3-L1 adipocytes mediate pro-tumorigenic effects on PDAC cells. However, heat-denaturation could also have an impact on the metabolite fraction of ACM. Therefore, we cannot rule out the contribution of metabolites secreted from 3T3-L1 adipocytes, which could potentially mediate pro-tumorigenic effects as well.

The tumor micro-environment influences the tumor proliferation, and invasion [70]. The characteristics of the malignant tumors are not just affected by their self-autonomous signaling, but also by paracrine and endocrine effects mediated by secreted soluble factors from the surrounding stromal cells [70]. Adipose tissue is linked to breast cancer tumorigenesis, as it is the most abundant component of the stroma in the breast tissue [71]. Conditioned media from 3T3-L1 adipocytes was shown to promote proliferation, and reduce apoptosis in breast cancer cell lines [70]. The adipocytes in close proximity to the tumors, often display modified characteristics like delipidation, and are called the cancer associated adipocytes (CAAs). The CAAs communicate with tumor cells through pro-inflammatory molecules, proteases etc. to promote tumor proliferation and invasiveness [72], [73].

Although the link between adipocytes and other cancer entities have been studied, there is not much literature on role of adipocytes in PDAC progression [74]. Recently, it was shown that 3T3-L1 adipocytes rescue the proliferation of murine PDAC/PanIN cells specifically under nutrient/glutamine deprived growth conditions, by secreting glutamine [74]. This study identifies glutamine transfer as a potential mechanism linking adipocytes to the proliferation of PDAC/PanIN cells [74].

3.2 Obesity leads to higher pancreatic tumor burden in distinct mouse models of metabolic dysregulation

Considering the global obesity pandemic, there is an urgent need to decipher the fundamental mechanisms linking obesity to tumorigenesis. BMI, and adiposity affect malignancies in a sex-dependent, and tumor site-specific manner [75]. Several mechanisms including the insulin and insulin-like growth factor-I axis, sex steroids, and adipokines, have been proposed to mediate the effects of obesity on malignant tumor progression [75]. Firstly, hyperinsulinemia associated with obesity, reduces the levels of IGF binding proteins -1 and -2 (IGFBP-1 and IGFBP-2, which under normal circumstances bind and inhibit the action of IGF-I), resulting in higher levels of free and biologically active IGF-I which promotes tumorigenesis [75]. Secondly, higher aromatase activity in the adipose tissue of obese post-menopausal women, has been associated with augmented conversion of androgenic precursors to estrogen, and estrogen is well known for its pro-tumorigenic effects on breast cancer [76], [77]. Lastly, dysregulated adipokine secretion by the adipose tissue in obesity, mediates tumor promoting effects. For e.g., the adipokine leptin is pro-inflammatory, and is significantly upregulated in obesity, and promotes growth of hematopoietic cells, and normal and transformed epithelial tissue, and promotes angiogenesis [78]. On the other hand, obesity induced reduction in the levels of the insulin sensitizing adipokine: adiponectin, promotes insulin resistance. Epidemiological studies indicate an inverse correlation between circulating adiponectin concentration and the incidence of breast, endometrial, and prostate cancer [75], [79], [80], [81], [82], [83].

Several researchers have tried to investigate the link between obesity and PDAC, however the underlying mechanisms involved are largely unknown. PDAC is known to be an aggressive malignancy characterized by desmoplastic stromal response, and resistance to known chemotherapeutics [35], [84], [85]. Inflammation plays a critical role in the initiation and progression of PDAC. Chronic inflammation mediated by pancreatitis, obesity, and multiple genetic and environmental factors support PDAC development [46].

Studies have showed that obesity leads to intra-pancreatic fat infiltration, which increases the incidence of pre-cancerous PanIN lesions [45]. Augmented adipose tissue hypoxia during obesity could also play a role in promoting metastasis and angiogenesis in PDAC tumors [61]. Adipose tissue is an important

component of the PDAC tumor micro-environment. Visceral adipose tissue is predominantly associated with obesity induced metabolic dysregulation. Recently, it was shown that a high-fat and high-calorie (HFHC) diet induces inflammation specifically in the peri-pancreatic adipose tissue of KrasG12D (KC) mouse model of PDAC, compared to KC mice on a low calorie diet [86]. This observation was supported by the presence of higher inflammatory foci, smaller sized adipocytes, and an altered cytokine expression in the inflamed peri-pancreatic adipose tissue of the HFHC fed KC mice [86]. Others have shown using an acinar cell specific model of oncogenic *Kras*, that High-fat diet (HFD) provides the external inflammatory stimulus for the activation of oncogenic *Kras* signaling which drives the progression of PanIN lesions to PDAC [48].

Interestingly, calorie restriction (CR) in mouse models transplanted with PDAC cells, reduces murine and human PDAC tumor growth, NF-κB activation, and downregulates pro-tumorigenic signaling in the tumors, in an insulin like growth factor-1 (IGF-1) dependent manner [87]. The beneficial effects of CR were further elaborated in spontaneous PDAC development, where CR in comparison to HFD, reduces PDAC desmoplasia and metastasis, and prolongs tumor free survival in KrasInk4a$^{+/-}$ mice, through reduced IGF-1 and Akt/mTOR signaling [88]. Therefore, CR plays a beneficial role in delaying the progression of PanIN lesions to PDAC by modulating IGF-1 signaling and reducing inflammation [87], [88].

We hypothesized that obesity accelerates PDAC progression, and that the transcriptional dysregulation/absence of *Tblr1* in the mouse adipose tissue is an underlying mechanism linking obesity and PDAC tumorigenesis. The ATKO (**A**dipocyte tissue specific **K**nock**O**ut of ***T****blr1*) mice were previously shown by our group, to have dysregulated adipose tissue metabolism, impaired lipolysis, and hypertrophic adipocytes [58]. These mice were also shown to gain a higher body weight upon high fat feeding, compared to control mice [58]. In line with our hypothesis, we demonstrated that subcutaneous Panc02 tumors grew significantly larger in both male and female ATKO mice, compared to the control mice. However, examination of the tumors did not reveal any differences in the histological features, or gene expression patterns. Also, *in vitro* exposure of PDAC cell lines to *Tblr1* kd ACM did not have any significant impact on tumor cell viability and proliferation, compared to the control CM. Therefore, with our current results we could not conclude that higher tumor volumes observed in the ATKO mice, was due to the absence of *Tblr1* alone. We concluded that the higher tumor burden in the ATKO mice could be an implication of the overall systemic effects of increased adiposity, and dysregulated adipose tissue metabolism in the ATKO mice.

We further demonstrated that tumor xenografts of murine Panc02 cells grow significantly larger in distinct congenital mouse models of obesity and MetS, i.e. db/db and ob/ob mice. Mouse models with loss-of-function mutation for leptin or LEPR, i.e. ob/ob and db/db mice, proceed to develop defective whole body energy metabolism reflected as obesity, diabetes, infertility, and immune dysfunction [89], [90]. The

above results from tumor implantation studies in ATKO, db/db, and ob/ob mice point to the conclusion that obesity indeed accelerates PDAC growth, and increases tumor burden in mouse models of metabolic dysfunction.

3.3 Leptin promotes chemo-resistance of PDAC cells to gemcitabine in vitro

Adipose tissue is no more considered merely as an energy storing organ, but as an active endocrine tissue secreting several bioactive factors called adipokines. Adipokines mediate the paracrine and endocrine action of adipose tissue on other organs to maintain overall energy homeostasis. Under healthy conditions, there is a balance between pro- and anti-inflammatory adipokines. However, under conditions of metabolic dysfunction or obesity, the balance is tilted towards pro-inflammatory cytokines, which leads to immune cell infiltration, and activation of pro-inflammatory M1 macrophages within the adipose tissue. All the above factors alter the tumor micro-environment, and provide potential tumor promoting signals.

Our efforts to identify secreted factors from dysfunctional adipose tissue, mediating pro-tumorigenic effects, led us to investigate the role of leptin. We identified leptin to be significantly upregulated in the iWAT of db/db mice, with subcutaneous Panc02 tumors. Interestingly, the Panc02 tumors grew significantly larger in these db/db mice, compared to wt mice.

Leptin is a 16 kDa polypeptide, which is the most abundant adipokine secreted by the adipose tissue. It is mainly involved in regulating appetite and whole body energy metabolism through its action on hypothalamic neurons. Obesity is associated with significant upregulation in the circulating levels of leptin, both in humans, as well as in mouse models of obesity. Leptin has been associated with the development of several malignancies, mainly via the JAK/STAT pathway upstream of PI3K/AKT3 signaling, and ERK1/2 signaling [91]. It has been reported that leptin expression goes up under hypoxic conditions, which often exists within solid tumors [92], [93]. Leptin has been linked to angiogenesis, and vascular remodeling in breast cancer [94].

The role of leptin in PDAC progression is controversial. It has been shown that leptin increases the invasiveness and metastasis of PDAC by upregulation of MMP-13 [95]. However, others showed that plasma leptin concentrations in newly diagnosed PDAC patients is significantly lower than in control subjects [96].

Gemcitabine is the standard mono-therapy for treating advanced PDAC with a response rate of less than 20% [97]. However, only recently in 2010, a new drug combination called FOLFIRINOX (FFX) was introduced for the clinical treatment of metastatic pancreatic cancer [98]. FFX consists of a combination

of chemotherapeutics including oxaliplatin, irinotecan, and 5-fluorouracil [98]. Chemo-resistance to standard chemotherapeutics is a major concern in the treatment of PDAC. Understanding the factors that promote chemo-resistance in PDAC would be instrumental in improving the existing treatment options for PDAC. Although, leptin signaling has been reported to play a role in tumor chemo-resistance, its role in PDAC chemo-resistance is not well understood. It has been demonstrated that a high expression of *Lepr* in glioblastoma is associated with increased tumor chemo-resistance to temozolomide [99]. Increased LEPR expression has been linked to enrichment of glioblastoma cells with stemmness markers, and it was proposed that the SOX-2/OCT4 signaling downstream to the STAT3 pathway maintains the stemness in LEPR positive cells, which modulates the chemo-resistance of glioblastoma to temozolomide [99]. Expression of LEP in gastro-oesophageal adenocarcinomas was shown to be associated with resistance to cisplatin and radiological treatment, and the pharmacological inhibition of LEPR improved sensitivity to cisplatin in highly drug-resistant glioblastoma cells [100].

Upon treating murine and human PDAC cell lines with recombinant leptin, we observed an increase in their viability *in vitro*. However, we could not demonstrate that this chemo-resistance was mediated through *Lepr* signaling because of the following observations: Firstly, there was no difference in the proliferation, and viability of wt and *Lepr* kd PDAC cells (Panc02, and AsPC1) when treated with gemcitabine. Secondly, subcutaneous Panc02 tumors generated by injecting wt and *Lepr* kd cells into wt mice, responded similarly to gemcitabine treatment *in vivo*. qPCR analysis confirmed that *Lepr* expression was restored in the kd tumors. We reasoned that the restoration of *Lepr* mRNA expression in the kd tumors must be beneficial to tumor growth, which could potentially promote the elimination of *Lepr* kd cells from the tumor. Also, we made an interesting observation that gemcitabine treatment increased the *Lepr* mRNA expression in both wt and *Lepr* kd cells. The effect of gemcitabine treatment on *Lepr* expression in PDAC cells needs further investigation. Finally, pharmacological inhibition of *Lepr* in Panc02 cells by anti-*Lepr* antibody did not enhance the chemo-resistance of human PDAC cells (Capan1, and AsPC1) towards gemcitabine. In conclusion, our results indicate that the effect of leptin on PDAC chemo-resistance is not consistent between *in vitro* and *in vivo* experimental systems, and further research is required in this regard, perhaps utilizing orthotopic tumor mouse models, to clearly understand the role of leptin in PDAC progression and chemo-sensitivity.

3.4 Outlook and summary

In summary our data shows that adipocyte conditioned media increases the proliferation, migration, and invasion of PDAC cell lines *in vitro*, and subcutaneous PDAC tumors grow significantly larger in mouse models of metabolic syndrome. In order to evaluate if there are stronger tumor promoting effects of dysregulated adipocyte conditioned media on PDAC cell lines, it would be critical to perform trans-well assays of PDAC cell lines with primary adipose tissue conditioned media from wt/obese/high fat fed mice. So far, we did not treat mature 3T3-L1 adipocytes with inflammatory cytokines like TNFα etc., which could potentially mimic the dysregulated and inflammatory state of the adipose tissue in an *in vitro* setting. The above experiments could elucidate if conditioned media from dysregulated adipose tissue, generated from primary or from TNFα treated 3T3-L1 adipocytes, further accelerates PDAC tumorigenesis *in vitro*, compared to the conditioned media from lean/healthy adipose tissue.

Going forward, it is important to identify if the tumor inducing effects from the adipocyte conditioned media are mediated by secreted protein factors, or by metabolites like fatty acids etc. released by the adipocytes. We previously exposed the conditioned media from 3T3-L1 cells to high temperature in order to heat inactivate the proteins. However, this procedure can potentially alter the integrity of some metabolites as well. Hence, it would be crucial to separate the proteins from the conditioned media using a milder procedure, like molecular weight cut-off filters. Culturing PDAC cell lines with such protein free ACM would clearly indicate if the secreted proteins are indeed mediating the observed pro-tumorigenic effects.

A comparative secretome analysis between lean and obese WAT would help in identifying potential differentially secreted candidates mediating pro-tumorigenic effects on PDAC progression. To this end, either primary SVF (stromal vascular fraction) differentiated to WAT *in vitro*, or mature primary adipocytes embedded in a collagen matrix could be employed. In addition, such analysis can be extended to different WAT depots, i.e. – visceral and subcutaneous WAT. Such an analysis would be instrumental in identifying secreted proteins, particularly from obese WAT that promote PDAC progression, and if they are differentially regulated in distinct WAT depots.

Finally, it is important to test and validate the effects of the identified secreted protein candidates using *in vivo* mouse models of PDAC. Although, tumor xenograft models are very useful for understanding tumor progression, they are not representative of the tumor micro-environment associated with PDAC. Hence, it would be necessary to orthotopically implant PDAC cells into mice, and evaluate the interaction between potential adipose tissue secreted factors and tumor progression. The schematic below depicts some of our key findings and the future prospects (Fig. 36).

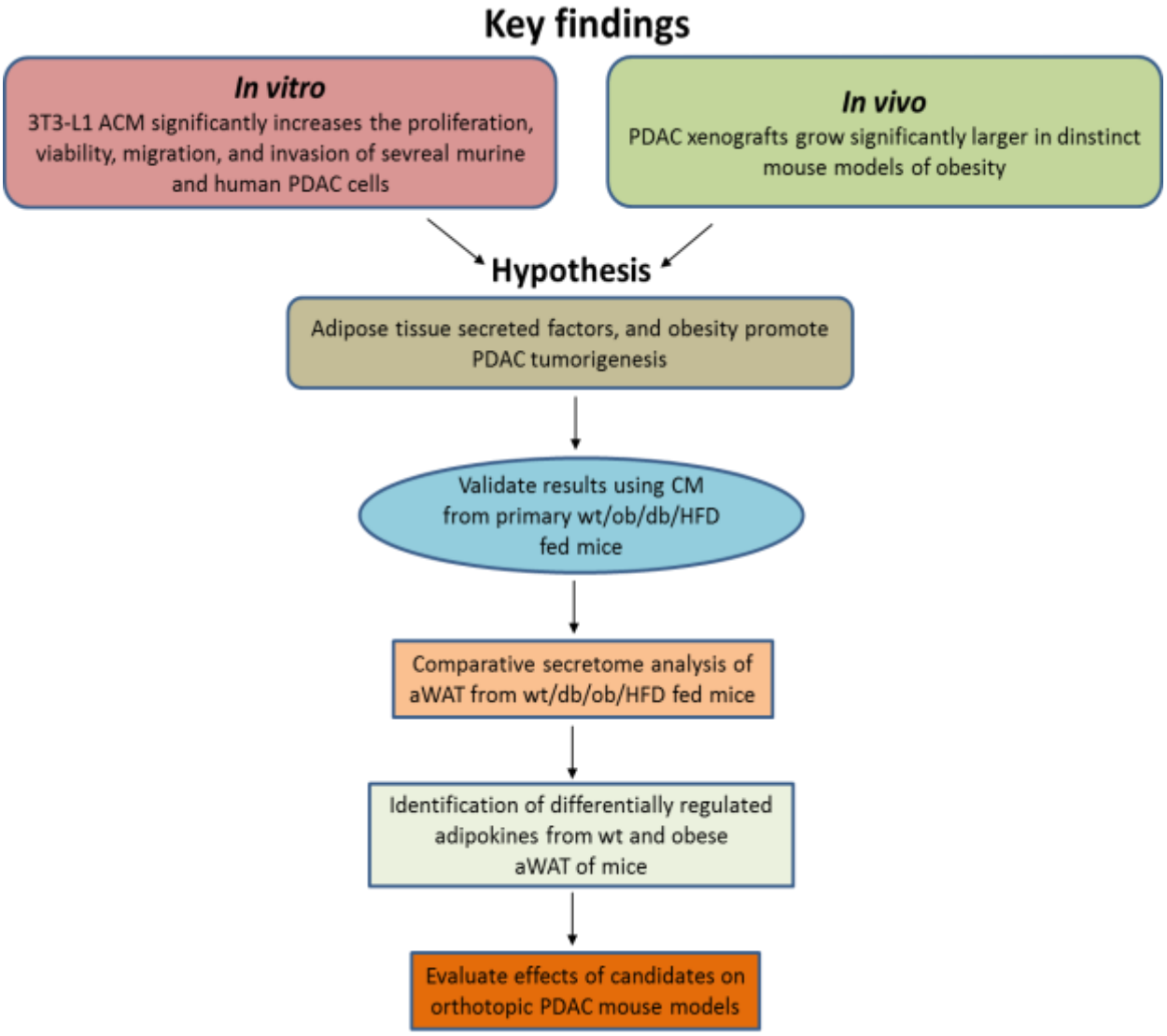

Fig. 36: Schematic representing current findings and future prospects: *3T3-L1 adipocyte conditioned media significantly increased proliferation, viability, migration, and invasion of PDAC cells in vitro. Panc02 xenografts grew significantly larger in distinct mouse models of obesity (db/db, and ob/ob mice). This led to the hypothesis that adipocyte secreted factors mediate PDAC progression. In future, these results must be validates using primary mouse ACM from wt mice and obese mice (ob/db/HFD-fed mice). Following this, comparative secretome analysis would help identify differentially regulated adipokines between wt and obese abdominal WAT (aWAT). Finally, the effects of identified candidates need to be validated in orthotopic mouse models of PDAC.*

4 METHODS

4.1 Molecular Biology

Transformation of *E.coli*

TOP10 competent *E.coli* strain was transformed by chemical transformation. 50 µl of cell suspension was thawed on ice and mixed with 0.1-1 µg of plasmid DNA. After 30 min incubation on ice, a heat shock at 42°C was applied for 30 s. Afterwards, 250 µl of SOC medium was added and cells were incubated at 37°C under vigorous shaking, and were subsequently plated onto LB agar plates containing the appropriate antibiotic.

Bacterial liquid cultures

Single colonies were inoculated into LB medium supplemented with the appropriate antibiotic. Depending on the amount of DNA needed, 2-200 ml cultures were inoculated. The cultures were incubated over night at 37°C under vigorous shaking (~160 rpm).

Preparation of plasmid DNA from *E.coli*

Plasmid DNA was isolated from *E.coli* bacterial cultures using commercially available kits, following the manufacturer's instructions (QIAprep Plasmid Miniprep Kit, Qiagen for small scale plasmid preparation; PureLink HiPure Plasmid Maxiprep Kit, Invitrogen for large scale plasmid preparation).

PCR

DNA from plasmids, cDNA or a genomic DNA was amplified by polymerase chain reactions using a thermocycler (PTC 200) and Phusion polymerase (Finnzymes). The primers used are listed in the material section. PCR reactions were set up following the manufacturer's instructions and were programmed according to the T_m of each individual primer pair and the length of the PCR product.

RNA isolation

A) From PDAC cell lines/3T3-L1 adipocytes

Cells were harvested in 1 ml QIAzol (Qiagen) and transferred to RNase free tubes. Lysates were incubated at room temperature for 5 min to release nucleoprotein complexes before adding 200 µl of chloroform. Mixtures were vortexed for 15 secs and then centrifuged for 30 min at 13,000 rpm, 4°C. The upper aqueous solution containing the RNA was transferred into a fresh reaction tube. The RNA phase was then mixed with equal volume of isopropanol and incubated at room temperature for 10 min, followed by a

10 min centrifugation step at 13,000 rpm, 4°C. The supernatant was aspirated and the pellet was washed once with 1 ml of 75% ethanol. The pellet was dried until translucent at RT and re-solubilized in 30 µl DNase/RNase free water. The samples were stored at -80°C until further use.

C) From frozen tissue

Frozen tissue samples were transferred into a 2 ml RNase/DNase-free reaction tube containing 1 ml QIAzol (Qiagen) and a pre-cooled stainless steel beads. The samples were lysed using the TissueLyser for 90 secs at a frequency of 30 Hz. Lysates were incubated at room temperature for 5 min to release nucleoprotein complexes before adding 200 µl of chloroform. Phase separation was performed as described in A). The upper phase was then transferred to a new tube containing 1 volume 100 % ethanol to precipitate nucleic acids. RNA was then purified using the RNeasy micro kit (Qiagen), following the manufacturer's instructions. RNA was eluted in 50 µl DNase/RNase free H_2O and stored at -80°C until further use.

Determination of RNA concentration

The RNA concentrations were measured using the NanoDrop ND- 1000 spectrophotometer. 1 uL of sample was placed on the sample holder and concentration was determined by spectrophotometric measurement at 260nm. Simultaneously, the absorbance ratio of 260 nm/280 nm was measured to assess sample contamination with protein.

cDNA synthesis

Complementary DNA was synthesized using the Fermentas cDNA synthesis kit, following the manufacturer's protocol. 200-1000 ng of RNA was used as the starting material, and the reverse transcription reaction was run in the thermocycler. Finally, the cDNA was diluted 10 fold in DNase/RNase free water and stored away at -20°C until further use.

Quantitative PCR

5 µl of the diluted cDNA samples obtained from reverse transcription were used for quantitative PCR. A master mix was prepared containing 10 µl *TaqMan* Gene Expression Assay Supermix, 4.5 µl DNase/RNase free water and 0.5 µl *TaqMan* probe per individual reaction. Technical triplicates of all samples were included. The *TaqMan* probes used were obtained from Applied Biosystems or MWG and are listed in the material section. Water was used as a negative control and samples containing no reverse transcriptase served as controls for genomic DNA contamination. 20 µl PCR reactions were transferred per well onto a MicroAmp Optical 96 well reaction plate and quantitative PCR was performed using the StepOnePlus Real Time PCR System (Applied Biosystems).

Gene expression profiling

Gene expression profiling was performed in tumor samples from wt and ATKO SC Panc02 tumors, or from the subcutaneous inguinal WAT of wt and db/db mice with Panc02 tumors. RNA isolation, cRNA synthesis and hybridization to Mouse Genome 430 2.0 arrays (Affymetrix, Freiburg) were performed according to the manufacturer's recommendations. Three arrays per sample were hybridized. CustomCDF by Brainarray with Entrez based gene definitions (Entrez basic version 13) was used to annotate the arrays (Sandberg R., 2007). The raw fluorescence intensity values were normalized applying quantile normalization. Differential gene expression was analyzed based on ANOVA using a commercial software package (SAS JMP8 Genomics, version 4, SAS Institute, Cary, NC). A false positive rate of a=0.05 with FDR correction was taken as the level of significance. Pathways belonging to various cell functions were obtained from public external databases (KEGG, http://www.genome.jp/kegg/). A Fisher's exact test was performed to detect the significantly regulated pathways.

4.2 Cell Biology

All experiments with eukaryotic cells were performed under sterile conditions. Cells were cultivated at 37°C, 5% CO_2 and 95% humidity. All media and additives were warmed to 37°C prior to use. A list of the media used for cell culture experiments is shown in Tab. 5.

Name	Medium	Serum	Antibiotic	Further Additives
3T3L1 culture	DMEM (1g/L glucose)	10% FBS	1% P/S	-
3T3L1 Differentiation	DMEM (4.5 g/L glucose)	10% FBS	1% P/S	See Tab. 6
3T3L1 virus infection	DMEM 1g/L glucose	-	-	-
Freeze medium	DMEM (4.5 g/L glucose)	20% FBS	-	10% DMSO
HEK293 culture	DMEM (4.5 g/L glucose)	10% FBS	1% P/S	
Primary adipocyte culture	DMEM	10% FBS	1% P/S	-
Primary adipocyte differentiation	DMEM	5% FBS	1% P/S	See Tab. 6
All PDAC cell line culturing	DMEM (4.5 g/L glucose)	10% FBS	1% P/S	-

Tab. 2: Media used for cell culture and virus experiments.

Thawing cells

Eukaryotic cells were stored in liquid nitrogen tanks in 1 ml aliquots containing 1 X 10^6 cells in freeze medium. Following thawing at 37°C, the suspension was added to 9 mL of DMEM with 10% FBS and 1% P/S (complete media), centrifuged at 2000 rpm for 3 mins to remove DMSO. The supernatant was aspirated and the pellet was re-suspended in 1 mL of complete media and added to 19 mL of complete media on a 15 cm cell culture dish.

Freezing cells

Eukaryotic cells were trypsinized and resuspended in freezing medium containing 20% FBS and 10% sterile DMSO. The cells were counted and diluted to $1X10^6$ cells/ml, and aliquoted in cryotubes as 1 mL aliquots in the freezing medium. The aliquots were placed in Mr. Frosty boxes, filled with isopropanol, for a gradual cooling, in -80 degree freezer for overnight. Next day, the cells were transferred to liquid N2 storage.

Cultivation of 3T3-L1 fibroblasts

3T3-L1 cells were cultivated on 15 cm tissue culture plates in 20 ml 3T3-L1 culture medium. Cells were never allowed to grow beyond 70% confluency, and a passage of 15 was never exceeded to avoid diminished differentiation capacity. For passaging, the cells were first washed in 1x PBS and trypsinized, then the detached cells were re-suspended in 10 ml of fresh medium. Cells were pelleted by centrifugation at 2000 rpm for 3 min and subsequently re-suspended in 10 ml fresh medium. After manual counting in a Neubauer counting chamber, $4x\ 10^4$ cells were plated onto a 15 cm tissue culture dish containing 20 ml medium. Cells were passaged every 3-4 days.

Differentiation of 3T3-L1 fibroblasts into adipocytes

3T3-L1 fibroblasts were differentiated into adipocytes by the addition of insulin, 3-isobutyl-1-methylxanthine (IBMX), dexamethasone (Dex), and ABP (L-ascorbate, d-biotin, pantothenic acid). Cells were cultivated on 10 cm plates until they reached confluency and then induced to undergo differentiation by adding 3T3-L1 differentiation media as shown in Tab. 6.

Differentiation	**Medium**	**Additives**
Day 1	3T3-L1 differentiation	1 μg/ml insulin 0.25 μM Dexamethasone 0.5 mM IBMX 1/1000 ABP stock solution
Day 3	3T3-L1 differentiation	1 μg/ml insulin 0.25 μM Dexamethasone 0.5 mM IBMX 1/1000 ABP stock solution
Day 5	3T3-L1 differentiation	1 μg/ml insulin 1/1000 ABP stock solution
Day 8	3T3L1 culture	None

Tab. 3. Media and additives for differentiation of 3T3-L1 fibroblasts.

Experiments could be performed 8-12 days after initiation of differentiation.

Cultivation of mouse and human pancreatic cancer cell lines

The pancreatic cancer cell lines were usually split twice a week, on Mondays and Fridays, as they grew and reached confluence very fast. All cells were grown in DMEM High glucose media with 10% FBS and 1% Penstrep. Following was the split ratio for the most commonly used PDAC cell lines:

Cell line	Splitting ratio	Approx. volume of addition from 10 mL suspension
Panc02	1:50	200 µl
Capan1	1:5	2 ml
Panc8680	1:20	500 µl
BxPC3	1:10	2 ml
AsPC1	1:5	2 ml

Tab. 4. Culturing conditions for PDAC cell lines.

Cultivation of human embryonic kidney (HEK) cells

HEK293 and HEK293A cells were cultured in HEK293 and HEK293A culture medium, respectively. The cells were cultivated either in 10 cm tissue culture plates containing 10 ml medium or in 15 cm plates with 25 ml medium. Cells were passaged at 70-90% confluency by re-suspension in 10 ml fresh medium, centrifugation (3 min, 2000 rpm), re-suspension of the pelleted cells in 10 ml medium and subsequent addition of the twentieth part of the cells to a new tissue culture plate. Cell number could be determined by using the Neubauer counting chamber.

Transfection with Lipofectamine 2000

For higher transfection efficiency HEK293 cells were transfected with Lipofectamine 2000 transfection reagent (Invitrogen). 3 µl of the reagent was added to 250 µl of serum free Opti-MEM medium. The mixture was combined with DNA which was diluted in the same medium, and the mixture was incubated in RT for 20 min to allow complex formation. The DNA/Lipofectamine complex was added dropwise to cells in antibiotic-free medium. Medium change to the normal culture medium was performed the following day.

Isolation of preadipocytes from adipose tissue

Preadipocytes were isolated from the stromal vascular fraction (SVF) of abdominal or inguinal white adipose tissue or from interscapular brown adipose tissue depots of male C57Bl6/N mice aged 6-9 weeks. Mice were sacrificed by cervical dislocation, sterilized with 70% ethanol and adipose tissue depots were dissected. After cleaning the fat pads, the pads were chopped until no pieces could be observed anymore and subsequently digested in 7 ml collagenase medium (DMEM containing 1.5 mg/ml type II collagenase and 0.5% BSA) for 1 h at 37°C and 180 rpm. To stop the reaction, 6 ml culture medium was added and adipocytes floated to the top of the tube, where they could be removed. If needed, 1 ml QIAzol reagent

(Qiagen) was added to 200 µl mature adipocytes to isolate RNA as described. The SVF was harvested by centrifugation at 1000 rpm, 10 min. The cell pellet was resuspended in culture medium, filtered through a 70 µm falcon strainer, and cells were plated to 12 well plates. One mouse harvested one 12 well plate abdominal preadipocytes, one 12 well plate inguinal preadipocytes, and half a 12 well plate brown preadipocytes. Cells were washed every day with warm culture medium until they reached confluency.

Differentiation of primary preadipocytes into adipocytes

Primary preadipocytes are differentiated into adipocytes by the addition of insulin, 3-isobutyl-1-methylxanthine (IBMX), dexamethasone and ABP (L-ascorbate, d-biotin, pantothenic acid). In case of preadipocytes harvested from brown adipose tissue, in addition triiodothyronine (T3) is added. Preadipocytes were cultivated until they reached confluency (approximately 1 week) and then induced to undergo differentiation by adding primary cell differentiation media as shown in Tab. 8.

Differentiation	Medium	Additives
Day 1	Primary adipocyte differentiation	1 µg/ml insulin 0.25 µM Dexamethasone 1/1000 ABP stock solution (3nM T3)
Day 3	Primary adipocyte differentiation	1 µg/ml insulin 0.25 µM Dexamethasone 1/1000 ABP stock solution (3nM T3)
Day 5	Primary adipocyte differentiation	1 µg/ml insulin 1/1000 ABP stock solution
Day 8	Primary adipocyte culture	none

Tab. 5: Media and additives for differentiation of primary adipocytes.

Experiments could be performed 8-12 days after initiation of differentiation.

Adenovirus harvest

Adenoviruses were harvested when 70-80% of the HEK293A cells were rounded and lost adhesion. For that purpose, the remaining adherent cells were rinsed off the tissue culture plate with a pipette and transferred to a centrifuge tube together with the non-adherent cells. Cells were pelleted by centrifugation (2000 rpm, 10 min, RT) and resuspended in 0.5-3 ml PBS-TOSH. The cell suspension was stored at -80°C. For cell disruption and virus release, 3 freeze-and-thaw cycles were performed. To this end the suspension was frozen in liquid nitrogen, thawed at 37°C and vortexed vigorously. Cell debris was removed by centrifugation at 3000 rpm for 5 min and the resulting crude virus lysate could be purified by CsCl gradient or used for further infection of HEK293A cells.

Adenovirus purification using cesium chloride gradient

Cesium chloride (CsCl) gradient centrifugation is a type of density gradient centrifugation for the purification of viral particles (Green et al. 2006). Confluent HEK293A on twenty 15 cm cell culture dishes were infected with crude virus lysate or purified adenovirus (1 µl per plate) and grown until 70-80% of the cells were rounded and lost adhesion, then they were harvested and lysed as described. PBS-TOSH was added to the crude lysate to a final volume of 20 ml. All solutions were adjusted to pH 7.2. The first gradient was layered with 9 ml 4.4 M CsCl, 9 ml 2.2 M CsCl and 20 ml virus in PBS-TOSH. After ultracentrifugation (2 hrs., 4 °C, 24,000 rpm, SW28 rotor) the virus band was removed and added to the same volume saturated CsCl. The second gradient was layered with 8 ml virus in CsCl, 1.5 ml 4.4 M CsCl und 1.5 ml 2.2 M CsCl. Following the second ultracentrifugation (3 hrs., 4 °C, 35,000 rpm, SW40Ti rotor) the virus band was removed in the smallest possible volume and dialyzed against PBS-glycerol over night at 4°C. 10% glycerol was added to the purified virus and aliquots were stored at -80°C.

Virus Titration using the Tissue Culture Infectious Dose 50 ($TCID_{50}$) method

The virus titer (plaque forming units, pfu) could be determined by $TCID_{50}$. For that purpose, 10,000 HEK293A cells were seeded in 100 µl virus titration medium in each well of a 96 well plate and infected with decreasing amounts of virus after 2 hrs. of adhesion. Serial dilutions of the virus up to 10^{-14} were prepared in titration medium and added to the cells. Double measurements were performed for each virus. 10-12 days after infection and incubation at 37°C the plaques were counted and the titer was calculated using the following formula:

$T = 10^{1+(s-0.5)} \times 10$ pfu / ml

(s = sum of positive wells starting from the 10^{-1} dilution; 10 positive wells per dilution = 1)

Transduction of 3T3-L1 fibroblasts with adenoviruses

2×10^4 3T3-L1 cells were seeded on 6 well plates and transduced with different amounts of adenovirus 72 hrs. after plating. MOIs of 100 to 100,000 were tested, with MOI 1000 being ideal for efficient transduction of the fibroblasts. The desired amounts of virus were diluted in low glucose DMEM without FCS and 0.5 µg/ml poly-L-lysin were added (Orlicky et al. 2001). After incubation at RT for 60-100 min the mixture was added to PBS-washed cells. After 90 min incubation at 37°C, 3T3-L1 culture medium was added and cells were incubated 72-96 hrs. until harvest. In case of subsequent differentiation, the differentiation process was started 24 hrs. after virus transduction.

Transduction of 3T3-L1 adipocytes with adenoviruses

Differentiated 3T3-L1 adipocytes on day 10 of differentiation were washed with PBS and trypsinized. The pelleted cells were then resuspended in 3T3-L1 culture medium and filtered through a 70 μM falcon strainer. Cells were counted, and 4 x 10^5 cells were plated to each well of a 12 well plate. For larger scale transductions, 4.8 x 10^6 cells were plated on 10 cm plates. 24 hrs later, floating cells were removed by washing with PBS and 3T3-L1 starve 1 medium was added. After 12 hrs incubation, cells were again washed in PBS and 3T3-L1 starve 2 medium was added for 12 hrs. Adenoviruses at an MOI of 500 were diluted in 3T3-L1 virus infection medium containing 0.5 μg/ml poly-L-lysin (250 μl medium per well or 2.5 ml per 10 cm plate). After incubation at RT for 60-100 min the mixture was added to PBS-washed cells. After 90 min incubation at 37°C, 3 volumes 3T3-L1 culture medium were added and cells were incubated 72-96 hrs until harvest.

Generation of lentivirus in HEK293T cells

Day 1: Seed HEK293T cells in 6-well plates (10^6 cells/well), in low antibiotic medium (High glucose, 10% FBS, P/S 1:1000, 2 ml/well), so that they are 60-80% confluent the following day.

Day 2: Mix

Solution a) 200μl Opti-MEM + 5ml lipofectamine 2000, incubate for 5 mins at RT

Solution b) pLKO1 1μg

psPAX2 1μg

pMD2.G 100ng

in 200μl Opti-MEM

Note: make master mix for packaging plasmids psPAX2 and pMD2.G and add different pLKO1 vectors afterwards.

- combine solutions and incubate 20-30 mins at RT
- change medium on HEK293T cells to 1.5 ml medium with low antibiotics
- dropwise add transfection-DNA mixture

Day 3: In the morning, change medium to high BSA medium (DMEM high glucose, 10% FBS + 1.1 g/100 ml supplemental BSA)

Day 4: Next day in the evening, collect virus, freeze at -80°C in aliquots

Transduction of PDAC cell lines with lentivirus

Day1: Plate 3 x 104 cells/well, on a 6-well plate (multiple plates, one plate for each virus), also include control wells without any virus

Day 2: Remove media and add virus + polybrene + media mixture to cells (different amounts, to choose the best one later)

Component	Volume (μl)	Volume (μl)	Volume (μl)
Virus	50 μl	100 μl	200 μl
Polybrene (1:1000)	1.5 μl	1.5 μl	1.5 μl
Media	1448.5 μl	1398.5 μl	1298.5 μl
Total	**1500 μl**	**1500 μl**	**1500 μl**

Tab. 6: Composition of transduction mix for infecting PDAC cells with lentivirus.

Day 3: In the morning, change media to low antibiotics media (DMEM high glucose, 10% FBS, 1:1000 P/S)

Day 4: Add fresh media with 1 μg/mL puromycin (stock puromycin: 10 mg/ml)

Day 5/6: Check for confluence, if there are too many cells, then trypsinize each well individually and re-plate with 1 μg/ml of puromycin containing media.

Day 8: Select for puromycin resistant cells. Many cells would float, and only infected cells would survive with puromycin.

Select and re-plate 2 x 96-well plates/virus (1 cell/well) and change media every 2-3 days. Allow for colony formation, and once the colonies are big enough, select 5 wells/virus and grow them in larger 10 cm dishes, and confirm knockdown by qPCR. Finally, after confirmation of target knockdown, freeze away the cells in liquid N2 for long-term storage.

CCK-8 Cell viability Assay

10uL of CCK-8 reagent was added to 100uL of media on top the cells in 96-well plates. The plate was incubated for 30 mins and 1 hr in the cell culture incubator and the absorbance was measured at 450nm.

Trans-well migration assay

Panc02/Capan1/BxPC3/Panc8680 cells were seeded onto the migration inserts in 24 well plates supplied by BD Falcon. Following assay conditions were used for specific cell lines as mentioned below:

S.No.	Cell line	Assay	Seeding density	Seeding Vol.	Chemoattractant vol.
1	Panc02	Migration	10,000	100 µl	1 ml
2	Panc02	Invasion	40,000	100 µl	1 ml
3	Panc8680	Migration	20,000	100 µl	1 ml
4	Capan1	Migration	100,000	100 µl	1 ml
5	BxPC3	Migration	40,000	100 µl	1 ml

Tab. 7: Migration and invasion assay conditions and seeding densities for different PDAC cell lines.

Cells were always seeded in serum free medium on the top chambers, and chemoattractant (Conditioned media/ Complete media with 10% FBS) was added to the bottom chambers. The plates were incubated overnight in the cell culture incubator. The next morning, the inserts were removed one by one, the media was aspirated, and the inside was wiped with a dry qTip, followed by a wet qTip (soaked in water). Following this, the inserts were fixed in methanol for 10 minutes. Afterwards, they were quickly in DPBS, and stained in 0.01% crystal violet (in water) solution for 15 mins. The inserts were washed thrice in water. All these solutions were pre-dispensed in 24 well plates. Finally, the inserts were inverted and carefully excised using a scalpel, and placed on top of mounting media on a glass slide. A cover slip was carefully placed on top of the inserts. The migrating or invading cells were manually counted, by taking images of 3-4 fields per insert.

Trans-well invasion assay

The invasion inserts were equilibrated for 45 mins in the cell culture incubator, with some DPBS on over the insert, and some in the bottom of the inserts. The DPBS, was removed and Panc02/Capan1 cells were seeded onto the invasion inserts, coated with matrigel, in 24 well plates, supplied by BD Falcon. Chemoattractant solution (Conditioned media/ Complete media) was added to the well bottom. The plates were incubated overnight in the cell culture incubator. The next morning, the inserts were removed one by one, the inside was wiped with a dry qTip, then with a wet qTip, and incubated for 10 mins in methanol, followed by quick wash in DPBS, then a 15 min incubation in 0,01% Crystal violet solution in water (filtered), and washed thrice in water. All these solutions are pre-dispensed in 24 well plates. Finally, the inserts are inverted and carefully cut out using a scalpel, and placed on a drop of mounting media on a glass slide. The migrating or invading cells are manually counted, by taking images of 3-4 fields per condition.

BrDU Proliferation Assay

BrDU assay was performed to measure proliferating cells. The BrDU kit from Cell Signaling was used and the assay was performed using manufacturer's protocol. Tumor cells were plated on 96-well black plates with transparent bottom, treated with leptin or gemcitabine or both for specific periods before they performing BrDU assay on them. Following are the cell densities used for different cell lines for BrDU assay.

Cell line	Cell density for BrDU assay	Time of incubation before assay
Panc02	4000	72 hours
Capan1	10000	72 hours
Panc8680	5000	72 hours
BxPC3	10000	72 hours
AsPC1	10000	72 hours

Tab. 8: BrDU assay conditions and seeding densities for different PDAC cell lines.

4.3 Animal experiments

The animals were housed according to international standard conditions with a 12 hrs dark, 12 hrs light cycle and regular unrestricted diet if not stated otherwise. Animal handling and experimentation was performed in accordance with NIH guidelines and approved by local authorities (Regierungspräsidium Karlsruhe). Blood was taken after cervical dislocation. Tissues including tumors, and fat pads were collected, weighed, snap-frozen in liquid nitrogen and used for further analysis.

Obesity models

8-12 week old ob/ob, or db/db mice were obtained from Charles River Laboratories (Brussels, BEL) and maintained on a 12 hrs light-dark cycle with regular unrestricted diet. All mice were procured from Jackson labs. Following are the ordering details:
db/db mice: B6.BKS. (D)-Lepr^{db}/J (#000697)
ob/ob mice: B6.Cg-Lep^{ob}/J (#000632
wt control mice: C57BL/6J (#000664)

Mice for SC tumor implantation

Male wt C57Bl6/J purchased from Charles River or C57Bl6/J mice from Barrier 2 within DKFZ at the age of 6-8 weeks were used for SC Panc02 tumor implantations.

Mice for isolation of primary preadipocytes

Male wt C57Bl6/J purchased from Charles River at the age of 6-9 weeks were used for the isolation of primary preadipocytes.

Adipocyte specific TBLR1 knockout mice

Adipocyte specific TBLR1 knockout mice were generated on C57Bl6 background (C57BL/6-Tbl1xr1(tm2273Arte) Tg(Fabp4-Cre)1Rev) by TaconicArtemis as described in 'Results'. Adipocyte specific

knockout was assessed by Southern Blot in various tissues with probes created by primers shown in 'Materials'.

Body composition analysis using Echo MRI

Mice were weighed and body composition was determined using magnetic resonance (Echo MRI, Echo Medical Systems, Houston).

Blood serum

Blood serum was obtained by incubation of blood samples at room temperature for 30 min and subsequent centrifugation for 1 hr at 3,000 rpm, 4°C. The serum (upper phase) was transferred to a new tube and stored at -80°C.

Tumor luminescence measurement and imaging using IVIS

The IVIS (**I**n **V**ivo **I**maging **S**ystem) was used to measure luminescence signal from luciferase expressing subcutaneous Panc02 tumors. The C57Bl6/J mice with tumors were gently shaved a day prior to imaging to prevent high background signal from black fur. On the day of imaging, the computer was turned on, and the camera was allowed to cool after opening the imaging software. The isoflurane level was visually checked and if less, was filled manually. The pump and oxygen supply were turned on. The mice were intraperitoneally injected with 10 μl/g of luciferase solution from a stock solution of 15mg/ml. They were placed in an anesthetizing chamber with 3% vaporized isoflurane for few minutes until unconscious. At any given point of time, only three mice could be imaged simultaneously, so they were staggered and treatment groups were measured side by side for comparison. They were carefully placed with the tumors facing up, inside the imaging chambers and the isoflurane level was reduced to 1%. Even while imaging, the mice were remained anesthetized as they were placed adjacent to nozzles supplying 1% isoflurane. Luminescence signal was measured and it was a direct measure of the tumor size. The instrument's camera needed time to cool down, and always stayed on as per manufacturer's instruction.

Glucose tolerance test

In a glucose tolerance test, glucose is injected in the peritoneum of fasted mice and blood samples are taken to determine how quickly the sugar can be cleared from the blood. Improved insulin signaling results in lower glucose levels as the sugar load induces a better clearance from the blood stream. Mice were fasted for 16 hrs prior to the experiment. The animals were transferred into fresh cages equipped with fresh water but no food. The following morning, the body weight and the initial blood glucose levels were determined by nicking the tail with a razor blade. Blood glucose was measured using a glucometer strip.

10 µl/g body weight of a 20% glucose solution were then injected intraperitoneally. Blood glucose was measured before injection and 20, 60, and 120 min after injection.

4.4 Biochemistry

Preparation of protein extracts

Cell lysis using RIPA Buffer

Cells were washed once with PBS, followed by addition of RIPA buffer supplemented with protease and phosphatase inhibitor. The plates were placed on ice for 30 minutes to promote complete lysis. Then the cells were scraped with a cell scraper and transferred to Eppendorf tubes. For viscous cell lysates, sonication was performed additionally to completely lyse the cells. Then, an appropriate volume of 2 x SDS sample buffer was added and the samples were boiled for 10 min at 95°C and stored at -20°C until further use.

Protein extracts from tissue samples

Protein extracts from tissue samples were prepared using the Tissue Lyser. Frozen tissue pieces or powder were transferred to 2 ml safe lock tubes containing ice-cold protein lysis buffer A containing protease and phosphatase inhibitors and a pre-cooled steel bead. The samples were immediately homogenized using the Tissue Lyser for 2 min at 30 Hz. The extracts were incubated on a rotating wheel for 1 hour and then transferred to fresh tubes (if using adipose tissues, the fat remains in the old tube). Then, extracts were supplemented with high salt supplement buffer and incubated for an additional hour on the wheel at 4°C. The protein concentration was determined using the BCA kit (Pierce) and samples were diluted in 5x SDS sample buffer and boiled for 10 min at 95°C.

Determination of Protein Concentration

Protein concentrations were determined using the BCA kit (Pierce) following the manufacturer's instructions. If SDS concentration of the samples was higher than 0.1 %, protein concentration had to be determined using the 2D-Quant kit (Amersham Biosciences) following the manufacturer's instructions. All measurements were performed in duplicates within the linear range of the BSA standard curves (0.1-2 mg/ml).

SDS Polyacrylamide Gel Electrophoresis (SDS-PAGE) and Immunoblotting

Protein samples in SDS sample buffer were loaded onto 6-12 % SDS-polyacrylamide gels and blotted onto nitrocellulose membranes using a wet blot system. Blotting was performed at 80 V for 70 minutes or 30 V overnight in transfer buffer. Membranes were subsequently blocked by incubation in 5% milk or 5% BSA dissolved in PBS-T/TBS-T for 1 hour. Primary antibodies diluted in 5 % milk, were incubated with the

membranes overnight at 4°C. The membranes were washed with PBS-T/TBS-T, the next day and incubated with the secondary antibody conjugated to horse radish peroxidase (HRP) at a dilution of 1:5000 for 1 hr. To detect specific bands, the enhanced chemiluminescence system (ECL) Western Blotting Detection Reagent was applied. The chemiluminescent signal produced by the blots was detected with the ChemiDoc detector (BioRad). Exposure times differed based on the quality of specific antibodies and protein concentrations. The results were quantified using the Image Lab software.

Determination of Free Fatty Acid Levels

Free Fatty Acids were determined in serum samples or cell supernatants using a colorimetric assay from WAKO (NEFA kit) following the manufacturer's instructions. 4 µl of serum samples or 20 µl of cell supernatants were measured in duplicates. A standard curve was determined using a dilution series of oleic acid. OD-values were determined at 540 nm.

Determination of Glycerol Levels

Glycerol content of serum or cell supernatants was measured using a calorimetric assay. The Free Glycerol component of the serum TG determination kit from Sigma was used for this assay. 4 µl of serum or 20 µl of supernatants were transferred to a 96well plate, 100 µl Free Glycerol Reagent were added and glycerol levels were measured at 540 nm against a glycerol standard.

Determination of Triglyceride Levels

TG levels were determined by separating TGs into one glycerol and three fatty acid molecules and measuring the glycerol using a colorimetric assay. The serum TG determination kit from Sigma was used for this assay. 4 µl of isolated hepatic TG, 4 µl of serum or 20 µl of cell supernatants were transferred to a 96well plate. In order to determine a blank value, 100 µl Free Glycerol Reagent were added to each well and the plate was incubated at 37°C for 5 min. Free glycerol levels were measured at 540 nm. In a second reaction (assay), 100 µl TG Reagent were added. This mixture contains the enzyme lipase, which catalyzes the release of fatty acids from TGs. Plates were incubated at 37°C for 5 min and measured at 540 nm. TG content (TG-bound glycerol) was determined by subtracting the free glycerol (blank) from the second measurement of total glycerol (assay).

Determination of Blood Glucose Levels

Blood glucose levels were determined using a drop of blood obtained from the tail vein and an automatic glucose monitor (One Touch, Lifescan).

4.5 Statistical Analysis

Statistical analyses were performed in GraphPad Prism 7 software, using a 1- or 2-way ANOVA (analysis of variance) with Bonferroni-adjusted post-tests, or t-test with one-factorial designs, respectively. A p value of < 0.05 was considered statistically significant. $*p < 0.05$, $**p < 0.01$, $***p < 0.001$.

5 MATERIAL

5.1 Instruments and equipment

Instrument/Equipment	Model	Company
Aspiration adaptor, 8-channel	Heraeus Function Line	Neolab (Heidelberg, Germany)
Bacterial Incubator		ThermoFisher Scientific (Schwerte, Germany)
Bacterial shaking incubator	Multitron Standard	Infors HT (Bottmingen, Switzerland
Balance	EW 2200-NM	Kern and Sohn (Balingen, Germany)
Bunsen Burner	Labogaz 206	Campingaz (Hattersheim, Germany)
Cell counter, automated	Countess™	Life Technologies™, Invitrogen™ (Darmstadt, Germany)
Cell culture hood	Cellgard Class II Biological safety cabinet	IBS Integrad Biosciences (Fernwald, Germany)
CO_2 incubator		Sanyo (Etten Leur, The Netherlands)
Counting chamber	BLAUBRAND®, Neubauer improved, Cat. No. 717805	Brand (Wertheim, Germany)
Digital Caliper		Bochem (Weilburg, Germany)
Echo MRI™ Whole Body Composition Analyser		Echo medical systems (Housten, TX, USA)
Fluorescence lamp for microscope	HXP 120C	Carl Zeiss (Oberkochen, Germany)
Fluorometer	QubitR 2.0	Life Technologies™, Invitrogen™ (Darmstadt, Germany)
Freezer (-20^{0}C)		Liebherr (Biberach, Germany)
Freezer, ultra-low temperature (-80^{0}C)	New Brunswick U101 Innova	Eppendorf (Hamburg, Germany)
Freezing Container	Mr. Frosty™, 5100-0001	ThermoFisher Scientific (Schwerte, Germany)
Gas anaesthesia system	XGI-8	Caliper Lifesciences (Rodgau, Germany)
Glucometer	OneTouch^R Ultra	Lifescan (Neckargemünd, Germany)
Immunoblot documentation	ChemiDoc™ XRS+Molecular Imager® with ImageLab™ Software	Biorad (München, Germany)
IVIS^R Optical Imaging System	Lumina II	Caliper LifeSciences (Rodgau, Germany)
LED Fluorescence Lamp for Axio Imager.M2	Colibri.2	Carl Zeiss (Oberkochen, Germany)
Magnetic stirrer	MR 30001 K	Heidolph (Schwabach, Germany)
Magnetic stirrer	Duomax 1030	Heidolph (Schwabach, Germany)
Magnetic stirrer	444-7076	VWR (Darmstadt, Germany)
Microscope	Axio ImagerM.2 with AxioCam HRc	Carl Zeiss (Oberkochen, Germany)
Microscope	Axiovert 40 CFL with AxioCam ICm1	Carl Zeiss (Oberkochen, Germany)

Instrument/Equipment	Model	Company
Microscope, automated	Olympus Cell^R	Olympus (Hamburg, Germany)
Microplate reader	Mithras LB 940	Berthold Technologies (Bad Wildbad, Germany)
Microplate reader, Varioscan LUX	Multimode	ThermoFisher Scientific (Schwerte, Germany)
Micropipette 0.2-2 µl	P2	Gilson (Limburg.Offheim, Germany)
Micropipette 1-10 µl	P10	Gilson (Limburg.Offheim, Germany)
Micropipette 2-20 µl	P20	Gilson (Limburg.Offheim, Germany)
Micropipette 10-100 µl	P100 N	Gilson (Limburg.Offheim, Germany)
Micropipette 50-200 µl	P200	Gilson (Limburg.Offheim, Germany)
Micropipette 100-200 µl	P1000	Gilson (Limburg.Offheim, Germany)
Micropipette, 8-channel, 0.5-10 µl	Research plus	Eppendorf (Hamburg, Germany)
Micropipette, 8-channel, 10-100 µl	Research	Eppendorf (Hamburg, Germany)
Microtome	RM2245	Leica (Wetzlar, Germany)
Microwave	700 W	Severin (Sundern, Germany)
Mouse cage system	Green Line IVC SealSafePlus	Tecniplast (Hohenpeißenberg, Germany)
Mouse housing cabinet, ventilated		Tecniplast (Hohenpeißenberg, Germany)
Mutistep pipette	Multipette® plus	Eppendorf (Hamburg, Germany)
Mutistep pipette	Multipette® M4	Eppendorf (Hamburg, Germany)
Nanodrop	ND-1000	ThermoFisher Scientific (Schwerte, Germany)
Orbital shaker	Duomax 1030	Heidolph (Schwabach, Germany)
pH meter	Qph 70	GHM Messtech, Greisinger (Regenstauf, Germany)
Pipetboy	acu	Integra (Fernwald, Germany)
Power supply for gel electrophoresis	PowerPac Basic™	Bio-Rad (München, Germany)
Power supply for Axio ImagerM.2	232	Carl Zeiss (Oberkochen, Germany)
Precision Balance	M-power AZ124	Sartorius (Göttingen, Germany)
Real-time PCR system	StepOnePlus	Life Technologies™, Invitrogen™ (Darmstadt, Germany)
Refrigerator (2-8 °C)		Liebherr (Biberach, Germany)
Rotating Wheel		Neolab (Heidelberg, Germany)
Sonicator	Bioruptor® Plus	Diagenode (Seraing, Belgium)
Tabletop centrifuge	Mikro 22R	Hettich (Newport Pagnell, United Kingdom)
Tabletop centrifuge	Heraeus Fresco 17	ThermoFisher Scientific (Schwerte, Germany)
Tabletop centrifuge	Heraeus Biofuge pico	ThermoFisher Scientific (Schwerte, Germany)
Tabletop centrifuge	Heraeus Biofuge primo	ThermoFisher Scientific (Schwerte, Germany)
Thermomixer	Comfort	Eppendorf (Hamburg, Germany)
Thermocycler	T3000	Biometra (Göttingen, Germany)
Tissue grinder (all-glass)	Dounce 7 mL	Kimble Chase (Meiningen, Germany)
Tissue Lyser	MM 400	Retsch (Hahn, Germany)
Titer plate shaker		ThermoFisher Scientific (Schwerte, Germany)
Vortex mixer	Genie	Scientific Industries (Bohemia, NY, USA)

Instrument/Equipment	Model	Company
Water bath		P-D Industriegessellschaft (Dresden, Germany)
Water filter system	TKA xCAD	ThermoFisher Scientific (Schwerte, Germany)

5.2 Consumables

Product	Company	Cat. No.
Cell scraper	Corning (Wiesbaden, Germany)	3010
Chamber slide, 8-well, Nunc-Lab-Tek	ThermoFisher Scientific (Schwerte, Germany)	177445
0.2 mL Combitips advanced®	Eppendorf (Hamburg, Germany)	0030 089.413
0.5 mL Combitips advanced®	Eppendorf (Hamburg, Germany)	0030 089.421
0.5 mL Combitips advanced®, sterile		0030 089.634
5 mL Combitips advanced®	Eppendorf (Hamburg, Germany)	0030 089.456
5 mL Combitips advanced®, sterile	Eppendorf (Hamburg, Germany)	0030 089.669
10 mL Combitips advanced®	Eppendorf (Hamburg, Germany)	0030 089.464
10 mL Combitips advanced®	Eppendorf (Hamburg, Germany)	0030 089.667
Countess™ cell counting chamber slides	Life Technologies™, Invitrogen™ (Darmstadt, Germany)	C10283
Cover slips 24X60 mm #1	Menzel (Braunschweig, Germany)	BB024060A1
2 mL cryogenic vials	StarLab (Hamburg, Germany)	E3110-6122
1.5 mL DNA LoBind tubes	Eppendorf (Hamburg, Germany)	0030 108.051
500 mL Filter system 0.22 um, polystyrene, nonpyrogenic	Corning (Wiesbaden, Germany)	430758
10 uL filter tip, graduated	StarLab (Hamburg, Germany)	S1121-3810
20 uL filter tip, graduated	StarLab (Hamburg, Germany)	S1120-1810
100 uL filter tip, graduated	StarLab (Hamburg, Germany)	S1120-1840
200 uL filter tip, graduated	StarLab (Hamburg, Germany)	S1120-8810
1000 uL filter tip, graduated	StarLab (Hamburg, Germany)	S1126-7810
Folded filters	Munktell (Bärenstein, Germany)	4.303.280
Genechip® Mouse Genome 430 2.0 Array	Affymetrix (High Wycombe, United Kingdom)	900496
Glucose test strips, One Touch® Ultra	Lifescan (Neckargemünd, Germany)	-
Histology casettes	NeoLab (Heidelberg, Germany)	7-0014
Imaging plate, 96-well clear bottom black wall	BD Falcon™ (Heidelberg, Germany)	353219
Injection needle Sterican® 0.4 X 20mm (27G)	B.Braun (Melsungen, Germany)	4657705
Inoculation loops 1 uL	Sarstedt (Nümbrecht, Germany)	86.1567.050
Insulin syringes, Micro-Fine™+ Demi, 0.3 mL	BD Medical (Heidelberg, Germany)	324826
MicroAmp® Optical Adhesive Film for qPCR	LifeTechnologies™, Applied Biosystems® (Darmstadt, Germany)	4311971

Product	**Company**	**Cat. No.**
Microtiter plate, 96-well (Nunc F96)	ThermoFisher Scientific (Schwerte, Germany)	260836
Nitrocellulose membrane, Protran BA 85, 0.45 um	GE Healthcare (Solingen, Germany)	10401196
Parafilm® M	Bemis® (Neenah WI, USA)	PM-996
Pasteur pipette, glass, long	WU Mainz (Bamberg, Germany)	
PCR Tubes, 8 strips, 0.2 mL	Greiner Bio-one (Frickenhausen, Germany)	673210
PCR tube lids, flat, 8 strip	Greiner Bio-one (Frickenhausen, Germany)	373250
Petri dish for Agar plates	Greiner Bio-one (Frickenhausen, Germany)	632180
10 uL Pipette tip	StarLab (Hamburg, Germany)	S1111-3700
200 uL Pipette tip	Steinbrenner Laborsysteme (Wiesenbach, Germany)	Tip-Tower Refill System
1000 uL Pipette tip	Steinbrenner Laborsysteme (Wiesenbach, Germany)	Tip-Tower Refill System
0.1 -10 uL pipette tips, ep T.I.P.S. ® LoRetention	Eppendorf (Hamburg, Germany)	0030 072.006
0.5-20 uL pipette tips, ep T.I.P.S. ® LoRetention	Eppendorf (Hamburg, Germany)	0030 072.014
1-200 uL pipette tips, ep T.I.P.S. ® LoRetention,	Eppendorf (Hamburg, Germany)	0030 072.022
50-1000 uL pipette tips, ep T.I.P.S. ® LoRetention,	Eppendorf (Hamburg, Germany)	0030 072.030
15 mL polypropylene centrifuge tubes	Greiner Bio-one (Frickenhausen, Germany)	188271
50 mL polypropylene centrifuge tubes	Greiner Bio-one (Frickenhausen, Germany)	227261
1.5 mL RNase-free centrifuge tubes, Multi® Safe Seal	Carl Roth (Karlsruhe, Germany)	AA80
14 mL round- bottom snap-cap tubes, polypropylene	BD Falcon™ (Heidelberg, Germany)	352059
1.5 mL safe-lock tube	Eppendorf (Hamburg, Germany)	0030 120.086
2 mL safe-lock tube	Eppendorf (Hamburg, Germany)	0030 120.094
5 mL safe-lock tube	Eppendorf (Hamburg, Germany)	0030 119.460
Scalpel, disposable, sterile, No. 21	Feather (Osaka, Japan)	
5 mL serological pipettes	BD Falcon™ (Heidelberg, Germany)	357543
10 mL serological pipettes	BD Falcon™ (Heidelberg, Germany)	357551
25 mL serological pipettes	BD Falcon™ (Heidelberg, Germany)	357525
50 mL serological pipettes	BD Falcon™ (Heidelberg, Germany)	357550
5 mL skirted tube	VWR (Darmstadt, Germany)	216-0153
Stainless steel beads, 5 mm	Qiagen (Hilden, Germany)	69989
1 mL syringe, Soft-Ject® Tuberkulin	Henke Sass Wolf (Tuttlingen, Germany)	5010-200V0
5 mL syringe	BD (Heidelberg, Germany)	309050
20 mL syringe	BD (Heidelberg, Germany)	300629
50 mL syringe	BD (Heidelberg, Germany)	300865
10 cm tissue culture plate	BD Falcon™ (Heidelberg, Germany)	353003
15 cm tissue culture plate	BD Falcon™ (Heidelberg, Germany)	353025
Tissue culture plate, 6-well	BD Falcon™ (Heidelberg, Germany)	353046
Tissue culture plate, 24-well	BD Falcon™ (Heidelberg, Germany)	353047
Tissue culture plate, 48-well	BD Falcon™ (Heidelberg, Germany)	353230

Product	Company	Cat. No.
Waste bags 200 X 300 mm	Carl Roth (Karlsruhe, Germany)	E706.1
Weigh boats 41 X 41 mm	Neolab (Heidelebrg, Germany)	1-1124
Weigh boats 89 X 89 mm	Neolab (Heidelebrg, Germany	1-1125
Whatman™ paper	GE Healthcare (Solingen, Germany)	3030 917

5.3 Kits

Product	Company	Cat. No.
BrDU Cell prliferation kit	Cell Signaling Technology	6813S
Click-iT® EdU Imaging Kit	LifeTechnologies™, Applied Biosystems® (Darmstadt, Germany)	C10338
CCK-8 assay kit	Sigma-Aldrich (München, Germany)	96992
DNase Set, Rnase-free	Qiagen (Hilden, Germany)	1023460
Enhanced Chemiluminescence (ECL) kit	Amersham Biosciences (Freiburg, Germany)	-
First strand cDNA synthesis kit, Fermentas	ThermoFisher Scientific (Schwerte, Germany)	K1612
Glucose (HK) assay kit	Sigma-Aldrich (München, Germany)	GAHK20-1KT
HR Series NEFA-HR (2) kit	Wako Diagnostics (Neuss, Germany)	276-76491
Pierce® BCA Protein assay kit	ThermoFisher Scientific (Schwerte, Germany)	23225
PureLink HiPure Plasmid Maxiprep kit	LifeTechnologies™, Invitrogen™ (Darmstadt, Germany)	K2100-06
RNeasy® Mini Kit	Qiagen (Hilden, Germany)	74106
Serum Triglyceride determination kit	Sigma-Aldrich (München, Germany)	TR0100
Superscript® Choice System for cDNA synthesis	LifeTechnologies™, Invitrogen™ (Darmstadt, Germany)	18090-019

5.4 Enzymes

Product	Company	Cat. No.
Collagenase type I	Sigma-Aldrich (München, Germany)	-
Proteinase K	ThermoFisher Scientific (Schwerte, Germany)	EO0491
RNase A 10 mg/mL	ThermoFisher Scientific (Schwerte, Germany)	EN0531

5.5 Plasmids

Product	Company	Cat. No.
Mission® shRNA Plasmid DNA, leptin receptor, mouse	Sigma-Aldrich (München, Germany)	SHCLND-NM_010704
Mission® shRNA Plasmid DNA, leptin receptor, human	Sigma-Aldrich (München, Germany)	SHCLND-NM_002303
pLKO.1-shRNA-scrambled	Addgene (Cambridge, MA, USA)	1864
pMD2.G	Addgene (Cambridge, MA, USA)	12259
psPAX2	Addgene (Cambridge, MA, USA)	12260

5.6 Chemicals and reagents

Product	Company	Cat. No.
Acetic acid	Sigma-Aldrich (München, Germany)	45731
Acrylamide/bis-acrylamide 37.5:1, 40% (Rotiphorese Gel 40 (37.5:1))	Carl Roth (Karlsruhe, Germany)	T802.1
Agarose	Carl Roth (Karlsruhe, Germany)	3810
Alexa Fluor 555, triethylammonium salt	Life Technologies™, Molecular Probes® (Darmstadt, Germany)	A20012
Ampicillin sodium salt	Sigma-Aldrich (München, Germany)	A9518
Antibody diluent, Background reducing	Dako (Hamburg, Germany)	X0590
APS (Ammonium persulfate)	Carl Roth (Karlsruhe, Germany)	9592
β-Mercaptoethanol	Sigma-Aldrich (München, Germany)	M7154
Biotin-blocking system (0.1% avidin solution and 0.01% biotin solution)	Dako (Hamburg, Germany)	X0590
Boric acid (H_3BO_3)	Sigma-Aldrich (München, Germany)	31146
Bromophenol blue, sodium salt	Sigma-Aldrich (München, Germany)	114405
BSA for cell culture: Albumin solution from bovine serum, 30% DPBS, sterile-filtered	Sigma-Aldrich (München, Germany)	A9576
BSA for immunoblotting and EdU assay: Albumin bovine Fraction V	Biomol (Hamburg, Germany)	01400.100
BSA fatty acid free	Sigma-Aldrich (München, Germany)	A8806
$CaCl_2$ (Calcium Chloride)	Carl Roth (Karlsruhe, Germany)	CN93
Chloroform ($CHCl_3$)	Carl Roth (Karlsruhe, Germany)	3313
CuSO4 (copper (II) sulfate petahydrate)	Sigma-Aldrich (München, Germany)	209198
DEPC (Diethylpyrocarbonate)	Sigma-Aldrich (München, Germany)	D5758
DMEM High Glucose Pyruvate (+ L-glutamine)	Life Technologies™, Gibco® (Darmstadt, Germany)	41966-029
DMEM Low Glucose Pyruvate (+ L-glutamine)	Life Technologies™, Gibco® (Darmstadt, Germany)	31885-023
DMSO (Dimethylsulfoxide) sterile for cell culture	Sigma-Aldrich (München, Germany)	D2650
DNA marker, Gene ruler, 100bp	ThermoFisher Scientific (Schwerte, Germany)	SM0241
DPBS, no $CaCl_2$, no $MgCl_2$	Life Technologies™, Gibco® (Darmstadt, Germany)	14190-094
DPBS 10x, no $CaCl_2$, no $MgCl_2$	Life Technologies™, Gibco® (Darmstadt, Germany)	14200-067
DTT (Dithiothreitol)	Applichem (Darmstadt, Germany)	A2948
EdU (5-ethynyl-2'-deoxyuridine)	Life Technologies™, Molecular Probes® (Darmstadt, Germany)	A10044
EGTA (Ethylene gycol-bis(2-aminoethylether)-*N,N,N',N'*-tetraaceticacid	Sigma-Aldrich (München, Germany)	E4378
Ethanol ≥ 99.8 %, denatured with approx. 1% methyl ethyl ketone (for histology)	Carl Roth (Karlsruhe, Germany)	K928
Ethanol, absolute	Sigma-Aldrich (München, Germany)	32205
Ethidium bromide solution, 1% / 10 mg/mL	Carl Roth (Karlsruhe, Germany)	2218

Product	**Company**	**Cat. No.**
Fetal bovine serum (FBS), US origin	Life Technologies™, Gibco® (Darmstadt, Germany)	26400-036
Fluorescent mounting medium	Dako (Hamburg, Germany)	S3023
Formaldehyde solution 37%	J.T. Baker (Deventer, The Netherlands)	7040
Formamide	Merck KGaA, Calbiochem (Darmstadt, Germany)	344206
Gemcitabine 40 mg/mL	HEXAL®	-
D-Glucose anhydrous	Applichem (Darmstadt, Germany)	A0883
Glycerol	Sigma-Aldrich (München, Germany)	15523
Glycine	Sigma-Aldrich (München, Germany)	33226
HEPES Buffer solution, 1M	Life Technologies™, Gibco® (Darmstadt, Germany)	15630-056
H_2O_2 (Hydrogen peroxide) solution, 30%	Merck KGaA, Calbiochem (Darmstadt, Germany)	1.07209
HCl (Hydrochloric acid) 37%	Sigma-Aldrich (München, Germany)	30721
Hoechst 33342, trihydrochloride trihydrate, 10 mg/mL	Life Technologies™, Molecular Probes® (Darmstadt, Germany)	H3570
IBMX (Isobutyl methylxanthine)	Sigma-Aldrich (München, Germany)	
IGEPAL® CA-630 (NP40 substitute)	Sigma-Aldrich (München, Germany)	56741
Imidazole	Merck KGaA, Calbiochem (Darmstadt, Germany)	4716
Insulin human recombinant expressed in yeast	Sigma-Aldrich (München, Germany)	I2643
Isoflurane	Baxter (Unterschleißheim, Germany)	I7403
KCl (Potassium chloride)	Carl Roth (Karlsruhe, Germany)	A137
KH_2PO_4 (Potassium dihydrogen phosphate)	Carl Roth (Karlsruhe, Germany)	3904
LB-Agar (Luria/Miller)	Carl Roth (Karlsruhe, Germany)	X969
LB-Medium (Luria/Miller)	Carl Roth (Karlsruhe, Germany)	X968
Lipofectamine® 2000 Transfection Reagent	Life Technologies™, Invitrogen™ (Darmstadt, Germany)	11668-019
Liquid DAB+ chromogen and substrate buffer	Dako (Hamburg, Germany)	K3468
$MgCl_2.6H_2O$ (magnesium chloride hexahydrate)	Sigma-Aldrich (München, Germany)	M9272
$MgSO_4.7H_2O$ (magnesium sulfate heptahydrate)	Applichem (Darmstadt, Germany)	A4101
Milk powder, skim milk extra grade	Gerbu (Heidelberg, Germany)	1602
MOPS (3-(*N*-morpholino)propanesulfonicacid	Sigma-Aldrich (München, Germany)	M3183
Mouse recombinant leptin	Peprotech	
Na_2HPO_4. $2H_2O$ (di-sodium hydrogenphoshate dehydrate)	Sigma-Aldrich (München, Germany)	30412
Na_3VO_4 (sodium orthovanadate)	Sigma-Aldrich (München, Germany)	S6508
NaCl (sodium chloride)	Sigma-Aldrich (München, Germany)	31434
NaF (sodium flouride)	Sigma-Aldrich (München, Germany)	S1504
$NaHCO_3$. $10H_2O$	Merck KGaA, Calbiochem (Darmstadt, Germany)	6391
NaOH (sodium hydroxide)	Sigma-Aldrich (München, Germany)	30620
Opti-MEM® I Reduced Serum Medium	Life Technologies™, Gibco® (Darmstadt, Germany)	31985-047
PageRuler™ prestained protein ladder	ThermoFisher Scientific (Schwerte, Germany)	26616

Product	Company	Cat. No.
Penicillin-streptomycin, liquid, 100x	Life Technologies™, Gibco® (Darmstadt, Germany)	15140-122
PMSF (phenylmethanesulfonyl fluoride)	Sigma-Aldrich (München, Germany)	P7626
Polybrene (hexadimethrine bromide)	Sigma-Aldrich (München, Germany)	H9268
Poly-L-Lysine hydrobromide	Sigma-Aldrich (München, Germany)	P2636
Ponceau S solution 0.1% in 5% acetic acid	Sigma-Aldrich (München, Germany)	P7170
Protease inhibitor cocktail	Sigma-Aldrich (München, Germany)	P8340
Protease inhibitor cOmplete	Roche (Mannheim, Germany)	04693116001
Protease inhibitor cOmplete, EDTA free	Roche (Mannheim, Germany)	04693132001
Puromycin	Sigma-Aldrich (München, Germany)	P8833
Pyruvate 100mM, 100x	Life Technologies™, Gibco® (Darmstadt, Germany)	11360-039
Qiazol lysis reagent	Qiagen (Hilden, Germany)	
RiboLock Ribonuclease Inhibitor	Fermentas, St. Leon Rot	
Roti®-Histofix 4% acetic acid free (pH 7.0), phosphate buffered formaldehyde solution	Carl Roth (Karlsruhe, Germany)	P087
SDS (sodium dodecyl sulfate)	Sigma-Aldrich (München, Germany)	D6750
Sodium acetate anhydrous	Applichem (Darmstadt, Germany)	A1522
Sodium deoxycholate	Sigma-Aldrich (München, Germany)	D6750
Standard chow diet	Kliba Nafag (Kaiseraugst, Switzerland)	3437
Sucrose	Sigma-Aldrich (München, Germany)	S1888
Taqman® Gene Expression Master Mix	Life Technologies™, Applied Biosystems® (Darmstadt, Germany)	4369016
TEMED (*N,N,N',N'*-teramethylethane-1,2-diamine)	Carl Roth (Karlsruhe, Germany)	2367
Tris (tris(hydroxymethyl)aminomethane)	Sigma-Aldrich (München, Germany)	T1503
Triton® X-100	Applichem (Darmstadt, Germany)	A1388
Tryphan blue solution, 0.4%	Life Technologies™, Invitrogen™ (Darmstadt, Germany)	T10282
0.25% Trypsin-EDTA (1x), Phenol red	Life Technologies™, Gibco® (Darmstadt, Germany)	25200-056
Tween® 20	Sigma-Aldrich (München, Germany)	P9416
Water, nuclease free	Life Technologies™, Gibco® (Darmstadt, Germany)	10977-035
Xylene	Merck KGaA, Calbiochem (Darmstadt, Germany)	1.08681

5.7 Antibodies

5.7.1 Primary Antibodies

Protein	Company	Cat. No.	Origin
AKT	Cell Signaling	9272	rabbit
β-Actin	Sigma	A5441	mouse
Caspase-3	Cell Signaling	9662	rabbit
Cleaved Caspase-3	Cell Signaling	9664S	rabbit

Protein	Company	Cat. No.	Origin
Cleaved PARP	Cell Signaling	9544S	mouse
CyclinD1	Cell Signaling	2926	mouse
Ki67	Dako	M7279	mouse
PARP	Cell Signaling	9542	rabbit
Phospho-AKT	Cell Signaling	9271	rabbit
Phospho-Histone H2A.X	Cell Signaling	9718	rabbit
Phospho-STAT3	Cell Signaling	9138S	mouse
p53	Cell Signaling	2524S	mouse
STAT3	Cell Signaling	12640S	rabbit
TBL1XR1	Novus Biologicals	NB600-270	rabbit
TBL1XR1	Abnova	H00079718-M01	mouse
β-Actin	Sigma	A5441	mouse
VCP	Abcam	11433	Mouse

5.7.2 Secondary Antibodies

Protein	Company	Origin
Anti-mouse IgG-HRP	Bio-Rad, Munich	goat
Anti-rabbit IgG-HRP	Bio-Rad, Munich	goat
Anti-chicken IgG-HRP	Chemicon, #AP162P	rabbit
Anti-goat IgG-HRP	Sigma, #sc-2020	donkey

5.8 Software

Product	Company
AxioVision	Zeiss
Graphpad Prism 7	GraphPad Software Inc., La Jolla, USA
Inkscape	Adobe
ImageJ	Freeware
ImageLab	Biorad
Microsoft Office	Microsoft, Unterschleißheim
ND-1000	Nanodrop
Photoshop	Adobe, San Jose, USA
QuantityOne	Bio-Rad, Munich
StepOne Plus sytem Software	

5.9 Solutions and Buffers

All buffers were diluted in H_20, unless otherwise stated.

10X MOPS:
200mM MOPS, 50mM NaAc, 10mM EDTA, pH 7.0

10X PBS:
1.4 M NaCl, 27 mM KCl, 100 mM Na_2HPO_4, 8 mM KH_2PO_4, 8 mM KH_2PO_4, pH 6.8

2X SDS Sample Buffer
120mM Tris/HCl pH 6.8, 4% SDS, 20% glycerol, 200 mM DTT, 0.01% bromophenol blue

5X SDS Sample Buffer
250 mM Tris/HCl pH 6.8, 0.5 M DTT, 10% SDS, 50% glycerol, 0.01% bromophenol blue

ABP Stock
50 mg/mL L-Ascorbate, 1 mM b-Biotin, 17 mM Pantothenic acid

Blocking Buffer
1x PBS, 0.1% Tween 20, 5% Milk powder

Coomassie stain
4 parts Coomassie Colloidal Blue, 1-part methanol

Destain for Coomassie stained gels
25% Isopropanol, 10% Acetic acid

0.1% crystal Violet Solution
1 mL of 2.3% stock crystal violet solution in 23 mL Milli Q H_20

RIPA Buffer
50 mM Tris pH 8.0, 150 mM NaCl, 1% NP40, 0.5% SDS, 10% Sodium deoxycholate
Always add protease and phosphatase inhibitors fresh, right before use

Krebs-Ringer Buffer
115 mM NaCl, 5.9 mM KCl, 1.2 mM NaH_2PO_4, 1.2 mM Na_2SO_4, 25 mM $NaHCO_3$, Adjust pH to 7.4

LB medium
10 g/l Trypton, 5 g/l Yeast extract, 10 g/l NaCl, pH 7.0

Oil Red O Stock
0.7 g Oil Red O, 200 mL Isopropanol, Stirred Overnight, sterile filtered

Oil Red O Working Solution
6 parts Oil Red O Stock solution, 4 parts H_2O

PBS-T
1x PBS with 0.1% Tween 20

SDS gel fixation buffer
25% Isopropanol, 10% Acetic acid

SDS running buffer (10x)
0.25 M Tris, 1.92 M Glycin, 1% SDS

TBE Buffer (10x)
100 mM Tris, 1 mM EDTA, 90 mM Boric acid, pH 8.0

TE Buffer
1 mM EDTS, 10 mM Tris HCl, pH 8.0

Transfer Buffer
25 mM Tris, 192 mM Glycine, 20% Methanol, 0.01% SDS

6 APPENDIX

6.1 Glossary

Abbreviation	Expansion
ABD	Abdominal
ABP	L-ascorbate, d-biotin, pantothenic acid
ACM	Adipocyte conditioned media
ANGPT1	Angiopoietin 1
AKT	Protein kinase B (PKB)
ANOVA	Analysis of variance
ATKO	Adipocyte specific TBLR1 knockout
BAT	Brown adipose tissue
BMI	Basal metabolic index
bp	Base pairs
BSA	Bovine serum albumin
BW	Body weight
cDNA	Complementary DNA
CM	Conditioned media
CNS	Central nervous system
Contrl	Control
DBD	DNA binding domain
Dex	Dexamethasone
DNA	Deoxyribonucleic acid
DTT	Dithiothreitol
FABP	Fatty acid binding protein
FBS	Fetal bovine serum
FCM	Fibroblast conditioned media
FFA	Free fatty acid
GC	Gastronemius muscle
GFP	Green fluorescent protein
H2AX	H2A histone family, member X
HDAC	Histone deacetylase
HDL	High density lipoprotein
HEK	Human embryonic kidney
HFD	High fat diet
IBMX	3-isobutyl-1-methylxanthine
ING	Inguinal
Ifu	Infectious units
IL-6	Intereukin 6
ip	Intraperitoneal
IR	Insulin resistance
IRS2	Insulin receptor substrate
aWAT	Abdominal white adipose tissue
iWAT	Inguinal white adipose tissue
kd	Knockdown
kDa	Kilo daltons
LCN2	Lipocalin 2
LBP	Lipopolysaccharide binding protein
LEP	Leptin
LEPR	Leptin receptor
LFD	Low fat diet
MetS	Metabolic syndrome

Abbreviation	Expansion
MOI	Multiplicity of infection
mRNA	Messenger RNA
ml	Milli liter
mM	Milli molar
NEFA	Non-esterified fatty acids
nM	Nano molar
NR	Nuclear receptor
OD	Optical density
OE	Overexpression
p-	Phospho-
PDAC	Pancreatic ductal adenocarcinoma
p53	Tumor protein p53
P/S	Penicillin/Streptomycin
PBS	Phosphate buffered saline
PCR	Polymerase chain reaction
PKA	Protein kinase A
PPARγ	Peroxisome proliferator-activated receptor gamma
PPI	Protein phosphatase inhibitor
qPCR	Quantitative polymerase chain reaction
RNA	Ribonucleic acid
RXR	Retinoic acid receptor
SAA3	Serum amyloid A3
SC	Subcutaneous
SEM	Standard error of means
shRNA	Small hairpin RNA
siRNA	Small interfering RNA
SVF	Stromal vascular fraction
TBL1	Transducin beta like
TBLR1	Transducin beta like receptor 1
TBP	Thymine binding protein
TG	Triglyceride
TNFα	Tumor necrosis factor a
TZD	Thiazolidinedione
UCP1	Uncoupling protein 1
VCP	Valosin containing protein
WAT	White adipose tissue
WHO	World health organization
wt	Wild-type
β-AR	Beta adrenergic receptor
μl	Micro liter
μM	Micro molar

6.2 Figures and tables

6.2.1 Figures

6.2.2 Tables

6.3 References

[1] S. O'Neill and L. O'Driscoll, "Metabolic syndrome: A closer look at the growing epidemic and its associated pathologies," *Obes. Rev.*, vol. 16, no. 1, pp. 1–12, 2015.

[2] J. Kaur, "A comprehensive review on metabolic syndrome," *Cardiol. Res. Pract.*, vol. 2014, 2014.

[3] B. M. Popkin, L. S. Adair, and S. W. Ng, "NOW AND THEN: The Global Nutrition Transition: The Pandemic of Obesity in Developing Countries," *Nutr Rev*, vol. 70, no. 1, pp. 3–21, 2013.

[4] J. B. Dixon, C. W. Le Roux, F. Rubino, and P. Zimmet, "Bariatric surgery for type 2 diabetes," *Lancet*, vol. 379, no. 9833, pp. 2300–2311, 2012.

[5] A. Giordano, A. Frontini, and S. Cinti, "Convertible visceral fat as a therapeutic target to curb obesity.," *Nat. Rev. Drug Discov.*, 2016.

[6] C. M. Kusminski, P. E. Bickel, and P. E. Scherer, "Targeting adipose tissue in the treatment of obesity-associated diabetes," *Nat. Publ. Gr.*, 2016.

[7] S. M. Grundy, "Drug therapy of the metabolic syndrome: minimizing the emerging crisis in polypharmacy.," *Nat. Rev. Drug Discov.*, vol. 5, no. 4, pp. 295–309, 2006.

[8] E. K. J. Gallagher, D. LeRoith, "Cognitive rehabilitation following traumatic brain injury: assessment to treatment.," *Mt. Sinai J. Med.*, vol. 77, no. 2, pp. 511–523, 2010.

[9] I. Lemieux, "Abdominal obesity and metabolic syndrome," *Nature*, vol. 444, no. December, pp. 881–887, 2006.

[10] G. Boden, "Effects of free fatty acids (FFA) on glucose metabolism: significance for insulin resistance and type 2 diabetes," *Exp Clin Endocrinol Diabetes*, vol. 111, no. 3, pp. 121–124, 2003.

[11] M. Roden, T. B. Price, G. Perseghin, K. F. Petersen, D. L. Rothman, G. W. Cline, and G. I. Shulman, "Mechanism of free fatty acid-induced insulin resistance in humans," *J. Clin. Invest.*, vol. 97, no. 12, pp. 2859–2865, 1996.

[12] X. Ma and S. Zhu, "Metabolic syndrome in the prevention of cardiovascular diseases and diabetes--still a matter of debate?," *Eur. J. Clin. Nutr.*, vol. 67, no. 5, pp. 518–21, 2013.

[13] and R. J. B. Christian K.Roberts, Andrea L.Hevener, "Metabolic Syndrome and Insulin Resistance: Underlying Causes and Modification by Exercise Training," *Compr Physiol*, vol. 3, no. 1, pp. 1–58, 2014.

[14] E. D. Rosen and B. M. Spiegelman, "Adipocytes as regulators of energy balance and glucose homeostasis.," *Nature*, vol. 444, no. 7121, pp. 847–853, 2006.

[15] S. S. Choe, J. Y. Huh, I. J. Hwang, J. I. Kim, and J. B. Kim, "Adipose Tissue Remodeling: Its Role in Energy Metabolism and Metabolic Disorders," *Front. Endocrinol. (Lausanne).*, vol. 7, no. April, pp. 1–16, 2016.

[16] R. C. M. Van Kruijsdijk, E. Van Der Wall, and F. L. J. Visseren, "Obesity and cancer: The role of dysfunctional adipose tissue," *Cancer Epidemiol. Biomarkers Prev.*, vol. 18, no. 10, pp. 2569–2578, 2009.

[17] N. Ouchi, J. L. Parker, J. J. Lugus, and K. Walsh, "Adipokines in inflammation and metabolic disease," *Nat Rev Immunol*, vol. 11, no. 2, pp. 85–97, 2011.

[18] E. Arner, P. O. Westermark, K. L. Spalding, T. Britton, M. Ryde, J. Frise, S. Bernard, and P. Arner, "Adipocyte Turnover : Relevance to Human Adipose Tissue," *Diabetes*, vol. 59, no. January, pp. 105–109, 2010.

[19] K. L. Spalding, E. Arner, P. O. Westermark, S. Bernard, B. a Buchholz, O. Bergmann, L. Blomqvist, J. Hoffstedt, E. Näslund, T. Britton, H. Concha, M. Hassan, M. Rydén, J. Frisén, and P. Arner, "Dynamics of fat cell turnover in humans.," *Nature*, vol. 453, no. 7196, pp. 783–787, 2008.

[20] S. Nishimura, I. Manabe, M. Nagasaki, Y. Hosoya, H. Yamashita, H. Fujita, M. Ohsugi, K. Tobe, T. Kadowaki, R. Nagai, and S. Sugiura, "Adipogenesis in Obesity Requires Close Interplay Between Differentiating Adipocytes, Stromal Cells, and Blood Vessels," *Diabetes*, vol. 56, no. 6, pp. 1517–26, 2007.

[21] R. H. Unger and P. E. Scherer, "Gluttony, sloth and the metabolic syndrome: A roadmap to lipotoxicity," *Trends Endocrinol. Metab.*, vol. 21, no. 6, pp. 345–352, 2010.

[22] Y. Y. Zhang, R. Proenca, M. Maffei, M. Barone, L. Leopold, and J. M. Friedman, "Positional

Cloning of the Mouse Obese Gene and Its Human Homolog," *Nature*, vol. 372, no. 6505. pp. 425–432, 1994.

[23] Y. Zhang and P. J. Scarpace, "The role of leptin in leptin resistance and obesity," *Physiol. Behav.*, vol. 88, no. 3, pp. 249–256, 2006.

[24] J. E. Brown, "Dysregulated adipokines in the pathogenesis of type 2 diabetes and vascular disease," *Br. J. Diabetes Vasc. Dis.* , vol. 12 , no. 5 , pp. 249–254, 2012.

[25] Y. Arita, S. Kihara, N. Ouchi, M. Takahashi, K. Maeda, J. Miyagawa, K. Hotta, I. Shimomura, T. Nakamura, K. Miyaoka, H. Kuriyama, M. Nishida, S. Yamashita, K. Okubo, K. Matsubara, M. Muraguchi, Y. Ohmoto, T. Funahashi, and Y. Matsuzawa, "Paradoxical decrease of an adipose-specific protein, adiponectin, in obesity.," *Biochem. Biophys. Res. Commun.*, vol. 257, no. 1, pp. 79–83, 1999.

[26] a H. Berg, T. P. Combs, X. Du, M. Brownlee, and P. E. Scherer, "The adipocyte-secreted protein Acrp30 enhances hepatic insulin action.," *Nat. Med.*, vol. 7, no. 8, pp. 947–953, 2001.

[27] N. Kubota, Y. Terauchi, T. Yamauchi, T. Kubota, M. Moroi, J. Matsui, K. Eto, T. Yamashita, J. Kamon, H. Satoh, W. Yano, P. Froguel, R. Nagai, S. Kimura, T. Kadowaki, and T. Noda, "Disruption of adiponectin causes insulin resistance and neointimal formation," *J. Biol. Chem.*, vol. 277, no. 29, pp. 25863–25866, 2002.

[28] M. A. McArdle, O. M. Finucane, R. M. Connaughton, A. M. McMorrow, and H. M. Roche, "Mechanisms of obesity-induced inflammation and insulin resistance: Insights into the emerging role of nutritional strategies," *Front. Endocrinol. (Lausanne).*, vol. 4, no. MAY, pp. 1–23, 2013.

[29] L. Boutens and R. Stienstra, "Adipose tissue macrophages: going off track during obesity," *Diabetologia*, vol. 59, no. 5, pp. 879–894, 2016.

[30] N. Hosogai, A. Fukuhara, K. Oshima, Y. Miyata, S. Tanaka, K. Segawa, S. Furukawa, Y. Tochino, R. Komuro, M. Matsuda, and I. Shimomura, "Adipose tissue hypoxia in obesity and its impact on adipocytokine dysregulation," *Diabetes*, vol. 56, no. 4, pp. 901–911, 2007.

[31] J. Ye, Z. Gao, J. Yin, and Q. He, "Hypoxia is a potential risk factor for chronic inflammation and adiponectin reduction in adipose tissue of ob/ob and dietary obese mice.," *Am. J. Physiol. Endocrinol. Metab.*, vol. 293, no. 4, pp. E1118–E1128, 2007.

[32] S. Fujisaka, I. Usui, M. Ikutani, A. Aminuddin, A. Takikawa, K. Tsuneyama, A. Mahmood, N. Goda, Y. Nagai, K. Takatsu, and K. Tobe, "Adipose tissue hypoxia induces inflammatory M1 polarity of macrophages in an HIF-1??-dependent and HIF-1??-independent manner in obese mice," *Diabetologia*, vol. 56, no. 6, pp. 1403–1412, 2013.

[33] L. Dhiraj, Yadav, Albert B., "The Epidemiology of Pancreatitis and Pancreatic Cancer," vol. 144, no. 6, pp. 1252–1261, 2014.

[34] A. Manuscript, "Genetic Susceptibility to Pancreatic Cancer," vol. 51, no. 1, pp. 14–24, 2013.

[35] N. Bardeesy and R. a DePinho, "Pancreatic Cancer Biology and Genetics," *Nat. Rev.*, vol. 2, no. 12, pp. 897–909, Dec. 2002.

[36] J. Klapman and M. P. Malafa, "Early detection of pancreatic cancer: Why, who, and how to screen," *Cancer Control*, vol. 15, no. 4, pp. 280–287, 2008.

[37] A. B. Lowenfels, P. Maisonneuve, E. P. DiMango, Y. Elitsur, L. K. Gates, J. Perrault, and D. C. Whitcomb, "Hereditary Pancreatitis and the Risk of Pancreatic Cancer," *J. Natl. Cancer Inst.*, vol. 89, no. 6, pp. 442–6, 1997.

[38] B. Farrow and B. M. Evers, "Inflammation and the development of pancreatic cancer," *Surg. Oncol.*, vol. 10, no. 4, pp. 153–169, 2002.

[39] C. X. Xu, H. H. Zhu, and Y. M. Zhu, "Diabetes and cancer: Associations, mechanisms, and implications for medical practice," *World J. Diabetes*, vol. 5, no. 3, pp. 372–380, 2014.

[40] A. E. Becker, Y. G. Hernandez, H. Frucht, and A. L. Lucas, "Pancreatic ductal adenocarcinoma: Risk factors, screening, and early detection," *World J. Gastroenterol.*, vol. 20, no. 32, pp. 11182–11198, 2014.

[41] C. S. Fuchs, G. A. Colditz, M. J. Stampfer, E. L. Giovannucci, H. David J., E. B. Rimm, W. C. Willett, and F. E. Speizer, "A Prospective Study of Cigarette Smoking and the Risk of Pancreatic Cancer Charles," *Arch Intern. Med.*, vol. 156, pp. 2255–2260, 1996.

[42] M. Pericleous, R. E. Rossi, D. Mandair, T. Whyand, and M. E. Caplin, "Nutrition and pancreatic cancer," *Anticancer Res.*, vol. 34, no. 1, pp. 9–21, 2014.

[43] K. Y. Wolin, K. Carson, and G. A. Colditz, “Obesity and Cancer,” *Oncologist*, pp. 556–565, 2010.
[44] E. E. Calle, C. Rodriguez, K. Walker-Thurmond, and M. J. Thun, “Overweight, Obesity, and Mortality from Cancer in a Prospectively Studied Cohort of U.S. Adults,” *New Engl. J.*, vol. 348, no. 17, pp. 1625–1638, 2003.
[45] V. Rebours, S. Gaujoux, G. D’Assignies, A. Sauvanet, P. Ruszniewski, P. Lévy, V. Paradis, P. Bedossa, and A. Couvelard, “Obesity and fatty pancreatic infiltration are risk factors for pancreatic precancerous lesions (PanIN),” *Clin. Cancer Res.*, vol. 21, no. 15, pp. 3522–3528, 2015.
[46] I. Gukovsky, N. Li, J. Todoric, A. Gukovskaya, and M. Karin, “Inflammation, autophagy, and obesity: Common features in the pathogenesis of pancreatitis and pancreatic cancer,” *Gastroenterology*, vol. 144, no. 6, pp. 1199–209.e4, Jun. 2013.
[47] J. Incio, H. Liu, P. Suboj, S. M. Chin, I. X. Chen, M. Pinter, M. R. Ng, H. T. Nia, J. Grahovac, S. Kao, S. Babykutty, Y. Huang, K. Jung, N. N. Rahbari, X. Han, V. P. Chauhan, J. D. Martin, J. Kahn, P. Huang, V. Desphande, J. Michaelson, T. P. Michelakos, C. R. Ferrone, R. Soares, Y. Boucher, D. Fukumura, and R. K. Jain, “Obesity-induced inflammation and desmoplasia promote pancreatic cancer progression and resistance to chemotherapy,” *Cancer Discov.*, 2016.
[48] B. Philip, C. L. Roland, J. Daniluk, Y. Liu, D. Chatterjee, S. B. Gomez, B. Ji, H. Huang, H. Wang, J. B. Fleming, C. D. Logsdon, and Z. Cruz-Monserrate, “A high-fat diet activates oncogenic Kras and COX2 to induce development of pancreatic ductal adenocarcinoma in mice,” *Gastroenterology*, vol. 145, no. 6, pp. 1449–1458, Dec. 2013.
[49] S. Lanza-Jacoby, G. Yan, G. Radice, C. LePhong, J. Baliff, and R. Hess, “Calorie restriction delays the progression of lesions to pancreatic cancer in the LSL-KrasG12D; Pdx-1/Cre mouse model of pancreatic cancer.,” *Exp. Biol. Med. (Maywood).*, vol. 238, pp. 787–97, 2013.
[50] H. Wang, A. Maitra, and H. Wang, “Obesity, intrapancreatic fatty infiltration, and pancreatic cancer,” *Clin. Cancer Res.*, vol. 21, no. 15, pp. 3369–3371, 2015.
[51] Y. A. Bulynko and B. W. O’Malley, “Nuclear receptor coactivators: Structural and functional biochemistry,” *Biochemistry*, vol. 50, no. 3, pp. 313–328, 2011.
[52] D. J. Mangelsdorf and R. M. Evans, “The RXR heterodimers and orphan receptors,” *Cell*, vol. 83, no. 6, pp. 841–850, 1995.
[53] M. Anbalagan, B. Huderson, L. Murphy, and B. G. Rowan, “Post-translational modifications of nuclear receptors and human disease,” *Nucl. Recept. Signal.*, vol. 10, no. Figure 1, p. e001, 2012.
[54] X. Li, W. Liang, J. Liu, C. Lin, S. Wu, L. Song, and Z. Yuan, “Transducin (β)-like 1 X-linked receptor 1 promotes proliferation and tumorigenicity in human breast cancer via activation of beta-catenin signaling.,” *Breast Cancer Res.*, vol. 16, no. 5, p. 465, 2014.
[55] J. Y. Li, G. Daniels, J. Wang, and X. Zhang, “TBL1XR1 in physiological and pathological states.,” *Am. J. Clin. Exp. Urol.*, vol. 3, no. 1, pp. 13–23, 2015.
[56] H. G. Yoon, D. W. Chan, Z. Q. Huang, J. Li, J. D. Fondell, J. Qin, and J. Wong, “Purification and functional characterization of the human N-CoR complex: The roles of HDAC3, TBL1 and TBLR1,” *EMBO J.*, vol. 22, no. 6, pp. 1336–1346, 2003.
[57] X.-M. Zhang, Q. Chang, L. Zeng, J. Gu, S. Brown, and R. S. Basch, “TBLR1 regulates the expression of nuclear hormone receptor co-repressors.,” *BMC Cell Biol.*, vol. 7, p. 31, 2006.
[58] M. Rohm, A. Sommerfeld, D. Strzoda, A. Jones, T. P. Sijmonsma, G. Rudofsky, C. Wolfrum, C. Sticht, N. Gretz, M. Zeyda, L. Leitner, P. P. Nawroth, T. M. Stulnig, M. B. Diaz, A. Vegiopoulos, and S. Herzig, “Transcriptional cofactor TBLR1 controls lipid mobilization in white adipose tissue,” *Cell Metab.*, vol. 17, no. 4, pp. 575–585, 2013.
[59] C. H. Lee, Y. C. Woo, Y. Wang, C. Y. Yeung, A. Xu, and K. S. L. Lam, “Obesity, adipokines and cancer: An update,” *Clin. Endocrinol. (Oxf).*, vol. 83, no. 2, pp. 147–156, 2015.
[60] U. Meier and A. M. Gressner, “Endocrine regulation of energy metabolism: Review of pathobiochemical and clinical chemical aspects of leptin, ghrelin, adiponectin, and resistin,” *Clin. Chem.*, vol. 50, no. 9, pp. 1511–1525, 2004.
[61] B. Bao, Z. Wang, Y. Li, D. Kong, S. Ali, S. Banerjee, A. Ahmad, and F. H. Sarkar, “The complexities of obesity and diabetes with the development and progression of pancreatic cancer,” *Biochim. Biophys. Acta - Rev. Cancer*, vol. 1815, no. 2, pp. 135–146, 2011.
[62] T. E. Nakajima, Y. Yamada, T. Hamano, K. Furuta, T. Matsuda, S. Fujita, K. Kato, T. Hamaguchi,

and Y. Shimada, “Adipocytokines as new promising markers of colorectal tumors: Adiponectin for colorectal adenoma, and resistin and visfatin for colorectal cancer,” *Cancer Sci.*, vol. 101, no. 5, pp. 1286–1291, 2010.

[63] S. Otake, H. Takeda, Y. Suzuki, T. Fukui, S. Watanabe, K. Ishihama, T. Saito, H. Togashi, T. Nakamura, Y. Matsuzawa, and S. Kawata, “Association of visceral fat accumulation and plasma adiponectin with colorectal adenoma: Evidence for participation of insulin resistance,” *Clin. Cancer Res.*, vol. 11, no. 10, pp. 3642–3646, 2005.

[64] T. Scholzen and J. Gerdes, “The Ki-67 protein: From the known and the unknown,” *J. Cell. Physiol.*, vol. 182, no. 3, pp. 311–322, 2000.

[65] M. Zanoni, F. Piccinini, C. Arienti, A. Zamagni, S. Santi, R. Polico, A. Bevilacqua, and A. Tesei, “3D tumor spheroid models for in vitro therapeutic screening: a systematic approach to enhance the biological relevance of data obtained.,” *Sci. Rep.*, vol. 6, no. August 2015, p. 19103, 2016.

[66] F. Sams-Dodd, “Target-based drug discovery: Is something wrong?,” *Drug Discov. Today*, vol. 10, no. 2, pp. 139–147, 2005.

[67] A. M. Edwards, C. H. Arrowsmith, C. Bountra, M. E. Bunnage, M. Feldmann, J. C. Knight, D. D. Patel, P. Prinos, M. D. Taylor, M. Sundström, P. Barker, D. Barsyte, M. H. Bengtson, C. Bell, P. Bowness, K. M. Boycott, C. Buser-Doepner, C. L. Carpenter, A. J. Carr, K. Clark, A. M. Das, D. Dhanak, P. Dirks, J. Ellis, V. R. Fantin, C. Flores, E. a. Fon, D. E. Frail, O. Gileadi, R. C. O’Hagan, T. Howe, J. T. R. Isaac, N. Jabado, P.-J. Jakobsson, L. Klareskog, S. Knapp, W. H. Lee, E. Lima-Fernandes, I. E. Lundberg, J. Marshall, K. B. Massirer, A. E. MacKenzie, T. Maruyama, A. Mueller-Fahrnow, S. Muthuswamy, J. Nanchahal, C. O’Brien, U. Oppermann, N. Ostermann, K. Petrecca, B. G. Pollock, V. Poupon, R. K. Prinjha, S. H. Rosenberg, G. Rouleau, M. Skingle, A. S. Slutsky, G. a. M. Smith, D. Verhelle, H. Widmer, and L. T. Young, “Preclinical target validation using patient-derived cells,” *Nat. Rev. Drug Discov.*, vol. 14, no. 3, pp. 149–150, 2015.

[68] B. Wang, P. C. Chandrasekera, and J. J. Pippin, “Leptin- and leptin receptor-deficient rodent models: relevance for human type 2 diabetes.,” *Curr. Diabetes Rev.*, vol. 10, no. 2, pp. 131–45, 2014.

[69] S. P. Poulos, M. V Dodson, and G. J. Hausman, “Cell line models for differentiation: preadipocytes and adipocytes.,” *Exp. Biol. Med. (Maywood, NJ)*, vol. 235, no. 10, pp. 1185–1193, 2010.

[70] P. Iyengar, T. P. Combs, S. J. Shah, V. Gouon-Evans, J. W. Pollard, C. Albanese, L. Flanagan, M. P. Tenniswood, C. Guha, M. P. Lisanti, R. G. Pestell, and P. E. Scherer, “Adipocyte-secreted factors synergistically promote mammary tumorigenesis through induction of anti-apoptotic transcriptional programs and proto-oncogene stabilization,” *Oncogene*, vol. 22, pp. 6408–6423, 2003.

[71] M. Zhao, C. I. Dumur, S. E. Holt, M. J. Beckman, and W. Lynne, “Multipotent adipose stromal cells and breast cancer development: think globally, act locally,” *Mol Carcinog.*, vol. 49, no. 11, pp. 923–927, 2010.

[72] Y. Y. Wang, C. Lehuédé, V. Laurent, B. Dirat, S. Dauvillier, L. Bochet, S. Le Gonidec, G. Escourrou, P. Valet, and C. Muller, “Adipose tissue and breast epithelial cells: A dangerous dynamic duo in breast cancer,” *Cancer Lett.*, vol. 324, no. 2, pp. 142–151, 2012.

[73] S. Hefetz-Sela and P. E. Scherer, “Adipocytes: Impact on tumor growth and potential sites for therapeutic intervention,” *Pharmacol. Ther.*, vol. 138, no. 2, pp. 197–210, 2013.

[74] K. A. Meyer, C. K. Neeley, N. A. Baker, A. R. Washabaugh, C. G. Flesher, B. S. Nelson, T. L. Frankel, C. N. Lumeng, C. A. Lyssiotis, M. L. Wynn, A. D. Rhim, and R. W. O’Rourke, “Adipocytes promote pancreatic cancer cell proliferation via glutamine transfer,” *Biochem. Biophys. Reports*, vol. 7, pp. 144–149, 2016.

[75] D. L. Roberts, C. Dive, and A. G. Renehan, “Biological mechanisms linking obesity and cancer risk: new perspectives.,” *Annu. Rev. Med.*, vol. 61, pp. 301–316, 2010.

[76] S. E. Bulun, D. Chen, I. Moy, D. C. Brooks, and H. Zhao, “Aromatase, breast cancer and obesity: A complex interaction,” *Trends Endocrinol. Metab.*, vol. 23, no. 2, pp. 83–89, 2012.

[77] R. C. Travis and T. J. Key, “Oestrogen exposure and breast cancer risk.,” *Breast Cancer Res.*, vol. 5, no. 5, pp. 239–47, 2003.

[78] L. Vona-Davis and D. P. Rose, “Adipokines as endocrine, paracrine, and autocrine factors in

breast cancer risk and progression," *Endocr. Relat. Cancer*, vol. 14, no. 2, pp. 189–206, 2007.

[79] E. Petridou, C. Mantzoros, N. Dessypris, P. Koukoulomatis, C. Addy, Z. Voulgaris, G. Chrousos, and D. Trichopoulos, "Plasma Adiponectin Concentrations in Relation to Endometrial Cancer: A Case-Control Study in Greece," *J. Clin. Endocrinol. {&} Metab.*, vol. 88, no. 3, pp. 993–997, 2003.

[80] L. Dal Maso, L. S. A. Augustin, A. Karalis, R. Talamini, S. Franceschi, D. Trichopoulos, C. S. Mantzoros, and C. La Vecchia, "Circulating adiponectin and endometrial cancer risk," *J. Clin. Endocrinol. Metab.*, vol. 89, no. 3, pp. 1160–1163, 2004.

[81] Y. Miyoshi, T. Funahashi, S. Kihara, T. Taguchi, Y. Tamaki, Y. Matsuzawa, and S. Noguchi, "Association of serum adiponectin levels with breast cancer risk.," *Clin. Cancer Res.*, vol. 9, no. 15, pp. 5699–704, 2003.

[82] C. Mantzoros, E. Petridou, N. Dessypris, C. Chavelas, M. Dalamaga, D. M. Alexe, Y. Papadiamantis, C. Markopoulos, E. Spanos, G. Chrousos, and D. Trichopoulos, "Adiponectin and breast cancer risk," *J.Clin.Endocrinol.Metab*, vol. 89, no. 0021–972X (Print), pp. 1102–1107, 2004.

[83] S. Goktas, I. Y. Mahmut, K. Caglar, A. Sonmez, S. Kilic, and S. Bedir, "Prostate cancer and adiponectin," *Urology*, vol. 65, no. 6, pp. 1168–1172, 2005.

[84] A. F. Hezel, A. C. Kimmelman, B. Z. Stanger, N. Bardeesy, and R. A. Depinho, "Genetics and biology of pancreatic ductal adenocarcinoma Genetics and biology of pancreatic ductal adenocarcinoma," vol. 1, pp. 1218–1249, 2006.

[85] An. Maitra and R. H. Hruban, "Pancreatic Cancer," *Annu. Rev. Pathol. Dis.*, vol. 3, pp. 157–188, 2008.

[86] K. M. Hertzer, M. Xu, A. Moro, D. W. Dawson, L. Du, G. Li, H.-H. Chang, A. P. Stark, X. Jung, O. J. Hines, and G. Eibl, "Robust Early Inflammation of the Peripancreatic Visceral Adipose Tissue During Diet-Induced Obesity in the KrasG12D Model of Pancreatic Cancer," *Pancreas*, vol. 45, no. 3, pp. 458–465, 2016.

[87] A. E. Harvey, L. M. Lashinger, D. Hays, L. M. Harrison, K. Lewis, S. M. Fischer, and S. D. Hursting, "Calorie restriction decreases murine and human pancreatic tumor cell growth, nuclear factor-κB activation, and inflammation-related gene expression in an insulin-like growth factor-1-dependent manner.," *PLoS One*, vol. 9, no. 5, p. e94151, 2014.

[88] L. M. Lashinger, L. M. Harrison, A. J. Rasmussen, C. D. Logsdon, S. M. Fischer, M. J. McArthur, and S. D. Hursting, "Dietary energy balance modulation of Kras- and Ink4a/Arf+/--driven pancreatic cancer: the role of insulin-like growth factor-I.," *Cancer Prev. Res. (Phila).*, vol. 6, no. 10, pp. 1046–55, 2013.

[89] J. M. Friedman, "Leptin at 14 y of age: An ongoing story," *Am. J. Clin. Nutr.*, vol. 89, no. 3, pp. 973–979, 2009.

[90] J. Park and P. E. Scherer, "Leptin and cancer: from cancer stem cells to metastasis," *Endocr Relat Cancer*, vol. 18, no. 4, pp. C25–9, 2011.

[91] D. Dutta, S. Ghosh, K. Pandit, P. Mukhopadhyay, and S. Chowdhury, "Leptin and cancer: Pathogenesis and modulation.," *Indian J. Endocrinol. Metab.*, vol. 16, no. Suppl 3, pp. S596–600, 2012.

[92] B. Wang, I. S. Wood, and P. Trayhurn, "Hypoxia induces leptin gene expression and secretion in human preadipocytes: Differential effects of hypoxia on adipokine expression by preadipocytes," *J. Endocrinol.*, vol. 198, no. 1, pp. 127–134, 2008.

[93] A. Grosfeld, J. Andre, and J. Pouysse, "Hypoxia-inducible Factor 1 Transactivates the Human Leptin Gene Promoter*," *Biochemistry*, vol. 277, no. 45, pp. 42953–42957, 2002.

[94] R. R. Gonzalez-Perez, V. Lanier, and G. Newman, "Leptin's pro-angiogenic signature in breast cancer," *Cancers (Basel).*, vol. 5, no. 3, pp. 1140–1162, 2013.

[95] Y. Fan, Y. Gan, Y. Shen, X. Cai, Y. Song, F. Zhao, M. Yao, J. Gu, and H. Tu, "Leptin signaling enhances cell invasion and promotes the metastasis of human pancreatic cancer via increasing MMP-13 production," *Oncotarget*, vol. 6, no. 18, pp. 16120–16134, 2015.

[96] A. Gąsiorowska, R. Talar-Wojnarowska, A. Kaczka, A. Borkowska, L. Czupryniak, and E. Malecka-Panas, "Role of adipocytokines and its correlation with endocrine pancreatic function in patients with pancreatic cancer," *Pancreatology*, vol. 13, no. 4, pp. 409–414, 2013.

[97] H. A. Burris, M. J. Moore, J. Andersen, M. R. Green, M. L. Rothenberg, M. R. Modiano, M. C.

Cripps, R. K. Portenoy, A. M. Storniolo, P. Tarassoff, R. Nelson, F. A. Dorr, C. D. Stephens, and D. D. Von Hoff, “Improvements in survival and clinical benefit with gemcitabine as first-line therapy for patients with advanced pancreas cancer: a randomized trial.,” *J. Clin. Oncol.*, vol. 15, no. 6, pp. 2403–2413, 1997.

[98] R. D. W. Marsh, M. S. Talamonti, M. H. Katz, and J. M. Herman, “Pancreatic cancer and FOLFIRINOX: a new era and new questions.,” *Cancer Med.*, vol. 4, no. 6, pp. 853–63, 2015.

[99] G. Han, L. Wang, W. Zhao, Z. Yue, R. Zhao, Y. Li, X. Zhou, X. Hu, and J. Liu, “High expression of leptin receptor leads to temozolomide resistance with exhibiting stem/progenitor cell features in gliobalastoma,” *Cell Cycle*, vol. 12, no. 24, pp. 3833–3840, 2013.

[100] G. H. Bain, E. Collie-Duguid, G. I. Murray, F. J. Gilbert, A. Denison, F. McKiddie, T. Ahearn, I. Fleming, J. Leeds, P. Phull, K. Park, S. Nanthakumaran, H. I. Grabsch, P. Tan, A. Welch, L. Schweiger, A. Dahle-Smith, G. Urquhart, M. Finegan, and R. D. Petty, “Tumour expression of leptin is associated with chemotherapy resistance and therapy-independent prognosis in gastro-oesophageal adenocarcinomas.,” *Br. J. Cancer*, vol. 110, no. 6, pp. 1525–34, 2014.